Smart4RES

Joint dispatch of RES and storage technologies towards a multi-service approach

D5.1 Joint dispatch of RES and storage technologies towards a multi-service approach

WP5, T5.1

Version V2.0

Authors:
Simon Camal (ARMINES)
Luca Santosuosso (ARMINES)
Akylas Stratigakos (ARMINES)
Dimitrios LAGOS (ICCS)
Inês Marques (EDP)
Catarina Martins (EDP)

Technical references

Project Acronym	Smart4RES
Project Title	Next Generation Modelling and Forecasting of Variable Renewable Generation for Large-scale Integration in Energy Systems and Markets
Project Coordinator	ARMINES – MINES Paris
Project Duration	November 2019 – April 2023

Deliverable	D5.1: Joint dispatch of RES and storage technologies towards a multi-service approach
Dissemination level	PU
Nature	R
Work Package	WP5- Modelling Tools for Integrating RES Forecasting in Electrical Grids, Electricity Markets and Storage Operation
Task	T5.1- Joint optimization and dispatch of RES power plants and storage
Lead beneficiary	ARMINES
Contributing beneficiaries	EDP, ICCS
Reviewers	Ricardo Silva (INESC TEC), Marcel Eijgelaar (DNV)
Due date of deliverable	28 February 2022

Document history

V	Date	Description
v0.1	20/01/2022	First draft containing contributions by all authors
v0.2	28/03/2022	Consolidated version by Task Leader
v0.3	19/04/2022	Reviews completed
v1.0	26/04/2022	Revised version
v2.0	28/04/2022	Final version submitted to the European Commission

This project has received funding from the European Union's Horizon 2020 research and innovation programme under grant agreement No 864337

Disclaimer

The present document reflects only the author's view. The European Climate, Infrastructure and Environment Executive Agency (CINEA) is not responsible for any use that may be made of the information it contains.

Table of Contents

This project has received funding from the European Union's Horizon 2020 research and innovation programme under grant agreement No 864337

List of Figures

This project has received funding from the European Union's Horizon 2020 research and innovation programme under grant agreement No 864337

This project has received funding from the European Union's Horizon 2020 research and innovation programme under grant agreement No 864337

This project has received funding from the European Union's Horizon 2020 research and innovation programme under grant agreement No 864337

List of Tables

This project has received funding from the European Union's Horizon 2020 research and innovation programme under grant agreement No 864337

Nomenclature

ACRONYMS

aFRR	automatic Frequency Restoration Reserve
AS	Ancillary Services
BESS	Battery Energy Storage System
BoL	Beginning of Life
BRP	Balancing Responsible Party
BSP	Balancing Service Provider
CCT	Cycling + Calendar with Threshold
DA	Day-Ahead
DDA	Deterministic Day-Ahead
DEMPC	Deterministic Economic MPC
DoD	Depth of Discharge
DRTMPC	Deterministic Reference Tracking MPC
ED	Economic Dispatch
EoL	End of Life
FCR	Frequency Containment Reserve
KPI	Key Performance Indicators
mFRR	manual Frequency Restoration Reserve
MPC	Model Predictive Control
NIIPS	Non-interconnected Island Power Systems
NMC	Nickel-Manganese-Cobalt
NoC	Number of Cycles
PV	Photovoltaic
RES	Renewable Energy Source

This project has received funding from the European Union's Horizon 2020 research and innovation programme under grant agreement No 864337

ROCOF Rate of Change of Frequency

RS Reference State

RT Real-Time

SC Simplified Cycling

SDA Stochastic Day-Ahead

SEMPC Stochastic Economic MPC

SoC State of Charge

SoH State of Health

ST Short-Term

TSO Transmission System Operator

VSS Value of the Stochastic Solution

WPP Wind Power Plant

PARAMETERS

η_c Charging efficiency of the BESS

η_d Discharging efficiency of the BESS

$\hat{y}$ RES production forecast

Ω Set of scenarios

π^B BESS degradation price

$\pi^{E,down}$ Imbalance price for downward deviations

$\pi^{E,up}$ Imbalance price for upward deviations

π^E Energy offer price

n^{100}_{EOL} Number of full cycles before End of Life.

T Trading period

w_1 Calendar weight

w_2 Cycling weight

w_B BESS degradation weight

w_M Market weight

x^{max} BESS maximum capacity

x^{min} BESS minimum capacity

$x^{thr,max}$ BESS maximum threshold capacity

$x^{thr,min}$ BESS minimum threshold capacity

This project has received funding from the European Union's Horizon 2020 research and innovation programme under grant agreement No 864337

VARIABLES

δ^R	Reserve deficit for the FCR AS
E^{down}	Energy offer downward deviation
E^{off}	Energy offer
E^{up}	Energy offer upward deviation
$p^{b,c}$	Power charged to the BESS
$p^{b,d}$	Power discharged from the BESS
R^{off}	Reserve offer for the FCR AS
x	Normalized battery capacity

SUBSCRIPTS

ω	Scenario
t	Time instant

SUPERSCRIPTS

DA	Day-Ahead
RT	Real-Time
ST	Short-Term

This project has received funding from the European Union's Horizon 2020 research and innovation programme under grant agreement No 864337

Executive Summary

The Deliverable D5.1 'Joint optimization and dispatch of RES power plants and storage' proposes new optimization approaches for the combined operation of Renewable Energy Sources (RES) and storage in two different settings, namely large RES power plants with integrated storage capacity (also called Hybrid RES power plants in the rest of the document). In isolated power systems the hybrid RES systems are composed by RES and battery energy storage systems (BESS) and will be mentioned separately since in islands with high RES penetration different services are described for the different components of the hybrid RES plant.

The first approach consists of a complete framework for the provision of multiple services by a Hybrid RES power plant integrating a Battery Energy Storage System (BESS). These services include the compensation of imbalances faced by the owner of the plant on the energy market, but also frequency-control Ancillary Services (AS). Specifically, the provided AS considered in this work are Frequency Containment Reserve (FCR) and automatic Frequency Restoration Reserve (aFRR).

The framework is based on a multi-objective optimization applied to a sequence of two models: (1) decision on the volumes of energy and services scheduled or traded by the hybrid RES plant; (2) short-term Model Predictive Control (MPC) of the hybrid RES plant, in particular of the BESS to efficiently implement the service delivery. The multi-objective formulation lets the decision-maker establish priorities between the performance of service provision and BESS degradation. An alternative approach based on machine learning is investigated to combine prediction and optimization into a single decision-aid model.

Operational constraints of a real-world hybrid RES plant, originating from the BESS technical characteristics and from contracts in place, have been integrated into the approach. Under simplified assumptions on AS prices, it is found that the proposed optimization framework integrating an economic MPC increases revenue for such a hybrid plant of at least 13% when the BESS adds FCR and aFRR to the compensation of imbalances on the energy market, which fulfills Smart4RES KPI 1.3.d (target $\geq$ 10 %).

An important result for the provision of multiple services is that the proposed economic MPC reduces the cost of BESS degradation significantly (at least 69%) compared to a standard reference tracking dispatch when the Hybrid plant offers energy and Frequency Containment Reserve (FCR). The methodology reaches a Technology Readiness Level (TRL) of 4 thanks to the integration of RES forecasts, day-ahead decision and short-term control.

The second approach optimizes the operation of a Hybrid plant in an isolated system. In isolated power systems the Hybrid plant plays a crucial role in the overall stability of the system. Specifically, the battery inverter have to provide several services, *e.g.* FCR, Frequency Restoration Reserves (FRR), grid forming operation, fault ride through, black start and synthetic inertia. In this deliverable, the services of the battery inverter required in small islands, with peak demand less than 5MW, will be defined. The actual case of Astypalea island is used to highlight the impact of the AS.

In addition, several of the aforementioned services (FRR,FCR, synthetic inertia) should be considered in the energy management of the island. A stochastic economic dispatch algorithm is developed that receives as input the forecasts from the tools developed in WP3 and considers also analytic expressions of frequency security correlated with the above services. This approach is evaluated using actual forecasts from installations in Rhodes island and static data from the small isolated island of Astpalea. The proposed approach is compared to 1) an existing formulation of the services in the economic dispatch to present its ability to predict more

This project has received funding from the European Union's Horizon 2020 research and innovation programme under grant agreement No 864337

accurately the frequency security in the system; 2) a deterministic economic dispatch to highlight the impact of novel forecast tools and energy management in the operation of the system. The Frequency Dynamic Economic Dispatch (FDED) proposed can achieve a reduction in load shedding in small island systems greater than 80% which fulfills Smart4RES KPI 1.3.a. Actual data from greek island systems were used to build the dynamic models, produce the forecasts based on Smart4RES tools in order to evaluate the method developed, reaching a TRL of Level 3.

Business cases will be analyzed in Smart4RES WP6 to further develop the decision-aid tools presented in this Deliverable. Finally, the key messages from this work are the following:

- Degradation-aware predictive control improves feasibility and profitability of multi-service provision by hybrid RES+BESS system
- Economic predictive control outperforms traditional reference tracking predictive control in the context of multiple services by a hybrid RES system
- The synthetic inertia service provision by a centralized BESS is crucial to maintain frequency security in non interconnected island operating in high RES penetration levels
- Grid forming control and less strict fault ride through requirements can increase the overall security of the system during faults and transitions between island states.
- The introduction of the different characteristics of BESS FCR and synthetic inertia compared to the diesel generators in the economic dispatch formulation can avoid the computation of frequency insecure control actions.
- Advanced forecasts modules (probabilistic) and optimization techniques that consider uncertainty (stochastic) increase the overall security in the system.

This project has received funding from the European Union's Horizon 2020 research and innovation programme under grant agreement No 864337

1 Introduction

1.1 Purpose and objectives of this Deliverable

This Deliverable aims to propose new decision-aid tools to support the provision of multiple services from storage systems that are jointly dispatched with RES production. Providing multiple services enables the increase of the profitability of the investments in storage by maximizing its value for power systems. It is also crucial in order to satisfy the stability of power systems under large renewable penetration.

The **objectives** of the Deliverable are the following:

1. Propose an optimization method for the scheduling/trading and control of a hybrid RES power plant integrating storage providing energy and AS.
2. Propose an optimization method of the dispatch of an isolated power system under large RES penetration, considering the provision of multiple AS by storage systems.
3. Identify the necessary services provided by a BESS for a small island system operating in high RES penetration levels.
4. Integrate forecasts of RES production (and load when applicable) into these methods based on real-world data.
5. Compare the value of the decision-aid tools to state-of-the-art approaches. After validation based on the Key Performance Indicators defined in Smart4RES D1.1, methods have reached a Technology Readiness Level of 3 to 4.
6. Identify some possible methodological convergences between the two decision-aid tools. This may serve to enhance the applicability of such tools to distinct Use Cases.

The document starts by defining the context of this work. Then the state of the art of similar decision-aid approaches in the context of service provision is reviewed, and contributions from the proposed approaches are explicitly stated. Finally, after presentation of case studies and evaluation metrics, results are presented and discussed.

This project has received funding from the European Union's Horizon 2020 research and innovation programme under grant agreement No 864337

1.2 Context

1.2.1 Offering in Electricity Market

This section presents an overview on the organization of short-term electricity markets where hybrid RES+BESS are anticipated to operate. This is justified in Europe where the transition from feed-in tariffs to direct market participation of RES has already started in many countries. For these hybrid RES plants, the provision of multiple services therefore means adding additional services to the offering of energy volumes and the reduction of costs associated with imbalances between offer and delivery.

Short-term electricity markets are mostly organized in day-ahead and intraday markets. RES production may be valorized in intraday electricity markets for various reasons, for instance hedging decisions taken at day-ahead or benefit from lower forecasting error as horizons shorten towards delivery. However, considering the heterogeneous structures of intraday markets throughout Europe, the present work focuses on day-ahead energy markets that share a higher degree of convergence in Europe.

On the day-ahead electricity market, the producer/consumer assumes the role of seller/buyer of bids from the market operator. A bid is defined by an energy volume, placed at a given *Market Time Unit* (MTU) to which it refers and a price (€/MWh). The purpose of the RES producer will be to sell the energy volume to the market, at the given MTU and for at least the price associated to the bid. The bid submission can go on until a specified time, known as *Gate Closure Time* (GCT). After GCT, once all selling and buying bids are known, the demand and offer curves are computed to determine the actual prices of the market and which bids are accepted.
For accepted bids, at the time of delivery, the amount of energy generated by a producer such as the hybrid system considered in this work is likely to differ from the bid volume, due to unforeseen availability and to forecasting errors in the case of RES production. These deviations generate imbalance penalties that must be paid by the Balancing Responsible Party (BRP) accountable for the producer to the Transmission System Operator (TSO), tasked to solve the imbalance using produced balancing AS. The payment of these imbalances is generally organized under a *single-price* or *dual-price* settlement. The *single-price* settlement becomes gradually the common standard for imbalance settlement in Europe due to its favourable economic properties, in plain words it should be a faithful price for the optimal recovery of costs associated to balancing needs of power systems. However, the *dual-price* settlement is considered in this Deliverable because this is the current settlement used in the real-world case studies of this work. In a *dual-price settlement* scheme, the prices of negative and positive deviations from the energy offer are distinct and computed following the total net imbalance of the power system, as shown in Fig.1. The principle of such a market is that BRP deviations which have the same sign as the total deviation of the market are penalized. In other words, the BRP pays the TSO for upward deviations (since the TSO compensates the deficit imbalance of the BRP by activating an upward regulation from balancing suppliers), while the BRP is paid by the TSO for downward deviations (since the TSO acquires the surplus imbalance from the BRP, although at a lower price than the day-ahead price, because this imbalance causes the activation of a downward regulation from balancing suppliers). These deviations are modelled in the proposed optimization approach because forecasting errors of RES production will cause deviations between day-ahead offers and available power at the balancing stage.
In this context, the present work aims at maximizing the provision of multiple services while protecting producers against high imbalance penalties that reduce their revenue. A major source of imbalance for a BRP operating such RES+BESS hybrid systems is the uncertain level of

This project has received funding from the European Union's Horizon 2020 research and innovation programme under grant agreement No 864337

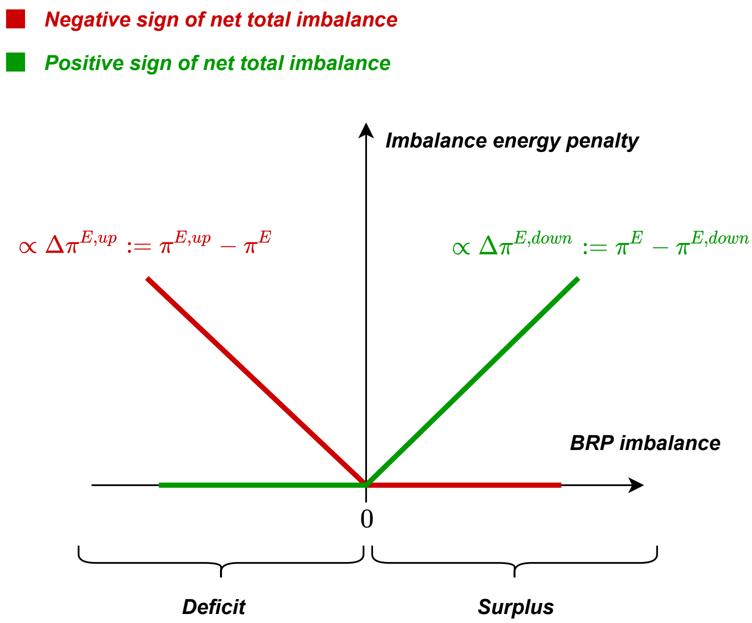

Figure 1: Imbalance price penalty computation.

RES production when the trading decision is made.

Fig.2 summarizes the value brought by energy storage in power systems. It is clear that storage addresses a wide range of use cases in power systems. Balancing AS appears in this summary as an additional use case for storage and will be included in the offer of the hybrid RES+BESS system. These balancing AS will be further described in the next subsection.

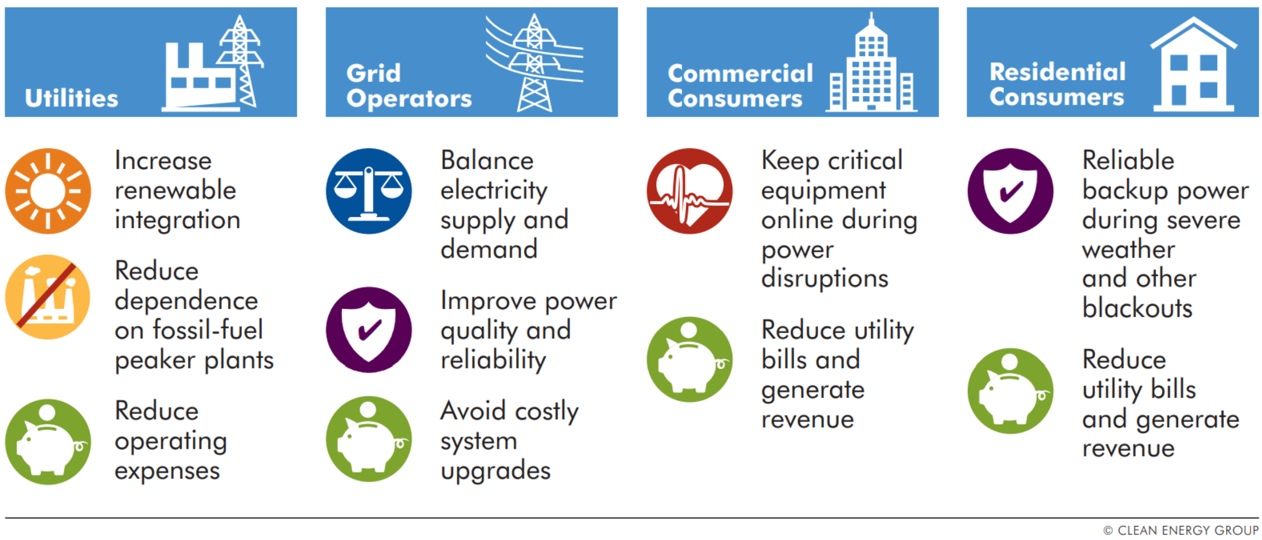

Figure 2: Value of storage in power systems [1].

1.2.2 Provision of Ancillary Services

Disturbances occur almost continuously in a power system. These disturbances create imbalances between the total power production and consumption levels and consequently the grid

This project has received funding from the European Union's Horizon 2020 research and innovation programme under grant agreement No 864337

frequency deviates from its nominal value ($50Hz$ in Europe). Active power reserves must be triggered in the next instants following a disturbance in order to avoid severe consequences going until a complete black-out. Figure 3 shows the three levels of activation of power reserve in European synchronous areas:

1. *Frequency Containment Reserve* (FCR).
2. *automatic Frequency Restoration Reserve* (aFRR).
3. *manual Frequency Restoration Reserve* (mFRR) and *Replacement Reserve* (RR)

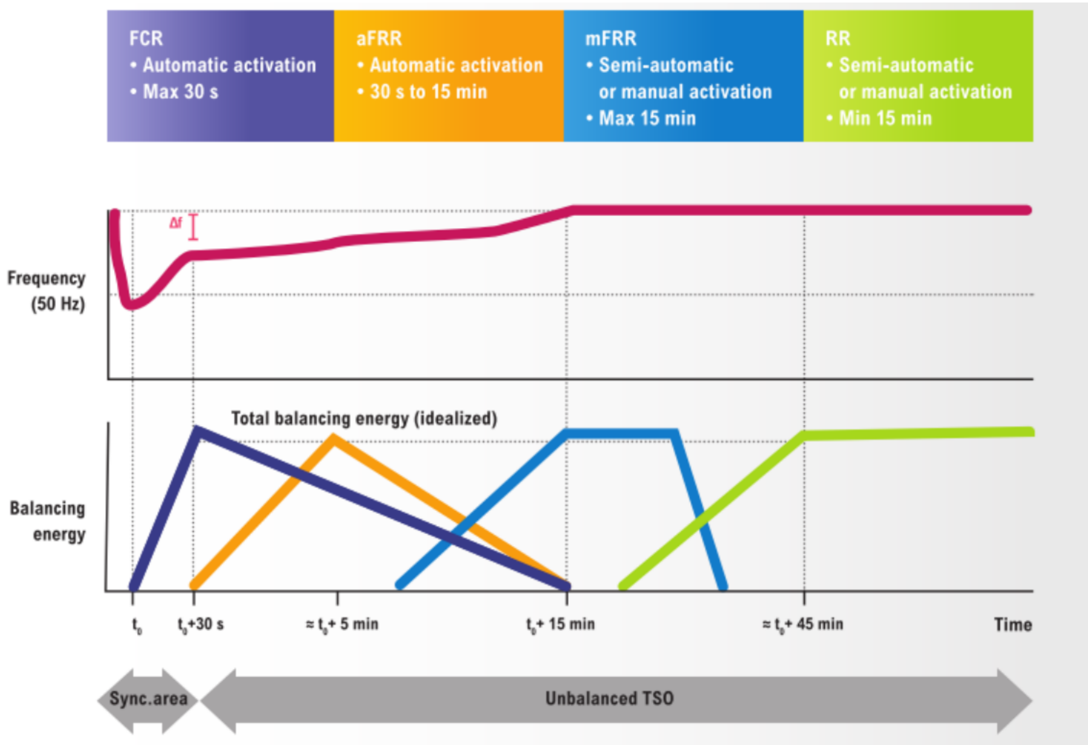

Figure 3: Frequency control scheme implemented in Europe [2].

The first of these levels is FCR, which is activated almost instantaneously over the whole synchronous area. The participating units have to fully deploy their reserves after several seconds, ranging from 2 to 30s according to its type [3]. Take for example the situation in Europe, in this case all the plants that take part in the FCR operations, assign a share of their power generation to this service and they regulate this part in a droop control mode. Due to this droop control, the active power of plant p is modulated in an inversely proportional way, with a factor K_p, with respect to the frequency deviation Δf from the nominal frequency, if this deviation is higher than the dead-band $db_{\Delta f}$:

$$FCR_p(\Delta f(t)) = -K_p \Delta f(t), \quad \forall \Delta f(t) \quad s.t. \quad |\Delta f(t)| \geq db_{\Delta f} \tag{1}$$

FCR constitutes a decentralized response in order to limit frequency deviations to a maximum of $200mHz$ and must be fully activated in less than $30s$.
Once the frequency deviations has been contained using FCR, the TSO activates the aFRR in its control area. The TSO sends to the BSPs some set points in order to restore the nominal frequency within 15 minutes at most (Figure 3). Thus, an operator p bidding an energy quantity E_p^{DA} on the day-ahead energy market and a reserve quantity $R_{aFRR,p}^{DA}$ on the day-ahead aFRR

This project has received funding from the European Union's Horizon 2020 research and innovation programme under grant agreement No 864337

market, will have its production modulated accordingly to the following rule:

$$Y_p(t) = E_p^{DA}(t) + E_p^{RT}(t) + \alpha_{aFRR}(t) R_{aFRR,p}^{DA}, \quad \forall t \in T_{validity}, \tag{2}$$

where $\alpha_{aFRR}(t) \in [-1, 1]$ is the set point sent by the TSO and $T_{validity}$ is the delivery period considered, also known as *product length* in the AS terminology. Finally the Balancing Service Providers (BSP) in charge of offering the mFRR and the RR services, replace those involved in the aFRR in order to restore and maintain the nominal situation. The increased participation of RES power plants on the energy market is challenging the provisioning of balancing AS, both in the size and in the efficiency. Accordingly to German TSOs, an increase of $40GW$ of RES capacity will imply an increase of balancing AS size of $1.5GW$ [4]. The TSO defines

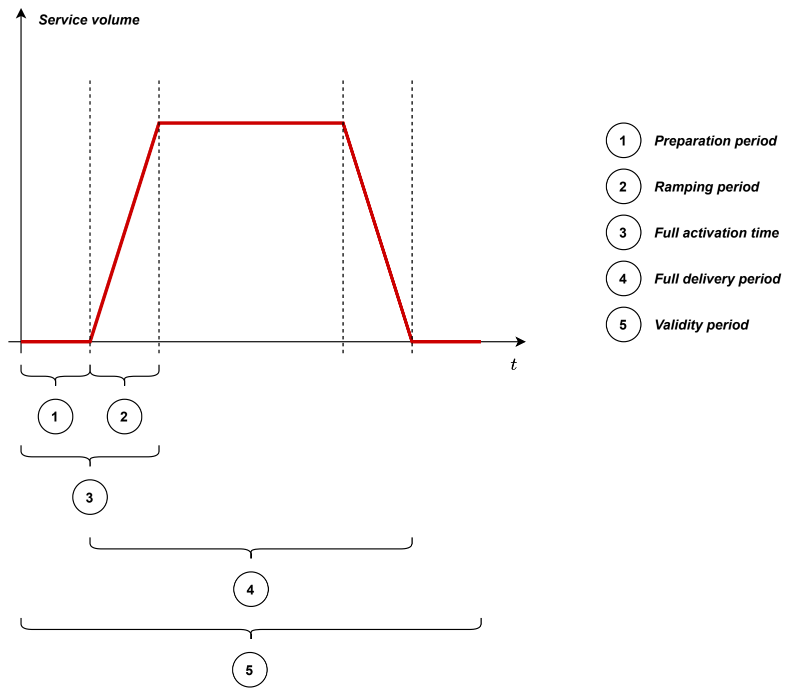

Figure 4: Standard balancing AS product.

some pre-qualification rules that must be met by the BSPs who are interested in joining the balancing AS markets. Thus a BSP must be able to provide, with minimum delay and high reliability, the AS product accordingly to frequency and automatic generation control signals. In Europe, this is currently regulated by the Electricity Balancing Guideline (EBGL), defined by the European Commission. The EBGL has defined a standard for the main temporal and volume characteristics of AS balancing products (Figure 4). It is doable nowadays to meet these constraints also with RES plants. The full activation time in Fig.4, at which it is required to start the delivery of 100% of the bid volume, can also be met by these kinds of power plants.

1.2.3 Hybrid Renewable Power Plants integrating on-site storage capacities

Battery Energy Storage Systems (BESS) can increase the reliability of RES dispatch, *e.g.* reduce the volumes of deviations between market offer and delivered RES production, but also provide other functionalities such as frequency control AS. The Cobadin Wind Farm in Romania, operated by EDP Renewables, is an example of a Hybrid Renewable Power Plant and is a case study in Smart4RES (Dataset n°7 in the Smart4RES Data Management Plan,

This project has received funding from the European Union's Horizon 2020 research and innovation programme under grant agreement No 864337

D1.4). The Cobadin Wind farm has a total installed capacity of 26 MW, having 13 Vestas turbines of 2 MW each and a BESS with an installed capacity of 1.26 MW / 1.344 MWh, with the aim of providing 1 MW/1hour at its point of coupling.

This specific plant has a limited BESS installed capacity (1.26 MW / 1.344 MWh) due to the fact that it has been set up in a demonstration project. It is clear that this capacity is not enough to compensate the hourly forecast deviations, that can be up to several MWh.

Prior to installing the system, EDPR has performed a cost-benefit analysis to estimate the optimal theoretical sizing of the BESS in the hybrid system. A simulation tool was developed in order to evaluate different scaling factors of the BESS capacity during an operation of several months. It was also verified that the behavior of the battery is accurately reproduced by means of software simulation. To do this, the energy moved by the BESS, considering different capacities, was computed using real production data, and real market prices were used to determine imbalance cost reduction. Technical values such as performance ratio and response time were also analysed to assess the performance of the storage system. The optimal battery size (expressed in both power and energy, in MW/MWh) for Cobadin was found to be 20MW/20MWh since once the capacity installed increases above 20 MW/20MWh, the CAPEX increase in order to capture more savings does not compensate. Similar conclusions have been achieved considering other EDPR wind farms.

In Figure 5 it is possible to observe the evolution of the imbalance cost savings and imbalance energy reduction as a function of the battery size, presented as the ratio between the battery capacity in MW and the wind farm installed capacity in MW.

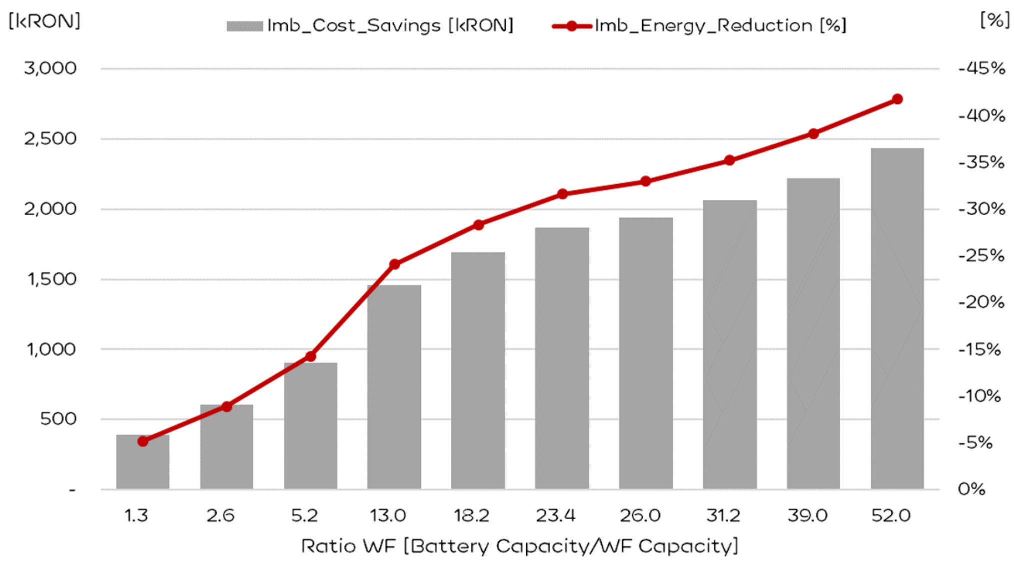

Figure 5: Reduction of imbalances on the energy market with increasing size of the BESS in the Cobadin hybrid system

The software that reproduced the BESS control system in Cobadin follows a rule-based algorithm that takes into account the deviation between the committed energy production and the energy produced by the wind turbine at each instant, and the battery state of charge (SOC). The algorithm starts by evaluating the deviation between the committed energy production and the energy produced at each instant, to determine if the battery should be charging or discharging. The second step is to evaluate the battery's SOC. If the battery should be charging but is fully

This project has received funding from the European Union's Horizon 2020 research and innovation programme under grant agreement No 864337

charged or should be discharging but has a SOC below the threshold, then the battery does not operate. Additionally, if the wind power produced by the turbines is below the minimum threshold of 0.1 kW, the battery also does not operate.

Next, it is presented an analysis to have a better comprehension of the battery behaviour and of the rules behind the algorithm. This analysis was performed for the week between 2018-09-22 and 2018-09-29. For this simulation, the scaling factor between the park size and battery size used was 15%, meaning that the battery size corresponds to 6.7 MW. During this week the produced energy exceeded the DA committed energy in approximately 42% of the time and was below the DA committed energy for 58% of the time. The battery was charging for approximately 22% of the time, discharging for 19% and did not operate for the remaining 59% of the time. The fact that the time percentages of the imbalances are quite higher than the percentage of time the battery was charging/discharging is an indicator that it was frequent to have the battery fully charged or discharged and that could not compensate for the deviations.

In Figure 6 it is possible to observe the committed DA energy, the energy produced by the wind turbines (WTG) and the total energy combining the wind turbines and the battery output. Figure 7 presents the deviations considering only the wind turbines vs the wind turbines combined with BESS, where deviations are defined as the energy generated by the wind turbines minus the committed DA energy. In average, the BESS reduces the deviation by 32.25%. The imbalance reduction is limited by two factors: the limited charging/discharging time of the storage system (41% of the total available time), and the small storage capacity compared to the amounts of imbalance to be compensated.

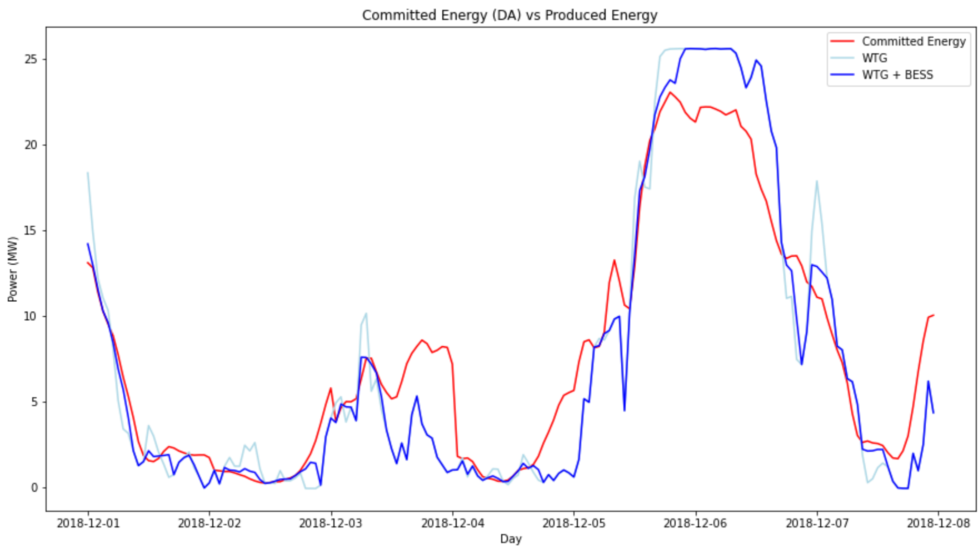

Figure 6: Time series of committed DA energy and produced energy with and without BESS in an operating Wind + Storage Hybrid RES plant in Romania (EDP-R / EDP New)

Figure 8 displays the factors taken into account for the decision to charge, discharge or keep the battery off. As mentioned before, the first step is to check whether we have a positive deviation, meaning the generation is above the committed energy or a negative deviation, meaning that the generation is below the committed energy. Then it is necessary to verify the current SOC of the battery to see if the intended action is feasible. For example, in Factor Number 4, the deviation is negative meaning we would need the battery to discharge to compensate the production of the wind turbines, however, since the SOC is already at the minimum, the battery is only available to charge. The opposite happens if we look at Factor Number 7, where the

This project has received funding from the European Union's Horizon 2020 research and innovation programme under grant agreement No 864337

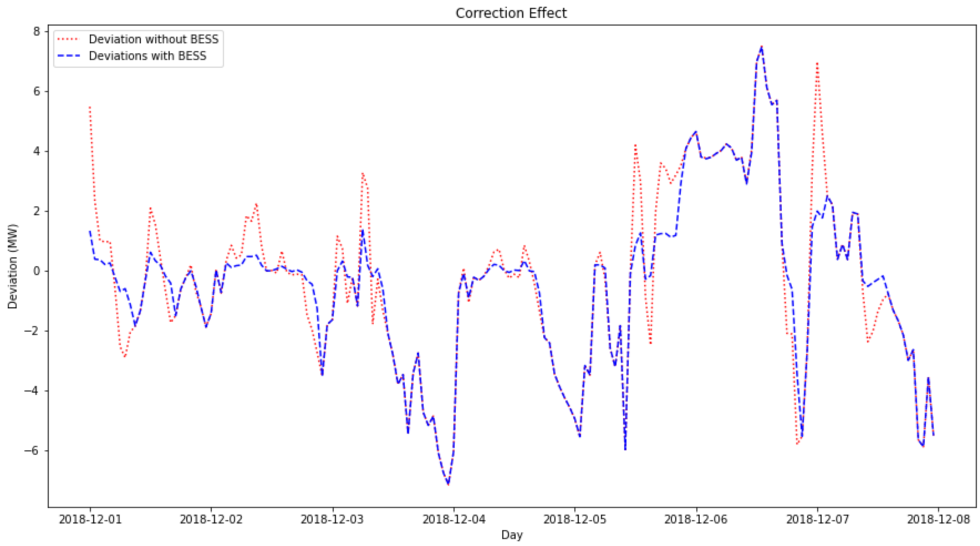

Figure 7: Deviations between committed DA energy and produced energy with and without BESS in an operating Wind + Storage Hybrid RES plant in Romania (EDP-R / EDP New)

Factor Number	Decision factors	Decision
1	Positive deviation, (PowerSetup - AuxCons) > 0 & (PowerSetup - AuxCons) > PotChargeEff * PMaxBESS, PowerSetup > 0	Charge
2	Positive deviation, (PowerSetup - AuxCons) > 0 & (PowerSetup - AuxCons) <= PotChargeEff * PMaxBESS, PowerSetup > 0	Charge
3	Negative deviation, (PowerSetup - AuxCons) <= 0 & <=PotChargeEff * PMaxBESS, PowerSetup < 0	Discharge
4	Negative deviation, SOC min - Only charge available, (PowerSetup - AuxCons) <= 0 & <=PotChargeEff * PMaxBESS, PowerSetup = 0	Off
5	Positive deviation, WTG power enough to charge, (PowerSetup - AuxCons) > 0 & (PowerSetup - AuxCons) > PotChargeEff * PMaxBESS, PowerSetup > 0	Charge
6	Positive deviation, WTG power enough to charge, (PowerSetup - AuxCons) > 0 & (PowerSetup - AuxCons) <= PotChargeEff * PMaxBESS, PowerSetup > 0	Charge
7	Positive deviation, SOC max - Only discharge available , (PowerSetup - AuxCons) <= 0 & <=PotChargeEff * PMaxBESS, PowerSetup = 0	Off

Figure 8: Dispatch rules implemented in an operating Wind + Storage Hybrid RES plant in Romania (EDP-R / EDP New)

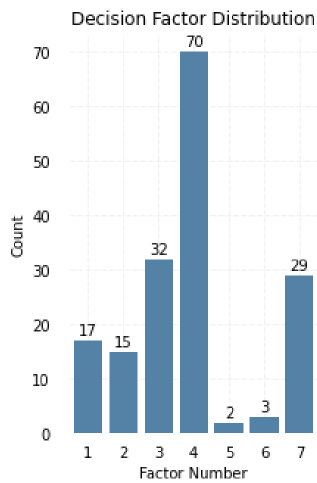

Figure 9: Distribution of dispatch rules

battery's SOC is at its maximum. The histogram plotted in Figure 9 provides an insight into the distribution of the several decision factors. It is possible to note that the battery reaches the minimum SOC very frequently, suggesting that a battery with a higher capacity would be more appropriate for this wind farm.

Figure 10 displays the committed DA energy and the energy generated at each instant together with the software decisions. In this plot it is possible to verify the phenomenon described before, for example between 2018-12-06 and 2018-12-07, where the battery cannot reduce the deviation due to being fully charged.

Using the software simulation, the battery energy management system has been confirmed to work correctly, although some additional improvements can be done. The BESS controls, as expected, have good dynamics with a response time of 1 sec. The actual charging/discharging power rates follow well the corresponding power setpoints, with a ratio of actual power delivery

This project has received funding from the European Union's Horizon 2020 research and innovation programme under grant agreement No 864337

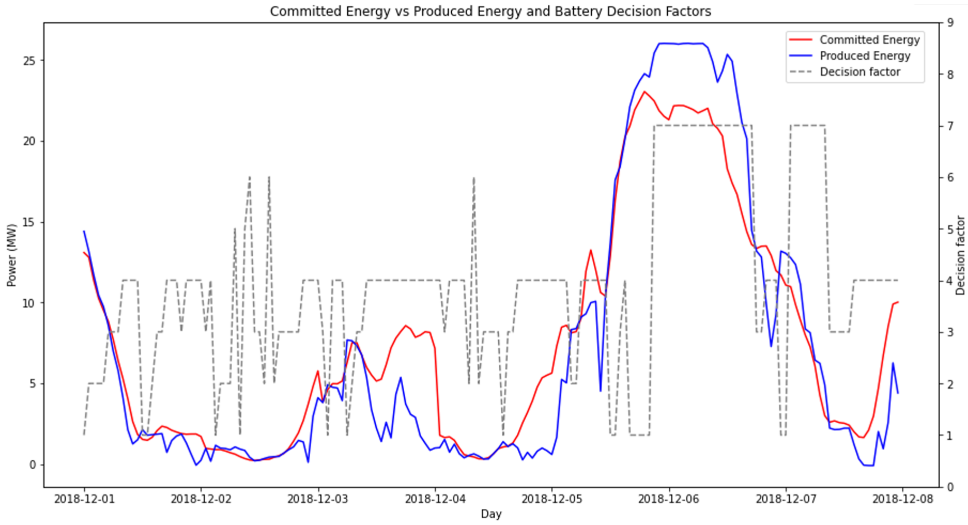

Figure 10: Time series of implemented Dispatch rules implemented in an operating Wind + Storage Hybrid RES plant in Romania (EDP-R / EDP New)

vs power setpoint that is above 90% during most situations. By testing different sizes (changing the scaling factor), it was found that the required installed energy of the BESS to compensate most of the deviations in Cobadin wind farm would need to be in the range of 20 MWh, which, taking into account current CAPEX estimations, is (still) not viable.

In order to increase the value of BESS, it is important to analyze the potential benefits of combining additional applications. The algorithm could also be improved by taking into account battery degradation among others.

1.2.4 Energy Storage and stability of isolated power system

Non-interconnected island power systems (NIIPS) are electrical systems isolated from the mainland grid that supply a geographical island or a group of islands. In large NIIPS and in interconnected systems, steam turbines, gas turbines, or combined cycle plants might be used to generate electricity. The electrification of small NIIPS, however, depends mainly on diesel generators. Diesel generators run on light or heavy fuel oil resulting in high operational costs, high greenhouse gas emissions and constrain the exploitation of the renewable energy potential. Another characteristic of these systems is that the load demand can present high seasonal variability, especially in islands with high seasonal tourism [5].

Due to these high expenditures, renewable energy sources (RES) are considered as viable solutions for the reduction of operational costs and greenhouse gas emissions in many NIIPS. However, despite the excellent renewable potential, especially wind and solar, that exists in many islands, RES production is limited for technical reasons. Power limitations relate to the technical constraints of conventional thermal units, *i.e.* their minimum loading limits (technical minima), as well as a RES operating limit due to stability purposes. More specifically, thermal generators are not operated below a certain level to avoid increased wear of their prime movers and increased maintenance requirements. Thus, at periods of low demand, the aggregated technical minima of thermal generators cover a significant portion of the load, leaving little headroom for RES operation. At the same time, a sufficient amount of conventional units is required to provide adequate levels of spinning reserves. A common practice applied by the island system operators is to consider reserves equal to the total RES generation. A total RES

This project has received funding from the European Union's Horizon 2020 research and innovation programme under grant agreement No 864337

generation outage is considered as a possible contingency, due to the intermittent behavior of RES production and the concentration of RES units in close geographical regions. For example, a simultaneous power outage of those units is probable due to voltage sags that exceed their ride-through capability caused by network faults. In addition, very high wind speeds that exceed the cut out speed of the wind turbines (WT) are also probable. In the case of RES outages, the operating thermal units need to compensate fast the resulting power deficit. Overall, large variations of RES production can cause significant frequency drops leading to load curtailment (tripping under frequency load shedding relays) and/or erroneous operation of loss of mains protection (that base their operation on frequency transients). Hence, a RES penetration limit is usually imposed in island systems depending on the island characteristics (size, type of conventional units, dispersion of RES generators, etc.). Typical values are between 30% to 40% of total capacity of operating diesel units or total demand in that period according to the island system operator practice [6].

Several initiatives have taken place in order to achieve high RES penetration levels (above 60% of the annual demand), especially in small island systems. To this end, new and advanced control solutions are necessary, as well as the introduction of energy storage [5]. Battery Energy Storage (BES) applications are vital because they offer the ability to provide system services (*e.g.* spinning reserve, frequency regulation and voltage control) allowing the operation of the islands with a reduced number of thermal units or even purely based on RES. Maintaining security of operation in NIIPS can be a difficult task even with the presence of a battery storage in the system. Without the necessary services provision the overall system security could be in jeopardy.

To begin with, NIIPS have limited mechanical inertia, according to the number of operating synchronous generators, since there is no interconnection with a stiff grid. Compared to interconnected systems, the overall frequency transients will be characterized by high Rate of Change of Frequency (ROCOF) both due to the limited system inertia (H_{sys}) and relative high disturbances (ΔP) due to the intermittent nature of RES generators, as presented by the following equation for the estimation of ROCOF.

$$ROCOF = \Delta P * f_{nom}/2H_{sys}$$

The overall reduced amounts of FCR provided by diesel generators at high RES penetration levels, as well as their restricted response time can lead to high ROCOF events with significant nadirs in frequency. To mitigate this effect, the battery storage unit should be able to provide emulated inertia services, to have a quick response after the transient and fast FCR provision to mitigate the frequency drop to avoid critical frequency nadirs.

To restore the frequency to its nominal value, the diesel generators in small NIIPS deploy automatically FRR (aFRR) though an isochronous control. Obviously, relying only on diesel generators to privide aFRR at high RES penetration levels, can result in inadequate levels of aFRR. Hence, the frequency can not be restored to its nominal value and the automatic nature of the deployment of FRR can result in diesel generator overload. To this end, it is crucial that the battery inverter also provides aFRR. According to the Greek Non Interconnected Island code, the units providing aFRR must maintain the provision service for at least 30 minutes, hence the battery unit should have sufficient headroom in its energy storage to maintain this service according to the code requirements.

To meet the desired goals of RES $\geq$ 60 % RES penetration annually in terms of energy supply (MWh), the island should operate also solely on inverter based generation on certain occasions.

This project has received funding from the European Union's Horizon 2020 research and innovation programme under grant agreement No 864337

In islands operating solely on RES and BESS, the battery unit needs to operate in grid forming mode to ensure voltage and frequency control of the system. It is also crucial to operate in grid forming mode, providing all of the aforementioned services in the presence of the other grid forming sources (conventional generators). This can be achieved by implementing a grid forming control in a virtual generator scheme in the battery inverter. The main advantage of this approach is that it will ensure smooth transitions when the conventional units connect or disconnect, without the need for communication or islanding detection schemes.The ability to form the grid allows the battery inverter to serve as a black start unit. This service will allow a faster restoration of the power supply in the island if the battery inverter control is able to mitigate the inrush currents that occur during the restoration of the system.

It is clear that the battery unit is the most critical asset for the island power supply security under high RES penetration levels. Hence, it is important for the BESS to remain connected during voltage sags that occur during faults. A Fault Ride Through service, therefore, should be supported to prevent the battery unit disconnecting during temporary voltage sags.

In addition, the RES units can also provide some of the aforementioned services.The downward FCR can be provided through frequency rise transients, while the upward FCR can be deployed if they are curtailed, reserving a portion of the available power for the provision of upward FCR. The provision of the aforementioned services, specifically the synthetic inertia, FCR, aFRR from the battery inverter, should be considered in the economic operation in the system. The necessary headroom in the active power and in the stored energy of the battery inverter to provide this services is linked mainly with the RES production, which is of uncertain nature. Thus, advanced forecast techniques are required to reduce the uncertainty in RES and Load forecast in order to control the battery unit and the remaining power sources in the island in the most secure and economic manner. A stochastic economic dispatch algorithm is proposed in this deliverable that uses as inputs the WP3 power ensemble forecasts to address this concern.

Finally, the services of inverter based resources differ in their time response considerably from the conventional diesel plants. Considering their services are similar can result in overestimation/underestimation of the offered services and the desired thresholds in frequency control. An approach to include the different unit characteristics in the provision of reserves and correlate them with frequency metrics (ROCOF, Nadir) in the constraints of the stochastic economic dispatch is also presented and evaluated.

This project has received funding from the European Union's Horizon 2020 research and innovation programme under grant agreement No 864337

2 State of the art

This Section analyzes briefly the state of the art of research on the two subjects addressed by this Deliverable, namely (1) optimization of the operation of RES combined with storage and (2) dispatch optimization in isolated power system considering storage participation.

2.1 Optimization of scheduling, trading and control of RES combined with storage

The optimization of scheduling or trading of storage capacities operating jointly with RES is an important topic in the power system literature. In [7], Correa-Florez et al. propose a framework for facing the problem of PV power plants participation in the day-ahead energy markets. Similarly to the approach proposed here, this work considers a hybrid system composed of RES generation and a storage system to bid on the electricity market. The storage system degradation is modeled, in the optimization problem, with a piecewise linearization of the relation between DoD and total admitted number of cycles before reaching EoL of the battery. Finally, the work shows how the performances (in terms of cost and risk) of the proposed framework are able to largely overcome those of the basic deterministic approach to the problem. Still this work can be extended and modified, in order to explicitly take into account the provision of ancillary services and by formulating the problem as a multi-objective optimization, in order to be able to assign different priorities to the various objectives. More importantly, this work is mostly focused on trading optimization, while the real-time control of the hybrid system is not taken into account in the analysis.

For controlling smart grids and power systems, Model Predictive Control has proven to be able to provide very efficient solutions, by explicitly solving an optimization problem. Many examples of this can be found in the literature, like [8], where the grid congestion problem is faced. Here Nair et al. show how an optimization method can overcome a rule-based approach when dealing with multiple objectives (*e.g.* grid congestion mitigation, BESS degradation) to be fulfilled. As stated in the previous analysis, when dealing with RES power generation, one must deal with the uncertain nature of the system. An MPC strategy which takes into account this necessity is provided by Dennis van der Meer et al. in [9]. One of the main contributions of this work stands in the proposed scenario-based stochastic economic model predictive control method, combining stochastic MPC with an economic-oriented optimization. Moreover, this method guarantees the feasability of the first implemented action without post-processing, by forcing the first MPC control action to coincide across all scenarios. However this work does not take into account the BESS degradation and the use case coincides only in part with that of [7]. Indeed the day-ahead trading problem of a hybrid RES+BESS system is not taken into account in [9], whose aim is just to compute an optimal schedule for the storage system. Another example of economic Model Predictive Control is provided in [10]. Here the controller is formulated as a linear programming problem, to tackle the problem of minimizing the cost of power generation, taking into account the operator's necessity to meet the contracts stipulated with TSOs. A simple way to formulate the MPC strategy is proposed, but still the presence of a storage system is neglected.

A framework integrating both trading and real time control of the system is proposed by [11]. A stochastic programming approach derives trading decisions and integrates linear decision rules to model the control actions of RES curtailment and storage charging and discharging. These rules are computed as a linear combination of past realizations of forecasting errors. Thus the control actions are not computed in a predictive way, by taking into account the future predicted evolution of the complete system like in [9]. This may lead to suboptimal BESS operations such

This project has received funding from the European Union's Horizon 2020 research and innovation programme under grant agreement No 864337

as for instance saturating storage because the expected RES production during the optimization horizon happens reaches higher levels than the average levels modelled via the collection of recent forecasting errors.

To conclude the analysis on the economic-oriented Model Predictive Controllers it must be said that the existing stability analysis for traditional MPC algorithms can not be extended to these kinds of controllers. Previous works have shown conditions for the asymptotic stability using terminal constraints in the MPC formulation [12]. Recent works [13] have proposed less constrained methods to ensure the same properties, in particular by substituting the hard terminal constraints with a terminal cost in the objective function[14]. This can bring many advantages, like the increase in the size of the feasible set of initial conditions or an improvement in the closed-loop properties.

Due to the high investment cost in storage, its degradation associated with cycling and ageing must be accurately modelled. In [15], Namor et al. account for BESS degradation directly inside the control strategy. In order to do this, the authors propose the concept of weighted energy throughput, which consists in a degradation model combining the simplicity of a linear model (easy to integrate into a control algorithm) with the consideration of two important aspects of degradation, namely cycling and calendar ageing.

Still this BESS degradation model can be extended in order to consider a third contribution to the storage ageing: the temperature effect. This effect is considered in [16], where Michiorri et al. propose an optimization problem to compute the optimal sizing of the storage in a hybrid system (PV + storage) as a consequence of thermal behaviour and ageing. This work is mainly focused in assessing the importance of battery thermal behavior and local climatic conditions in the storage ageing, but also the cycling effect is taken into account in the model. A function for computing temperature ageing is obtained as a consequence of the interpolation of datasheet data and then linked to the battery cost of degradation in a linear way. Thus, even if this work extends the degradation model in the direction of thermal ageing, conversely to the previous case, the calendar contribution is not taken into account and the parameters of the proposed linear relations are not validated with experiments.

This analysis of the existing studies shows that still some gaps are present in the literature. It is uncommon to find a work that proposes a complete approach for the sequence of day-ahead decision (*e.g.* scheduling or trading) and short-term control of an hybrid system (RES + BESS). Either the problem is only focused on the trading only, neglecting the presence of near real-time control actions, or conversely only on the control strategy. In the cases in which both problems are considered, the BESS degradation is not take into account in a complete way or the optimization problem is not a multi-objective one, so the operator doesn't have the possibility to vary the strategy depending on the desired objective. In addition to this, the existing works are mostly focused on providing energy only, while the presence of ancillary services is mostly neglected. Finally, when control strategies are introduced in the framework that controls the system in real time, these are simplified linear strategies which do not optimize the control actions in a predictive manner. To the best of the authors knowledge, the combination of economic model predictive control with a stochastic scenario-based representation of the uncertainty has not been proposed for the application of multi-service provision by a renewable producer integrating storage.

This project has received funding from the European Union's Horizon 2020 research and innovation programme under grant agreement No 864337

2.2 Dispatch optimization in isolated power systems considering storage participation and security constraints

To reach high RES penetration levels the introduction of BESS is crucial [5]. Despite the concerns presented for the operation of island with high RES penetration, a significant presence of RES based installed capacity has already taken place in insular energy grids since these regions are preferable due to high availability of RES. Moving further towards an increasing share of RES an evolution of the island code is necessary [17].

The most critical security aspect is the frequency security. In systems with high RES penetration, thus reduced physical inertia, new frequency regulation services are emerging aiming to take full utilization of a BESS unit. Several new services have been introduced in grid codes, *e.g.*, Enhanced Frequency Response (EFR) of U.K., Fast Frequency Response of Ireland (FFR-IR), FFR of Australia (FFR-AUS) and Dynamic Regulation Signal (RegD) of PJM, although they differ in names and types. Some of them describe the fast deployment of FCR, *i.e.* in less than 2s, while other (Dynamic Regulation Signal (RegD) of PJM) refer to the BESS participation with FRR in system security [3]. In bulk power systems these services are part of the balancing market. In a small non-interconnected islands there are usually contractual agreements or grid code requirements that makes mandatory the provision of these services by critical units, like the BESS. The hybrid plant operator is usually compensated with a fixed price for each MWh produced to ensure adequate return of investment. The levels of AS are dictated by the islands dispatch control or automatic generation control and their levels can not be modified by the hybrid plant operator.

The BESS AS, that could be requested for islands operating in high RES penetration levels, can include the Fault Ride Through (FRT) and dynamic voltage support during faults, the reactive power provision and voltage support at normal operating conditions, the FCR and aFRR provision, the grid forming capability, etc. Those services are described for exampled in the greek NII code [18]. However, it is not clear if those services are adequate.

The provision of emulated inertia (or synthetic inertia) by a BESS unit have shown promising performance for low inertia power grids especially during the transient of frequency disturbances and its impact has been studied in non-interconnected islands (NII) too [19]. However, this service is not included in any grid codes yet. Part of this work is focused to discuss the impact of the AS mainly in frequency control and discuss whether it should be considered in future grid codes to enhance NII system security.

At the same time, the economic operation of a small island in those conditions usually incorporates AS by the BESS unit, mainly aFRR and FCR. In addition, it has been shown that the main contribution of storage lies in the provision of fast response reserves that facilitate the integration of increased intermittent RES generation [20]. In such formulations, the necessary levels of upward FCR and aFRR are selected to compensate RES generation variations, *e.g.* by selecting specific factors for each power RES source, *i.e.* solar or wind [20]. The downward reserves are selected to compensate load variations. Usually, in such formulation the diesel generators and BESS reserves are considered identical.

However, given that island's physical inertia may be highly scarce at times when high RES production coincides with low demand, the FCR levels should be selected that specific frequency metrics do not exceed certain security thresholds. In this context, the research community is increasingly focused on implementing various frequency-security constraints in Economic Dispatch (ED) and Unit Commitment (UC). The key challenge lies on the mathematical complexity of incorporating the differential-equation-driven frequency evolution into the algebraic-equation-

This project has received funding from the European Union's Horizon 2020 research and innovation programme under grant agreement No 864337

constrained optimisation problem [21]. To accurately have an estimation of the frequency transients in the ED formulation those works consider in the optimization problem the provision of synchronised and synthetic inertia, the different dynamics of FCR provided by thermal and BESS units [21].

Those works consider the synthetic inertia provided by a BESS unit as a constant amount similar the physical ones. However, during a transient the BESS unit could restrict its synthetic inertia provision if its power output reach its nominal ratings [22]. Therefore the necessary available power of the BESS unit should be guaranteed in order to provide effectively the synthetic inertia in an island system with high RES penetration.

Our work aims to propose a methodology to derive linear rules that can be used in an ED or UC formulation that take into account:

- physical inertia of thermal units
- synthetic inertia by a central BESS unit including also the guarantees that the total amount of its synthetic inertia are available
- the different characteristics of FCR provision by BESS and diesel generators
- correlation with specific frequency related metrics (frequency nadir, ROCOF)

Apart from the frequency security during transient conditions the ED algorithm must consider also constraints for the BESS state of charge, power balance, generator constraints and adequate aFRR for the horizon considered. Thus those constraints and the economic operation of the system is strongly correlated with the uncertainty in RES production and load. Especially in small systems that both the consumers are limited and the RES power plants the forecasts could have significant errors that can lead to insecure control actions from the economic dispatch. Several approaches have been proposed to deal with uncertainty in the FDUC formulation, *e.g.*, interval optimization and stochastic optimization [23] or robust formulation [24]. In this work, a stochastic approach is implemented to address uncertainty in small NII using probabilistic forecasts from the tools developed in the work package 3 of Smart4RES project.

This project has received funding from the European Union's Horizon 2020 research and innovation programme under grant agreement No 864337

3 Overview of the methodology

The methodology employed in this Deliverable is summarized in Figure 11. It gives an overview of the workflow including the contributions of each partner.

The multi-objective optimization framework of the Hybrid RES+BESS system developed by ARMINES integrates the operational constraints and existing dispatch rules of a real hybrid system described by EDP. This framework makes use of trajectories of RES production at multiple time frames, derived by ARMINES. State-of-the-art machine learning technologies are implemented to generate trajectories that can be easily adapted to different problem configurations such as the different time frames required for day-ahead for scheduling/trading, and intraday for control.

The provision of multiple services by storage systems is also applied to the context of isolated power systems and validated on power system data provided by HEDNO, including existing reserve requirements and storage constraints for scheduling in isolated power systems. Based on this data, ICCS designs a battery inverter to provide multiple advanced ancillary services for systems with low inertia. This design is then incorporated into a stochastic economic dispatch (ED) that integrates frequency constraints. The ED uses ensemble forecasts of RES production and load at the level of the isolated power system as an input.

The dashed arrows in the Figure below represent potential perspectives of integration between the different solutions, towards future solutions of higher technological maturity. A first possible future integration is the refinement of the Hybrid system optimization framework with specific constraints on ancillary services in isolated power systems (*e.g.* fast FCR (activation in less than 1 s) and synthetic inertia). A second possible future integration consists in including controllable RES hybrid systems into the ED of an isolated power system.

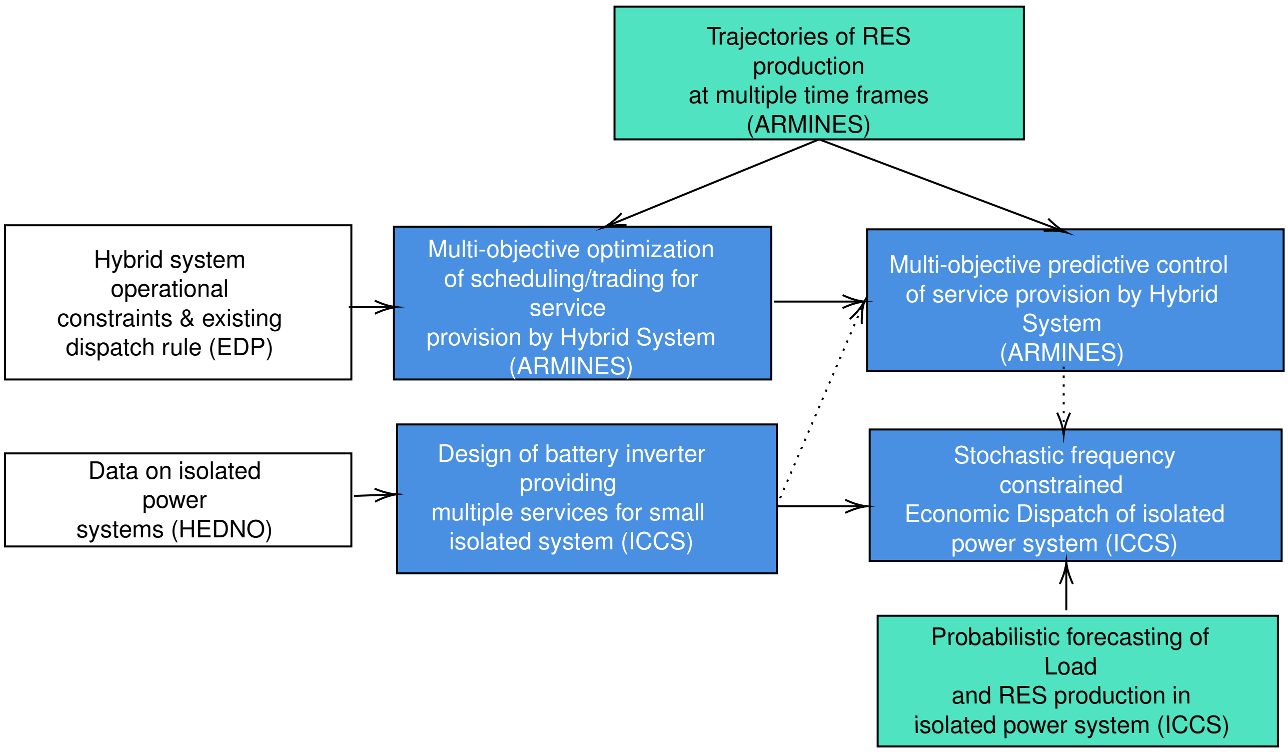

Figure 11: Overview of the methodology including contributing Smart4RES partners

This project has received funding from the European Union's Horizon 2020 research and innovation programme under grant agreement No 864337

4 Optimization method for the provision of multiple services by a renewable hybrid system

This Section presents an optimization method for a renewable hybrid system that provides multiple services. As presented in the Introduction, a renewable hybrid system is a RES plant that integrates an on-site BESS. The multiple services considered in this work are energy production, frequency-control Ancillary Services and the reduction of imbalances between offered market quantities and actual delivery.

The content of this Section is based on the Master Thesis report of Luca Santosuosso for the degree of Master of Science in Control Engineering by Sapienza University of Rome, Italy (academic year 2020/2021). This work has been supervised by S.Camal and G.Kariniotakis from ARMINES / MINES Paris - PSL University. The methodology and case studies have been adapted to the purposes of the present Deliverable. A submission of an article based on this work to an IEEE PES journal or to Applied Energy is scheduled for May 2022.

4.1 Optimization Framework

The proposed method constitutes a complete framework for the joint provision of energy and AS through trading and control of the system. The objectives of the framework are the maximization of revenue and the minimization of the Battery Energy Storage System (BESS) degradation. This framework integrates decisions taken at different stages. To better understand the motivation of the sequences of stages in the framework, consider for the moment that the Hybrid System provides its production to the energy market only. The proposed framework applied to energy only is shown in Fig.12. It consists of three different stages:

1. **Forecast Stage**, a preliminary step which consists in computing forecasts for all the uncertain variables of the problem. These variables comprise RES production, and market quantities *e.g.* prices on the day-ahead and balancing energy market. Here for the sake of simplicity only RES forecasting is employed. Market quantities are assumed to be known. Please refer to Appendix 1 for a description of the forecasting methodology and obtained results. The RES production forecast consists of a set of Ω trajectories $(\hat{y}_{\omega,t}, \quad \forall(\omega, t) \in \{\Omega \times T\})$ reproducing the temporal correlation in the RES production signal over an optimization period T.

2. **Day-Ahead (DA) Trading Stage**, which consists in computing, on the basis of the DA forecasts, the energy offer $\mathbf{E}^{off,DA}$ on the DA market, in addition to the expected upward/downward deviations $\mathbf{E}^{up,DA}$, $\mathbf{E}^{down,DA}$ from this offer and the expected scheduled SOC for the battery $\mathbf{x}^{DA}$ obtained as a consequence of the trading and BESS charging decisions computed at DA stage. The trading optimization is performed via two model variants: a deterministic model (*i.e.* $\hat{y}$ is a single average trajectory) and a stochastic model where decision variables are derived based on the expectation of the uncertain realization of production $\mathbb{E}_\omega\{.\}$. Non-anticipativity is ensured so that the day-ahead offer is independent from the uncertainty realizations that occur after the offer has been decided: $\mathbb{E}_\omega\{\mathbf{E}^{off,DA}\} = \mathbf{E}^{off,DA}$.

3. **Short-Term (ST) Control Stage**, which consists in computing the actual set of control actions to be implemented on the basis of the intraday forecasts (updated forecasts for short-term horizons *i.e.* next hours) and of the DA energy offer. Different MPC strategies are implemented and analyzed. The general control strategy aims to minimize the devia-

This project has received funding from the European Union's Horizon 2020 research and innovation programme under grant agreement No 864337

tions from the DA energy offer because, as discussed in Section 1.2.1, an optimal trading strategy for energy should minimize on average the volume of deviations. As output from the MPC controller, the operator will receive a charging/discharging setpoint for the BESS $\mathbf{p}^{b,d,ST}$. The MPC also returns the actual expected energy delivery $\mathbf{E}^{del,ST}$. This is not the exact delivery that will be observed in real time, because the result of the MPC still relies on a RES production forecast. The actual real time delivery will be a consequence of the actual RES production instead.

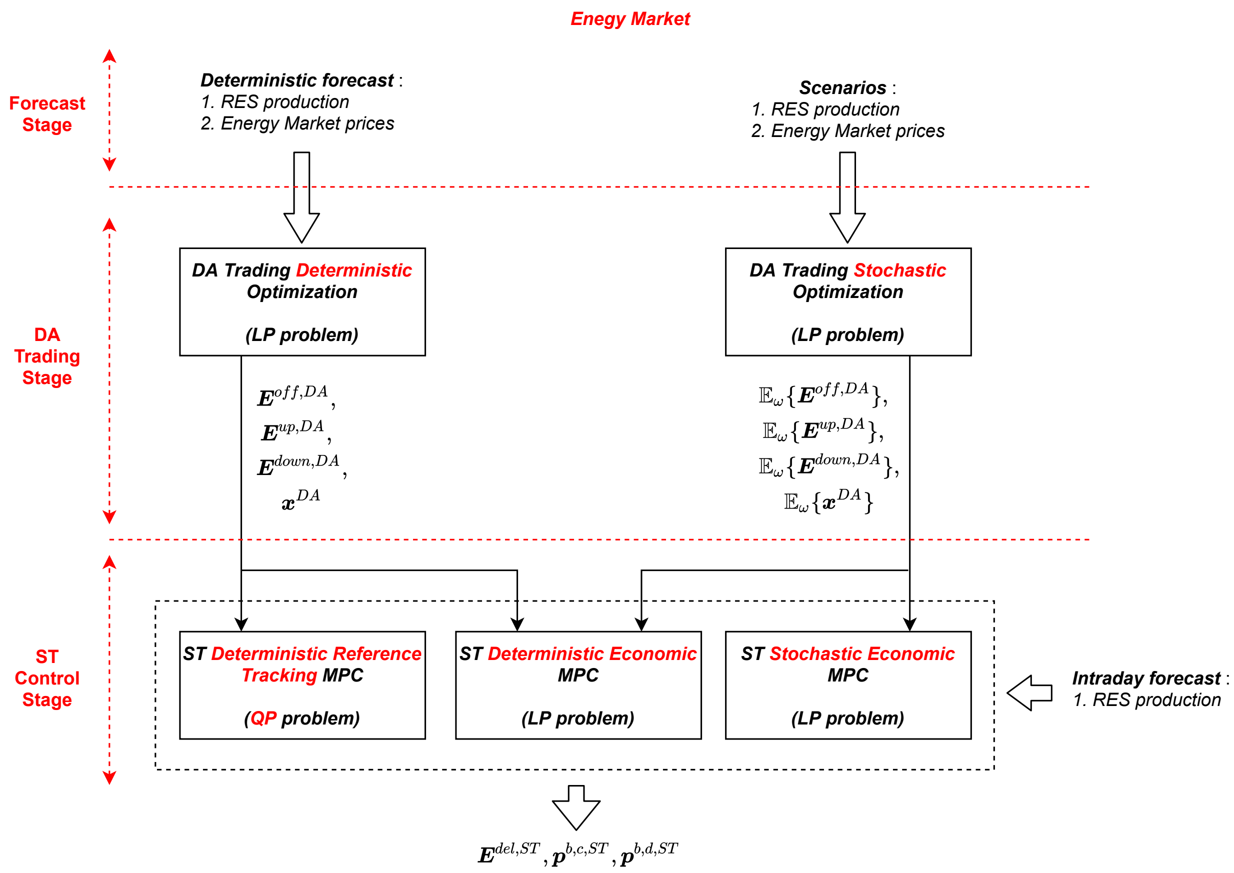

Figure 12: Framework general scheme for energy market only.

We now motivate the introduction of *deviations* from the energy offer E_t^{off} in the problem. Neglect the presence of the BESS and consider only the energy market, then the *balancing constraint* of the system assumes the form:

$$E_t^{off} - E_t^{up} + E_t^{down} = y_t, \quad \forall t \in T, \tag{3}$$

meaning that the RES production y_t should equal, at every t, the energy offer E_t^{off} plus the deviations from this offer (E_t^{up} and E_t^{down}). As a consequence of this formulation, when the production is higher than the energy offer, it will be observed a downward deviation. Conversely, when the energy production is lower that the offer, it will be observed an upward deviation. These deviations are modelled as variables because they can be directly affected by their corresponding imbalance penalty prices in the optimization problem.

The complete framework follows the structure presented above, extended by the provision of ancillary services. Fig.13 shows the structure of the framework when offering energy + reserve, where new terms associated to the reserve provision are highlighted in green. Reserve can be

This project has received funding from the European Union's Horizon 2020 research and innovation programme under grant agreement No 864337

a single reserve product, *e.g.* FCR or aFRR, or a combination of both. Here the DA optimization and ST control problems are modified in order to take into account also reserve provision offered on the DA market and the deviations from this reserve, called *deficit*. In particular, the reserve offer on the DA market is given by the vector $\mathbf{R}^{off,DA}$, the deficit of the reserve at DA is given by $\delta^{R,DA}$, while the actual reserve delivery after the computation of the ST control actions to be implemented, is given by the vector $\mathbf{R}^{del,ST}$. In this framework the reserve delivery is not optimized at ST stage and it is assumed to follow, at ST, the exact reserve delivery computed at DA. More on this will be explained in the following sections. Adding reserve to the problem requires additional inputs, namely reserve prices and short-term activation signals triggered by the TSO to activate the frequency-control AS as a function of the balancing needs of the network. The activation signals depend on the observed frequency for FCR and on a designed setpoint for aFRR.

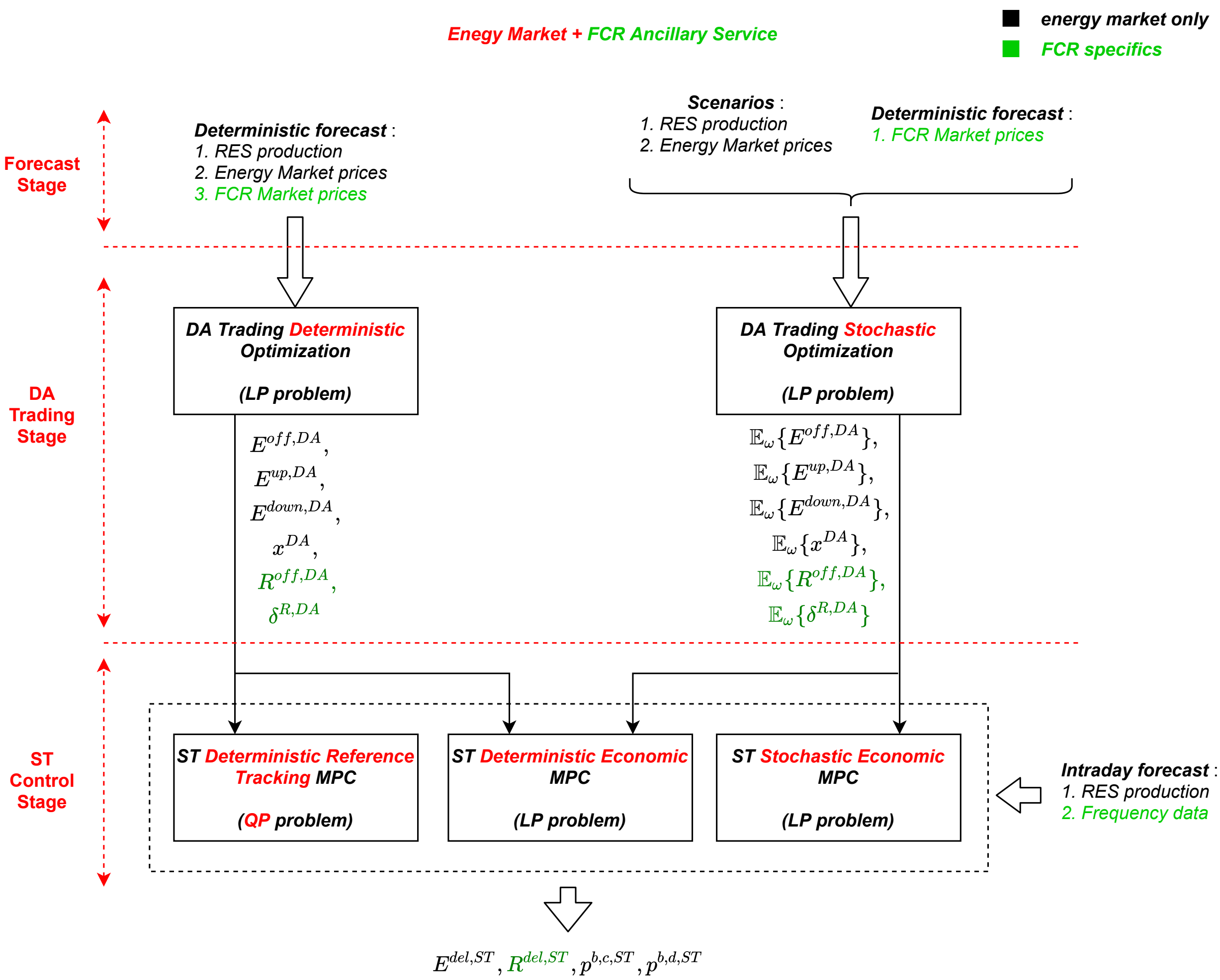

Figure 13: Framework general scheme for energy market + ancillary service.

4.2 Battery Energy Storage System (BESS)

Battery degradation is a complex physico-chemical process which depends significantly on the technology of the the battery (cathode, anode, electrolyte, a.o.) and on the operating conditions, mainly State of Charge (SoC), Depth of Discharge (DOD), Charge/Discharge currents, cell temperature, a.o. An option for the degradation model is to implement a mechanical-chemical

This project has received funding from the European Union's Horizon 2020 research and innovation programme under grant agreement No 864337

degradation model, for example by following the approaches presented in [25], but these require accurate information on the cell physical properties and corresponding data. To simplify the degradation model, in this work it is proposed a model at the macro-level of a complete battery rack which quantifies the decrease in the energy capacity of the battery. The following assumptions hold:

1. The fast degradation observed in the Beginning of Life (BoL) of Li-ion battery due to the formation of the Solid Electrolyte Interphase is neglected. This is justified in this subject because it is an operational problem and not a planning problem where a new battery has to be installed.
2. At End of Life (EoL) other factors increase the degradation rate. Again, as the present subject is operational it is assumed that the battery remains usable at the end of the optimization period, and therefore the terminal phase of degradation can be neglected.

These assumptions enable to justify a linear degradation of the battery capacity dependent on cycling and on the time in operation for calendar ageing tests. The former degradation phenomenon is shown in Fig.14, where the y-axis represents the State of Health, here defined as the operational cell capacity normalized by the initial cell capacity, and called below *capacity retention*. The latter ageing factor is presented in Fig.15, where y-axis represents the *capacity retention*. Thus, in this work, the degradation of the BESS is understood as the reduction of capacity retention. As shown in both figures, the capacity retention of the storage system decreases with the cycling and calendar ageing factors. In particular:

- **Cycling ageing** is associated to the number of charging/discharging cycles of the storage system. The higher the number of cycles the higher the degradation.
- **Calendar ageing** is associated to the time at which the storage systems is kept at certain levels of SoC. The longer the BESS is kept at high levels of SoC, the higher the degradation.

To be fair it should be mentioned another important source of degradation, due to the temperature of the BESS. However, large storage systems like those considered in this work are typically installed in special containers with a dedicated cooling system. Thus they can be assumed to work at a constant favorable temperature, in such a way that temperature ageing becomes negligible.

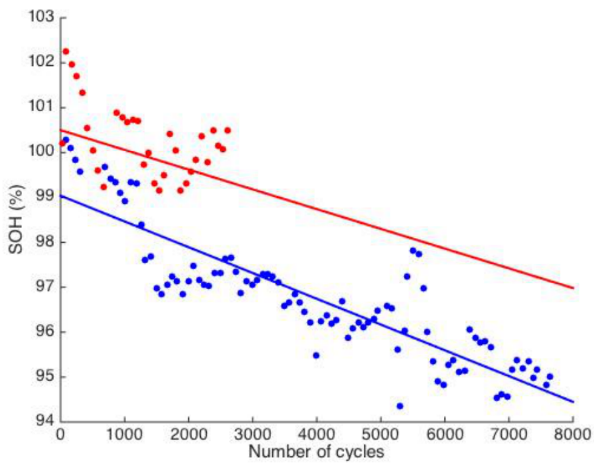

Figure 14: Cycling ageing test in laboratory for a Lithium-Ion battery at 1.5C (red) and 4C (blue) [26].

This project has received funding from the European Union's Horizon 2020 research and innovation programme under grant agreement No 864337

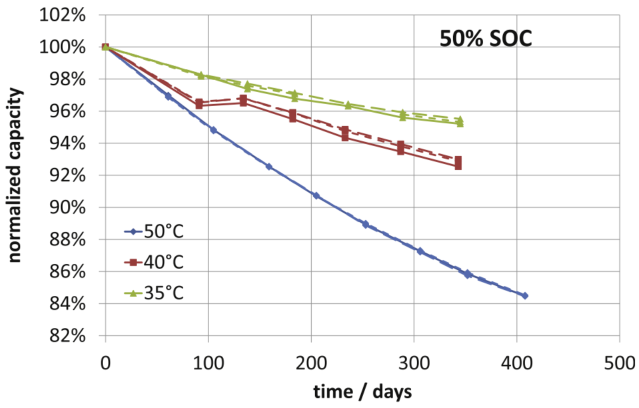

Figure 15: Calendar ageing test in laboratory for a Lithium-Ion battery kept at constant SoC [27].

Further specific assumptions will be presented in the case study to accommodate with the existing data sets. Using linear functions neglects the non-linear relation between the maximum Number of Cycles (NoC) and the DoD. It is clear that such a model approximates significantly the behaviour of the degradation process. However, it has the advantage of simplifying the integration of degradation into the optimization problem compared to a piece-wise approximation of the NoC-DoD curve, which requires the use of multiple binary variables to detect charging/discharging cycles and corresponding DoD intervals.
As a consequence of the previous reasoning, it is possible to formulate two different models to take into account cycling and calendar ageing, a simplified one and a complete one. Moreover, it could be possible that the operator is interested in explicitly keeping the battery at a desired reference value, maybe for control purposes. Thus, a total of 3 different models for the storage degradation have been implemented and tested in this work:

- A **Simplified Cycling** (SC) degradation model, to explicitly take into account cycling degradation, which is usually the main source of degradation.
- A **Cycling + Calendar with Threshold** (CCT) degradation model, to explicitly account for cycling and calendar ageing.
- A **Reference State** (RS) model, to impose a desired reference state to the BESS.

Call x_t the energy stored inside the BESS at time t, then the SC degradation model can be formulated as:

$$\frac{1}{T}\sum_{t\in T}\pi^B \cdot |x_t - x_{t-1}| \tag{4}$$

Where T is the time interval of interest for the degradation and π^B is the cost associated to one complete cycle of BESS charge/discharge. This model is able to capture the cycling effect, by considering the absolute difference in the BESS state at time t and $t-1$, but it completely neglects the calendar ageing. Thus it may happen that the storage system is kept, for long periods of time, at very high or very low values of SoC. This will impact badly on the storage health.
To solve the limitations of the SC degradation model, a slightly more complex model is pro-

This project has received funding from the European Union's Horizon 2020 research and innovation programme under grant agreement No 864337

posed. This is the CCT degradation model:

$$\begin{cases} \frac{1}{T}\sum_{t\in T}\pi^B\cdot(w_1\cdot x_t + w_2\cdot|x_t - x_{t-1}|) & \text{if } x_t \geq x^{thr,max} \\ \frac{1}{T}\sum_{t\in T}\pi^B\cdot w_2\cdot|x_t - x_{t-1}| & \text{else} \end{cases} \tag{5}$$

$$\text{with} \quad x_t \geq x^{min} \tag{6}$$

Where T and π^B have the same meaning of that of the previous model, while w_1 and w_2 are weights used to take into account the different contribution in degradation of the cycling and calendar effects, $x^{thr,max}$ is the maximum BESS threshold state and x^{min} is the minimum BESS admissible state.
A graphical explanation of the CCT degradation model is provided in Fig.16. The figure shows the 3 different zones in which the possible set of states of the BESS is divided:

- *Desired zone*: this is the zone in between x^{min} and $x^{thr,max}$. In this zone the CCT model behaves as the SC one, thus here only cycling ageing is take into account, while calendar degradation is neglected.
- *Calendar degradation zone*: the battery state is allowed to enter this zone, even reaching the maximum SoC, but the model will also take into account, in addition to cycling degradation, calendar degradation.
- *Danger zone*: this zone is forbidden, in the sense that x_t can not reach state values below x^{min}, since this will damage the storage system. Thus, this must be implemented as a hard constraint in the model.

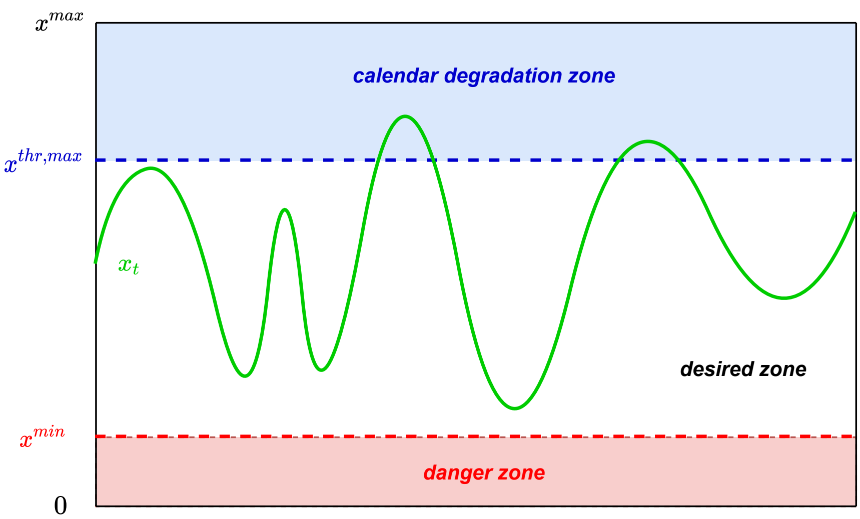

Figure 16: Graphical description of the CCT degradation model at eq.(5).

To complete the set of possible situations, there is only one case when the model gives a null degradation for BESS. This is the case when the storage system state is not used and it is kept outside the calendar degradation zone:

$$\begin{cases} x_t - x_{t-1} = 0 \\ x^{min} \leq x_t < x^{thr,max} \end{cases} \tag{7}$$

The last degradation model presented in his work is the RS model. This can be described by the following equation:

$$\frac{w_{ref}}{T}\sum_{t\in T}|x_t^{ref} - x_t| \tag{8}$$

Where x_t^{ref} is the desired state at time t and w_{ref} is a weight that can be used to modulate the importance that the operator wants to give to following the desired state. The strategy behind this model is completely different from that of the SC and CCT degradation models. In this case cycling and calendar ageing are not taken into account, unless the BESS resides in a state that is has been identified as optimal, *i.e.* for which the BESS has minimum degradation. On one hand, identifying this optimal state is highly unlikely to be possible in real cases. On the other hand, the advantages of using this kind of degradation model for control purposes are clear. Indeed the BESS is usually used to control the energy delivery of a plant, *i.e.* it can be charged when the system faces an energy surplus or discharged when the system faces a lack of energy. Thus it is a common practice in control algorithms to keep the battery at roughly half of its charge, in order to maximize the control degree on the system.
Unfortunately this strategy doesn't account for cycling nor calendar degradation of the BESS, thus one should choose which approach is more suited for a given problem. Since this work aims to be as much as possible economic-oriented in order to take into account the main concerns of the industry world, the CCT model will be particularly focused in the simulations presented in the next chapter. Indeed this is the only one, among the 3 models presented, which explicitly takes into account the economic cost of BESS degradation.

4.3 Day-Ahead Trading Optimization

The next sections present different *multi-objective optimization problems* to optimize trading on the energy and Ancillary Services markets, while minimizing the degradation of the storage system. The main objective of this optimization framework is to propose an approach that is scalable to a different number of provided services, and is robust in terms of mitigation of the uncertainty's impact on costs and quality of service provision. The scalability is addressed by presenting an incremental modelling complexity, starting with the provision of energy only, before providing energy and Ancillary Services. A stochastic formulation is proposed to ensure the robustness, which is evaluated by comparison with a deterministic version of the problem.

4.4 Modelling Assumptions

The following assumptions hold for the optimization of trading and control:

1. The uncertain RES production is modelled by state-of-the art trajectories reproducing realistically the temporal correlations in the RES production signal. The forecast $\hat{y}$ is derived at day-ahead horizon for trading and at short-term horizon (up to a few hours ahead) for control.
2. Dual-price imbalance on the energy market.
3. Reserve deficits δ are potential deviations of the reserve capacity offer, as illustrated in Figure 17. These deviations are reductions in the reserve capacity that are highly penalized in the reserve market.The excess of reserve at the balancing stage, *i.e.* disposing of more reserve than offered at day-ahead, is not penalized because it is not detrimental to the power system.
4. FCR provision is symmetrical (equal capacity for upward and downward reserve) while aFRR provision is asymmetrical.
5. No uncertainty on prices.

6. No curtailment of the RES production to minimize positive imbalances on the energy market, *i.e.* RES production is curtailed only in cases of downward reserve provision or partial upward reserve provision, and to the extent that it is optimal to curtail RES rather than charge the storage. This corresponds to the operational policy of hybrid systems such as the one considered in the case study. Note that a decision variable modelling RES curtailment for the minimization of positive imbalances can be added to the methodology as a further decision variable without major impact on the model structure.

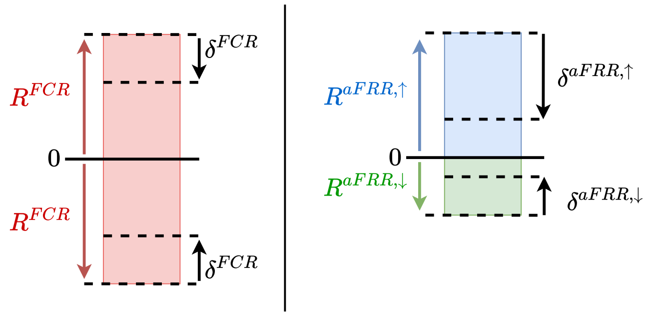

Figure 17: Different models for FCR and aFRR offers and deficits. On the left side, the FCR offer (in red) is symmetric as well as the upward and downward deficits (δ^{FCR}). On the right side, the aFRR upward and downward offers are in general different ($R^{aFRR,\uparrow} \neq R^{aFRR,\downarrow}$), as well as their deficits ($\delta^{aFRR,\uparrow} \neq \delta^{aFRR,\downarrow}$).

The optimization problems presented compute the optimal offer of energy and other potential services on the entire trading horizon $t \in T$. This offer can be made exclusively on the energy market, when considering the *Provision of Energy* use case, or on both energy and Ancillary Services markets (FCR, aFRR), under the *Provision of Energy and Ancillary Services* use case. The offer depends on the storage capacity, the market prices and the RES production forecast.

The section below presents the stochastic optimization model proposed to solve the trading problem.

4.4.1 Stochastic optimization

The stochastic optimization relies on a discretization of the uncertainty by means of a set Ω of scenarios. For each one of these scenarios $\omega \in \Omega$ a RES production forecast trajectory $\hat{y}_{\omega,t}$ is available. The optimization problems presented in this section are solved over the whole trading horizon T, for each scenario $\omega \in \Omega$. In the end, the size of these problems will be $|T| \times |\Omega|$.

A graphical representation of this multi-scenario problem is given in Fig.18. The Trading problem is formulated as a two-stage problem for which a set of scenarios Ω is available and each of those scenarios is associated to a particular trajectory for the uncertainty. Call z^{fs} the *first stage* decisions of the problem then, depending on the realization of the uncertainty, different *second stage variables* decisions ($z^{ss}(\omega = 1, t = T)$, $z^{ss}(\omega = 2, t = T)$, ...) will be computed in each scenario ω. First-stage decisions are offers on the markets of interest (energy only or energy + Ancillary Services) and second-stage decisions are charging/discharging setpoints for the BESS and resulting deviations between offer and delivery of the hybrid system at the balancing stage.

This project has received funding from the European Union's Horizon 2020 research and innovation programme under grant agreement No 864337

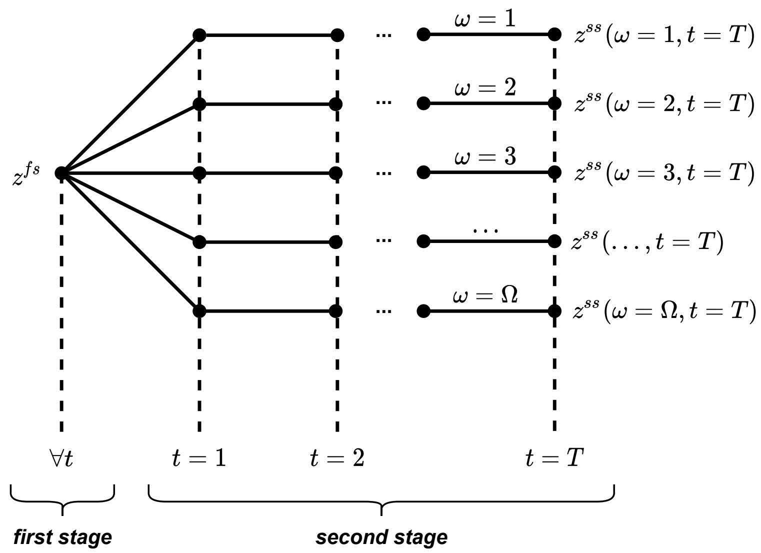

Figure 18: Graphical representation of a two-stage stochastic optimization

4.4.2 Provision of Energy

In this part, the Hybrid RES plant + BESS system trades only on the energy market. The decisions taken at the DA stage are defined by the column decision vector

$$\mathbf{d^{DA}_{\omega,t}} = \text{col}(\mathbf{E^{DA}_{\omega,t}}, \mathbf{P^{DA}_{\omega,t}}) \quad \forall \omega, t \tag{9}$$

in which the partitions

$$\begin{aligned} \mathbf{E^{DA}_{\omega,t}} &= \text{col}(E^{off,DA}_{t}, E^{\uparrow,DA}_{\omega,t}, E^{\downarrow,DA}_{\omega,t}) \quad \forall \omega, t \\ \mathbf{P^{DA}_{\omega,t}} &= \text{col}(p^{b,c,DA}_{\omega,t}, p^{b,d,DA}_{\omega,t}) \quad \forall \omega, t \end{aligned} \tag{10}$$

represent respectively the decisions on the energy market (offer and imbalances), and the charging and discharging decisions for the energy storage at time t for scenario ω.

The parameters of this study are the price vector $\boldsymbol{\pi}^{\mathbf{E}}_{\mathbf{t}}$ which represents, in compact form, the prices for the day-ahead contracted energy volume, upward and downward deviations in the energy balancing market respectively, and the BESS efficiency vector $\boldsymbol{\eta}$.

$$\boldsymbol{\pi}_{\mathbf{E,t}} = \text{col}(-\pi_{E,t}, \pi_{E^{\uparrow},t}, -\pi_{E^{\downarrow},t}) \quad \forall t \tag{11}$$

$$\boldsymbol{\eta} = \text{col}(\eta_c, -1/\eta_d). \tag{12}$$

Then, the problem of computing the optimal offer on the energy market, given the technical constraints of the system and the RES production forecast, can be formulated as a *multi-objective mixed-integer non-linear programming* problem expressed right below. The non-linearity comes from the absolute value integrated into the estimation of the variation of the BESS state. The absolute value is linearized by the integration of auxiliary variables modelling the negative and positive component of $x_t - x_{t-1}$.

The different objectives are the expected cost from Energy Trading (ET) $\mathbb{E}_{\Omega,T}[ET]$ and the expected cost of the BESS Degradation (BD) $\mathbb{E}_{\Omega,T}[BD]$, weighted by w_M and w_B respectively:

This project has received funding from the European Union's Horizon 2020 research and innovation programme under grant agreement No 864337

$$\mathbb{E}_{\Omega,T}[\text{ET}] = \frac{1}{\Omega}\frac{1}{T}\sum_{\omega\in\Omega}\sum_{t\in T}\boldsymbol{\pi}_{\mathbf{E,t}}{}^{T}\mathbf{E}^{\mathbf{DA}}_{\boldsymbol{\omega},\mathbf{t}} \tag{13}$$

$$\mathbb{E}_{\Omega,T}[\text{BD}] = \frac{\pi^{B}}{\Omega\cdot T}\sum_{\omega\in\Omega}\sum_{t\in T}\begin{cases} cl_{\omega,t}+cy_{\omega,t}, & \text{if } x_{\omega,t}\geq x^{thr,max} \\ cy_{\omega,t}, & \text{else} \end{cases}. \tag{14}$$

where the *calendar ageing factor* $cl_{\omega,t}$ and the *cycling ageing factor* $cy_{\omega,t}$ are:

$$cl_{\omega,t} = w_1\cdot x_{\omega,t}, \tag{15}$$

$$cy_{\omega,t} = w_2\cdot |x_{\omega,t}-x_{\omega,t-1}| \tag{16}$$

The resulting *multi-objective mixed-integer linear programming* problem writes as follows:

$$\underset{\mathbf{d}^{\mathbf{DA}}_{\boldsymbol{\omega},\mathbf{t}}}{\arg\min} \quad w_M\mathbb{E}_{\Omega,T}[ET]+w_B\mathbb{E}_{\Omega,T}[BD] \tag{17}$$

subject to:

$$\begin{pmatrix}+1\\-1\\+1\end{pmatrix}^{T}\mathbf{E}^{\mathbf{DA}}_{\boldsymbol{\omega},\mathbf{t}}+\Delta t\begin{pmatrix}+1\\-1\end{pmatrix}^{T}\mathbf{P}^{\mathbf{DA}}_{\boldsymbol{\omega},\mathbf{t}} = \hat{y}^{DA}_{\omega,t}, \tag{18a}$$

$$x^{DA}_{\omega,t+1} = x^{DA}_{\omega,t}+\Delta t\cdot\boldsymbol{\eta}^{T}\mathbf{P}^{\mathbf{DA}}_{\boldsymbol{\omega},\mathbf{t}}, \tag{18b}$$

$$x^{DA}_{\omega,0} = x^{DA}_{\omega,T} \tag{18c}$$

$$x^{min}\leq x^{DA}_{\omega,t}\leq x^{max}, \tag{18d}$$

$$0\leq\Delta t\cdot p^{b,c,DA}_{\omega,t}\leq x^{max}\cdot b^{c}_{\omega,t}, \tag{18e}$$

$$0\leq\Delta t\cdot p^{b,d,DA}_{\omega,t}\leq x^{max}\cdot b^{d}_{\omega,t}, \tag{18f}$$

$$b^{c}_{\omega,t}+b^{d}_{\omega,t}\leq 1, \tag{18g}$$

$$0\leq E^{off,DA}_{t}\leq y^{max}+x^{max}, \tag{18h}$$

$$E^{\uparrow,DA}_{\omega,t}\geq 0,\ E^{\downarrow,DA}_{\omega,t}\geq 0,\ p^{b,c,DA}_{\omega,t}\geq 0,\ p^{b,d,DA}_{\omega,t}\geq 0, \tag{18i}$$

$$b^{c}_{\omega,t}\in\{0,1\},\ b^{d}_{\omega,t}\in\{0,1\}, \tag{18j}$$

for $\omega\in\{1,2,...,\Omega\}$ and $t\in\{1,2,...,T\}$.

The problem is solved by considering a *discrete* hybrid system, every Δt in a *trading horizon* T and for each *scenario* ω in the set of possible scenarios Ω. Moreover:

- η_c is the charge efficiency of the storage system.

This project has received funding from the European Union's Horizon 2020
research and innovation programme under grant agreement No 864337

- η_d is the discharge efficiency of the storage system.

with $\eta_c \neq \eta_d$ in general.
It is important to notice that the energy offer $E_t^{off,DA}$ is not scenario dependent. Thus this is the *first stage* decision of the problem, that must be computed before the realization of the uncertainty.
The constraints pertain to three different groups:

- *Hybrid RES plant coupled with BESS balancing constraints* (18a), to enforce the balance of the system by stating that the sum of energy offer plus its deviations and reserve offers plus their deficits should equal the energy production plus the energy charge/discharged to/from the BESS.
- *BESS technical constraints* (18b)-(18d), to enforce the discrete time evolution of the storage system, its initial state and the upward and downward limits of the BESS state x_t.
- *Power technical constraints* (18e)-(18g), to enforce that the power charged/discharged to/from the BESS, in Δ_T, can be at most equal to its total capacity. To guarantee that no simultaneous charging and discharging of the BESS happens, the binary variables $b^c_{\omega,t}$ and $b^d_{\omega,t}$ are used.
- *Market coherency constraints* (18h)-(18j), to enforce the market rule that imposes to offer a total amount of energy at most equal to the total capacity of the hybrid system ($y^{max} + x^{max}$).

Weights w_M and w_B give more importance to the revenue achieved on the energy market or to the degradation of the BESS. As a consequence of this, in order to have a coherent implementation of the problem, the following constraint must be enforced:

$$w_M + w_B = 1 \tag{19}$$

4.4.3 Provision of Energy and Ancillary Services

In this use case the system provides simultaneously energy and Ancillary Services. We present here the full formulation when FCR and aFRR are provided. The formulation for energy + FCR is a simplified version of the problem presented in this section. The previous optimization problem ((18)) is extended by adding decision vectors for reserve provision. The decision vector now writes:

$$\mathbf{d^{DA}_{\omega,t}} = \text{col}(\mathbf{E^{DA}_{\omega,t}}, \mathbf{FCR^{DA}_{\omega,t}}, \mathbf{aFRR^{DA}_{\omega,t}}, \mathbf{P^{DA}_{\omega,t}}). \tag{20}$$

in which the partitions

$$\begin{aligned} \mathbf{FCR^{DA}_{\omega,t}} &= \text{col}(\delta^{FCR,DA}_{\omega,t}, R^{FCR,DA}_t) \\ \mathbf{aFRR^{DA}_{\omega,t}} &= \text{col}(\delta^{aFRR,\uparrow,DA}_{\omega,t}, \delta^{aFRR,\downarrow,DA}_{\omega,t}, R^{aFRR,\uparrow,DA}_t, R^{aFRR,\downarrow,DA}_t) \end{aligned} \tag{21}$$

named FCR and aFRR represent the FCR and aFRR reserves and deficits, respectively. The offer of FCR is symmetrical and aFRR is asymmetrical.

Additional price vectors are introduced below to denote prices for reserve provision and penalty in case of deficit in reserve provision.

$$\begin{aligned} \boldsymbol{\pi}_{\mathbf{FCR,t}} &= \text{col}(\pi_{\delta,FCR,t}, -\pi_{FCR,t}) \\ \boldsymbol{\pi}_{\mathbf{aFRR,t}} &= \text{col}(\pi_{\delta,aFRR\uparrow,t}, \pi_{\delta,aFRR\downarrow,t}, -r_{aFRR\uparrow,t}, -r_{aFRR\downarrow,t}) \end{aligned} \tag{22}$$

This project has received funding from the European Union's Horizon 2020 research and innovation programme under grant agreement No 864337

While FCR is a capacity-only reserve market, the aFRR market procures both reserve capacity and balancing energy, with distinct prices for upward and downward directions ($\pi_{aFRR,bal,\uparrow}$, $\pi_{aFRR,bal,\downarrow}$). Then, the upward and downward aFRR offer revenues are given by the sum of revenues for reserve capacity and for the delivery of balancing energy. The amount of balancing energy depends on the estimated activation signal $\hat{\alpha}$. The activation signal corresponds to the share of the reserve capacity offered by the hybrid system that is effectively activated by the TSO. In the case of FCR, the activation signal follows a droop control proportional to the observed grid frequency. The activation signal of aFRR consists of a non-linear setpoint sent by the TSO [28].

Thus, the upward aFRR offer reward is defined as:

$$r_{aFRR\uparrow,t} = \pi_{aFRR\uparrow,t} + \hat{\alpha}_{aFRR\uparrow,t} \cdot \pi_{aFRR,bal\uparrow,t}, \tag{23}$$

and, similarly, the downward aFRR offer reward is defined as:

$$r_{aFRR\downarrow,t} = \pi_{aFRR\downarrow,t} + \hat{\alpha}_{aFRR\downarrow,t} \cdot \pi_{aFRR,bal\downarrow,t}, . \tag{24}$$

Finally, the activation signal is applied to the offers and deficits associated to FCR and aFRR:

$$\begin{aligned} \hat{\boldsymbol{\alpha}}_{\mathbf{FCR,t}} &= \text{col}(-\hat{\alpha}_{FCR,t}, \hat{\alpha}_{FCR,t}) \\ \hat{\boldsymbol{\alpha}}_{\mathbf{aFRR,t}} &= \text{col}(-\hat{\alpha}_{aFRR,\uparrow,t}, \hat{\alpha}_{aFRR,\downarrow,t}, \hat{\alpha}_{aFRR,\uparrow,t}, -\hat{\alpha}_{aFRR\downarrow,t}) \end{aligned} \tag{25}$$

The multi-objective optimization problem now becomes:

$$\underset{\mathbf{d^{DA}_{\omega,t}}}{\arg\min} \quad w_M\{\mathbb{E}_{\Omega,T}[ET] + \mathbb{E}_{\Omega,T}[AST]\} + w_B\mathbb{E}_{\Omega,T}[BD] \tag{26}$$

where the costs associated to Ancillary Service Trading (AST) write:

$$\mathbb{E}_{\Omega,T}[\text{AST}] = \frac{1}{\Omega}\frac{1}{T}\sum_{\omega=1}^{\Omega}\sum_{t=0}^{T-1}[\boldsymbol{\pi}_{\mathbf{FCR,t}}{}^T\text{FCR}^{\mathbf{DA}}_{\boldsymbol{\omega},\mathbf{t}} + \boldsymbol{\pi}_{\mathbf{aFRR,t}}{}^T\mathbf{aFRR}^{\mathbf{DA}}_{\boldsymbol{\omega},\mathbf{t}}] \tag{27}$$

subject to the following constraints:

$$\begin{pmatrix} +1 \\ -1 \\ +1 \end{pmatrix}^T \mathbf{E}^{\mathbf{DA}}_{\boldsymbol{\omega},\mathbf{t}} + \hat{\boldsymbol{\alpha}}_{\mathbf{FCR,t}}{}^T\text{FCR}^{\mathbf{DA}}_{\boldsymbol{\omega},\mathbf{t}} + \hat{\boldsymbol{\alpha}}_{\mathbf{aFRR,t}}{}^T\text{aFRR}^{\mathbf{DA}}_{\boldsymbol{\omega},\mathbf{t}} + \Delta t \begin{pmatrix} +1 \\ -1 \end{pmatrix}^T \mathbf{P}^{\mathbf{DA}}_{\boldsymbol{\omega},\mathbf{t}} = \hat{y}^{DA}_{\omega,t}, \tag{28a}$$

BESS technical constraints (18b)-(18d),

Power technical constraints (18e)-(18g),

$$E^{off,DA}_t + R^{FCR,DA}_t + R^{aFRR,\uparrow,DA}_t - R^{aFRR,\downarrow,DA}_t \leq y^{max} + x^{max}, \tag{28b}$$

$$0 \leq E^{off,DA}_t \leq y^{max} + x^{max}, \tag{28c}$$

$$0 \leq R^{FCR,DA}_t \leq y^{max} + x^{max}, \tag{28d}$$

$$0 \leq R^{aFRR,\uparrow,DA}_t \leq y^{max} + x^{max}, \tag{28e}$$

$$0 \leq R^{aFRR,\downarrow,DA}_t \leq y^{max} + x^{max}, \tag{28f}$$

$$\begin{aligned} &E^{\uparrow,DA}_{\omega,t} \geq 0,\ E^{\downarrow,DA}_{\omega,t} \geq 0,\ \delta^{FCR,DA}_{\omega,t} \geq 0, \\ &\delta^{aFRR,\uparrow,DA}_{\omega,t} \geq 0,\ \delta^{aFRR,\downarrow,DA}_{\omega,t} \geq 0,\ p^{b,c,DA}_{\omega,t} \geq 0, \end{aligned} \tag{28g}$$

This project has received funding from the European Union's Horizon 2020 research and innovation programme under grant agreement No 864337

for $\omega \in \{1, 2, ..., \Omega\}$ and $t \in \{1, 2, ..., T\}$.

The principles of the balancing constraint (28b) are explained in Fig. 19, where a generic reserve variable R replaces FCR and aFRR for the sake of simplicity. The red line in the figure is the total offer on the energy+reserve market, while the blue dotted line is the total amount of energy available (RES production + energy charged/discharged to/from the BESS). When these 2 curves do not match, it means that deviations are present. While in the previous case it was possible to observe only deviations from the energy offer ($E_t^{\uparrow,DA}$ and $E_t^{\downarrow,DA}$), in this case also deviations from the AS offer are present ($\delta_t^{R,DA}$). For the energy offer it is possible to deviate in two different directions (upward and downward) and different prices are associated to different deviation directions. On the other hand it makes sense to consider only scarcity of reserve or upward deviation ($\delta_t^{R,DA}$), called *deficit*. A surplus of reserve is not detrimental to the system and therefore are neither rewarded nor penalized.

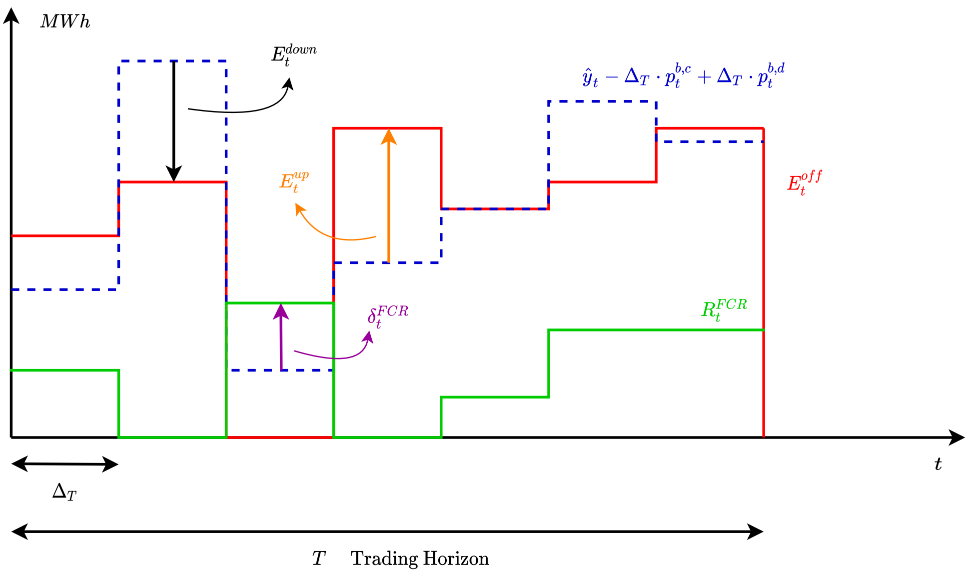

Figure 19: Graphical description of the balancing constraint (28b) of the Hybrid RES plant + BESS system.

This section ends with a note on the estimation of the AS activation signal. A day-ahead estimation of the activation signal could consist in a prediction of the AS activation signal, based on explanatory variables related to AS market volumes and position of the offer of the Hybrid System (HS) among all AS capacity offers. Some works that predict the imbalance volume on the energy market have been proposed *e.g.* [29]. However the day-ahead prediction of the activated volume of an AS such as aFRR or the variations of grid frequency is very challenging and is not the focus of the present Deliverable. Instead, the estimated activation corresponds to the average activation over a rolling past period T_{activ} representative of recent balancing market conditions, *i.e.* in the order of several days. Due to the symmetrical nature of FCR, the average activation signal over a market trading interval (*e.g.* 15 min to 1h) is mostly zero. For aFRR, we assume that the HS is activated as an average reserve supplier in the aFRR market, due to a *pro rata* aFRR activation or a central position in the offering curve of aFRR market. The actual values of the estimated activation are presented in the Case Study in Section 5.

This project has received funding from the European Union's Horizon 2020 research and innovation programme under grant agreement No 864337

$$\hat{\alpha}_{FCR,t} = \mathbb{E}_{t\in T_{\text{activ}}}[\alpha_{FCR,t}] \tag{29}$$
$$\hat{\alpha}_{aFRR,\uparrow,t} = \mathbb{E}_{t\in T_{\text{activ}}}[\alpha_{aFRR,\uparrow,t}] \tag{30}$$
$$\hat{\alpha}_{aFRR,\downarrow,t} = \mathbb{E}_{t\in T_{\text{activ}}}[\alpha_{aFRR,\downarrow,t}] \tag{31}$$

4.5 Short-Term Control

Once the day-ahead offer is made, it is still possible to optimize in the short-term (ST) horizon and this is done in the ST stage of the proposed framework. See Fig.12 for the case of energy only and Fig.13 for the case of energy + AS. This means that, given a DA offer that cannot be modified at this stage, it is still possible to control the BESS of the system in order to maximize the revenue and minimize the costs. The control is based on an update of the RES forecast at intraday horizon. The intraday forecasting error is lower than the day-ahead forecasting error associated to the DA decision (cf. Appendix 1), therefore the short-term control is expected to be able to improve the objective due to the improved information on the expected RES production level.
Different strategies for controlling this system are proposed in the following, all based on Model Predictive Control (MPC). MPC is chosen because it is well suited to multi-objective optimization, versatile in the formulation of objectives and constraints, and enables to easily assess the impact of forecasting performance on the control actions. Reinforcement Learning could be an alternative but it is more difficult to understand how actions are decided. Finally, Linear Decision Rules could be implemented in a stochastic optimization to model the control of the system. These rules are implemented in the Machine Learning alternative (cf Section 4.8), however restricting control to actions linearly dependent on the realization of the uncertainty may be suboptimal, especially in a multi-service setting where activation signals and cost vary in non-linear patterns over the control horizon. It is worth to point out that, apart from special price situations, in all cases the general purpose of the control should be that of minimizing the deviations from the DA offer. Indeed the market will pay the operator for the offer, while the operator will face penalties for the deviations from the DA bid. The economic objectives of this work can be optimized at this stage directly by implementing an economic version of the MPC. This approach is compared with a standard reference tracking MPC that tracks the DA offers on the energy and AS markets (which should indirectly maximize the revenue on the market) and BESS DA schedule (which is the optimal scheduling for the storage in the ideal case in which the DA forecast is perfect). The resulting control is expected to be suboptimal regarding the economic objective but may remain valid when the objective of tracking multiple services is at least as important as economic results.

4.6 Traditional Model Predictive Control

The first strategy that we propose is a traditional **Deterministic Reference Tracking MPC** (**DRTMPC**) approach. This is used as a benchmark for the evaluation of the following economic-oriented MPC strategies.
Define the *energy delivery* E_t^{del} at time $t \in \{1, 2, ..., T\}$ as the energy offer plus its deviations:

$$E_t^{del} = E_t^{off} - E_t^{\uparrow} + E_t^{\downarrow}, \tag{32}$$

This project has received funding from the European Union's Horizon 2020 research and innovation programme under grant agreement No 864337

then, given the past information up to time t, we define the vectors

$$ee_{t+k|t} = E^{del,DA}_{t+k} - E^{del,ST}_{t+k|t}, \tag{33}$$
$$eb_{t+k|t} = x^{DA}_{t+k} - x^{ST}_{t+k|t}, \tag{34}$$
$$\delta^2_{t+k|t} = (\delta^{FCR,ST}_{t+k|t})^2 + (\delta^{aFRR,\uparrow,ST}_{t+k|t})^2 + (\delta^{aFRR,\downarrow,ST}_{t+k|t})^2 \tag{35}$$

for $k \in \{0, 1, ..., N-1\}$, where N is the prediction horizon of the control strategy. The terms (33)-(35) define respectively the error between ST and DA energy delivery, the error between ST and DA BESS scheduling and the penalisation for AS deficits evaluated at the ST stage. Moreover, define the deterministic ST BESS power commands vector

$$\mathbf{P^{ST}_{t+k|t}} = \text{col}(p^{b,c,ST}_{t+k|t}, p^{b,d,ST}_{t+k|t}) \tag{36}$$

and the tracking ST decision vector as

$$\mathbf{d^{ST}_{t+k|t}} = \text{col}(\mathbf{P^{ST}_{t+k|t}}, E^{del,ST}_{t+k|t}, \delta^{FCR,ST}_{t+k|t}, \delta^{aFRR,\uparrow,ST}_{t+k|t}, \delta^{aFRR,\downarrow,ST}_{t+k|t}). \tag{37}$$

First, a single trajectory $\hat{y}^{ST}_t$ of uncertain renewable power generation is computed at an intraday horizon. Then, the optimization problem of this traditional MPC strategy at time $t \in \{1, 2, ..., T\}$ is formulated as a *multi-objective quadratic programming* problem. The objective function (38a) includes three contributions: (*i*) the DA energy delivery tracking, (*ii*) the DA BESS scheduling tracking, (*iii*) the penalisation for deficits on the AS. The same weights are applied on the multiple objectives as in the trading optimization problem, so that the sequential framework trading+control follows coherent objectives.

$$\underset{\mathbf{d^{ST}_{t+k|t}}}{\arg\min} \quad w_M \cdot \sum_{k=0}^{N-1} (ee^2_{t+k|t} + \delta^2_{t+k|t}) + w_B \cdot \sum_{k=0}^{N} eb^2_{t+k|t} \tag{38a}$$

subject to

$$E^{del,ST}_{t+k|t} + R^{FCR,del,ST}_{t+k|t} + R^{aFRR,del,ST}_{t+k|t} + \Delta_k \begin{pmatrix} +1 \\ -1 \end{pmatrix}^T \mathbf{P^{ST}_{t+k|t}} = \hat{y}^{ST}_{t+k}, \tag{38b}$$

$$x^{ST}_{t+k+1|t} = x^{ST}_{t+k|t} + \Delta_k \boldsymbol{\eta}^T \mathbf{P^{ST}_{t+k|t}}, \tag{38c}$$
$$x^{ST}_{t|t} = x_t, \tag{38d}$$
$$x^{ST}_{t+k|t}, x^{ST}_{t+N|t} \in [x^{min}, x^{max}], \tag{38e}$$

$$\delta^{FCR,ST}_{t+k|t} \in [0, R^{FCR,DA}_{t+k}], \tag{38f}$$
$$\delta^{aFRR,\uparrow/\downarrow,ST}_{t+k|t} \in [0, R^{aFRR,\uparrow/\downarrow,DA}_{t+k}], \tag{38g}$$
$$p^{b,c/d,ST}_{t+k|t} \in [p^{c/d,min}, p^{c/d,max}], \tag{38h}$$

This project has received funding from the European Union's Horizon 2020 research and innovation programme under grant agreement No 864337

for $k \in \{0, ..., N-1\}$, where x_t is the current storage energy capacity.
The block of constraints integrates the balancing constraints and BESS technical constraints similarly than for the trading stage. Among these constraints, condition (**??**) is particularly important and it takes the name of *terminal constraint* in the MPC terminology. This is used to guarantee stability and recursive feasibility of this controller. At time t, the BSP estimates the activation signals ($\hat{\alpha}_{FCR,t}$, $\hat{\alpha}_{aFRR\uparrow,t}$ and $\hat{\alpha}_{aFRR\downarrow,t}$) and these are fixed over the whole prediction horizon of the controller in order to compute, by means of (39) and (40), the reserve deliveries ($R^{FCR,del,ST}_{t+k|t}$ and $R^{aFRR,del,ST}_{t+k|t}$).

$$R^{FCR,del,ST}_t = \hat{\alpha}_{FCR,t} \cdot (R^{FCR,DA}_t - \delta^{FCR,ST}_t) \tag{39}$$

$$\begin{aligned} R^{aFRR,del,ST}_t &= \hat{\alpha}_{aFRR\uparrow,t} \cdot (R^{aFRR,\uparrow,DA}_t - \delta^{aFRR,\uparrow,ST}_t) + && (40)\\ &- \hat{\alpha}_{aFRR\downarrow,t} \cdot (R^{aFRR,\downarrow,DA}_t - \delta^{aFRR,\downarrow,ST}_t), && (41) \end{aligned}$$

To conclude, a graphical description of the DRT-MPC is provided in Fig.20. The figure shows that the process to be controlled is the BESS schedule and the control actions are computed as a consequence of the errors defined above (*predicted errors* (33)-(35)) and on the basis of the quantities computed at DA stage. If AS are taken into account in the problem, the MPC will receive the DA reserve offers and deficits as well. In previous paragraphs (*Provision of Energy* and *Provision of Energy and Ancillary Services*) the formulation of the optimization problems of the MPC is provided for both cases.

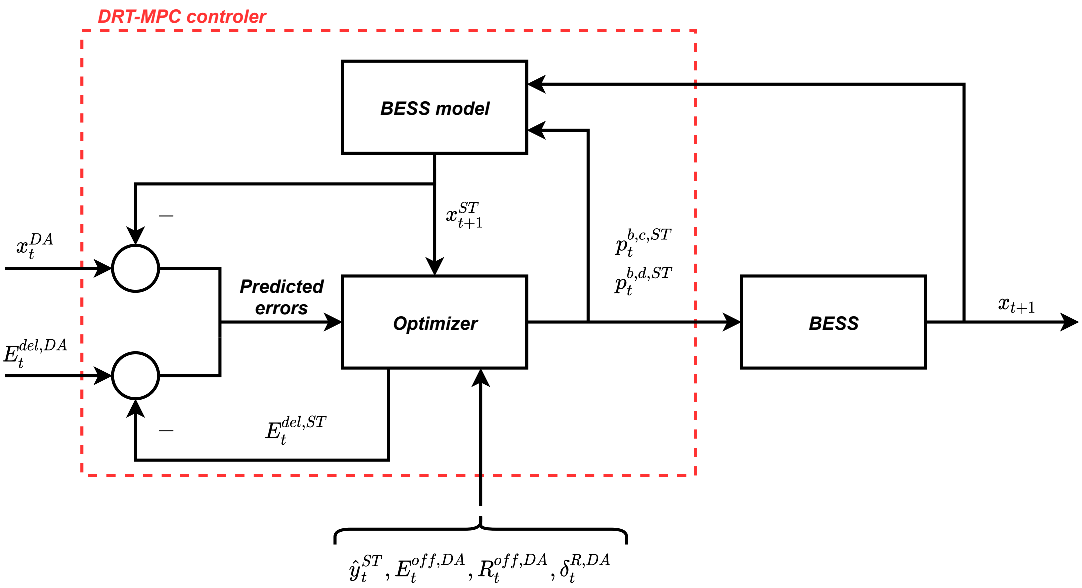

Figure 20: DRT-MPC scheme

4.7 Economic Model Predictive Control approaches

As an alternative to the traditional DRTMPC approach, we propose two economic-oriented MPC strategies: a **Stochastic Economic MPC** (**SEMPC**) approach and a **Deterministic Economic MPC** (**DEMPC**) approach. In the former we consider a set of scenarios Ω for the realization of uncertainties, while in the latter this set is reduced to a singleton.

This project has received funding from the European Union's Horizon 2020 research and innovation programme under grant agreement No 864337

First, a new set of trajectories $\hat{y}^{ST}_{\omega,t}$, for $\omega \in \{1, 2, ..., \Omega\}$, of uncertain renewable power generation is computed at intraday horizons $k = 0, 1, ..., N - 1$.

Define the vectors

$$\mathbf{P^{ST}_{\omega,t+k|t}} = \text{col}(p^{b,c,ST}_{\omega,t+k|t}, p^{b,d,ST}_{\omega,t+k|t}), \tag{42}$$

$$\boldsymbol{\delta}^{\mathbf{E,ST}}_{\boldsymbol{\omega},\mathbf{t+k|t}} = \text{col}(E^{\uparrow,ST}_{\omega,t+k|t}, E^{\downarrow,ST}_{\omega,t+k|t}), \tag{43}$$

$$\boldsymbol{\delta}^{\mathbf{AS,ST}}_{\boldsymbol{\omega},\mathbf{t+k|t}} = \text{col}(\delta^{FCR,ST}_{\omega,t+k|t}, \delta^{aFRR,\uparrow,ST}_{\omega,t+k|t}, \delta^{aFRR,\downarrow,ST}_{\omega,t+k|t}) \tag{44}$$

and the economic ST decision vector as

$$\mathbf{d^{E,ST}_{\omega,t+k|t}} = \text{col}(\mathbf{P^{ST}_{\omega,t+k|t}}, \boldsymbol{\delta}^{\mathbf{E,ST}}_{\boldsymbol{\omega},\mathbf{t+k|t}}, \boldsymbol{\delta}^{\mathbf{AS,ST}}_{\boldsymbol{\omega},\mathbf{t+k|t}}). \tag{45}$$

Moreover the vectors

$$\boldsymbol{\pi}^{\boldsymbol{\delta},\mathbf{E}}_{\mathbf{t+k}} = \text{col}(\pi^{E,\uparrow}_{t+k}, \pi^{E,\downarrow}_{t+k}), \tag{46}$$

$$\boldsymbol{\pi}^{\boldsymbol{\delta}}_{\mathbf{t+k}} = \text{col}(\pi^{\delta,FCR}_{t+k}, c^{\delta,\uparrow,aFRR}_{t+k}, c^{\delta,\downarrow,aFRR}_{t+k}) \tag{47}$$

denote, in a compact form, imbalance penalties on the energy and AS markets.
Then, the SEMPC strategy optimizes, at time $t \in \{1, 2, ..., T\}$, the ST economic decision variables for each $k \in \{0, 1, ..., N-1\}$, over the whole set of scenarios Ω. The optimization problem of the SEMPC strategy is formulated as the following *multi-objective non-linear programming* problem.

$$\underset{\mathbf{d}^{\mathbf{ST}}_{\boldsymbol{\omega},\mathbf{t+k|t}}}{\arg\min} \quad w_M \cdot \{\mathbb{E}_{\Omega,N}[ED] + \mathbb{E}_{\Omega,N}[ASD]\} + w_B \cdot \mathbb{E}_{\Omega,N}[BD] \tag{48a}$$

where

$$\mathbb{E}_{\Omega,N}[BD] \text{ is given by (5)}, \tag{48b}$$

$$\mathbb{E}_{\Omega,N}[ED] = \frac{1}{\Omega N} \sum_{\omega=1}^{\Omega} \sum_{k=0}^{N-1} \boldsymbol{\pi}^{\boldsymbol{\delta},\mathbf{E}}_{\mathbf{t+k}}{}^{T} \boldsymbol{\delta}^{\mathbf{E,ST}}_{\boldsymbol{\omega},\mathbf{t+k|t}}, \tag{48c}$$

$$\mathbb{E}_{\Omega,N}[ASD] = \frac{1}{\Omega N} \sum_{\omega=1}^{\Omega} \sum_{k=0}^{N-1} \boldsymbol{\pi}^{\boldsymbol{\delta}}_{\mathbf{t+k}}{}^{T} \boldsymbol{\delta}^{\mathbf{AS,ST}}_{\boldsymbol{\omega},\mathbf{t+k|t}} \tag{48d}$$

subject to

$$E^{off,DA}_{t+k} + \begin{pmatrix} -1 \\ +1 \end{pmatrix}^{T} \boldsymbol{\delta}^{\mathbf{E,ST}}_{\boldsymbol{\omega},\mathbf{t+k|t}} + R^{FCR,del,ST}_{\omega,t+k|t} +$$

$$+ R^{aFRR,del,ST}_{\omega,t+k|t} + \Delta_k \begin{pmatrix} +1 \\ -1 \end{pmatrix}^{T} \mathbf{P}^{\mathbf{ST}}_{\boldsymbol{\omega},\mathbf{t+k|t}}$$

$$= \hat{y}^{ST}_{\omega,t+k}, \tag{48e}$$

$$x^{ST}_{\omega,t+k+1|t} = x^{ST}_{\omega,t+k|t} + \Delta_k \boldsymbol{\eta}^{T} \mathbf{P}^{\mathbf{ST}}_{\boldsymbol{\omega},\mathbf{t+k|t}}, \tag{48f}$$

$$x^{ST}_{\omega,t|t} = x_{\omega,t}, \tag{48g}$$

$$x^{ST}_{\omega,t+k|t}, x^{ST}_{\omega,t+N|t} \in [x^{min}, x^{max}], \tag{48h}$$

$$E^{\uparrow,ST}_{\omega,t+k|t}, E^{\downarrow,ST}_{\omega,t+k|t} \in \mathbb{R}_{+}, \tag{48i}$$

$$\delta^{FCR,ST}_{\omega,t+k|t} \in [0, R^{FCR,DA}_{t+k}], \tag{48j}$$

$$\delta^{aFRR,\uparrow/\downarrow,ST}_{\omega,t+k|t} \in [0, R^{aFRR,\uparrow/\downarrow,DA}_{t+k}], \tag{48k}$$

$$p^{b,c/d,ST}_{\omega,t+k|t} \in [p^{c/d,min}, p^{c/d,max}] \tag{48l}$$

for $k \in \{0, ..., N-1\}$ and $\omega \in \{1, 2, ..., \Omega\}$, where x_t is the current storage energy capacity.
In the above formulation, the objective function (48a) includes three contributions: (*i*) the *energy deviations* cost term (48c), accounting for the cost of deviating from the DA energy offer, (*ii*) the *ancillary service deficits* cost term (48d), accounting for the cost of deviating from DA reserves offers, (*iii*) the *BESS degradation* cost term (5). Moreover, the meaning of the constraints is the same as those from the DRTMPC.
Once the optimal BESS power commands $\mathbf{P}^{ST}_{\omega,t}$ have been computed for each scenario ω, the commands that are actually implemented at time t are obtained as the average BESS power commands on all scenarios:

$$\mathbf{P}^{ST}_{t} = \frac{\sum_{\omega=1}^{\Omega} \mathbf{P}^{ST}_{\omega,t}}{\Omega}. \tag{49}$$

It is then necessary to implement a post-processing operation to ensure the feasibility of $\mathbf{P}^{ST}_{t}$. Finally, the deterministic version of the economic MPC (DEMPC) is derived by replacing the full uncertainty distribution by a singleton representing the expected RES trajectory. It serves as a benchmark to the traditional DRTMPC approach.

This project has received funding from the European Union's Horizon 2020 research and innovation programme under grant agreement No 864337

4.8 Machine-Learning alternative for trading and control

This section concludes the proposed multi-objective methodology for service provision by hybrid RES systems. The approach presented above is a “forecast-then-optimize” approach, that requires first modeling each of the uncertain variables, deriving forecasts, and finally solving an optimization problem. In this standard approach, the learning component (forecasting) is independent of the downstream optimization problem.

In contrast, a decision-aid approach based on Machine-Learning (ML) is proposed here to tackle the trading and control problem with an integrated approach. By doing so, decisions are taken based on value-oriented objectives without the need to develop separate a forecasting model for each uncertain variable. This constitutes a significant simplification of the model chain as will be illustrated further below. Furthermore, the obtained ML models are generic and can be readily adapted to different system configurations.

The approach integrates forecasting and optimization into a single decision-aid model, published by A. Stratigakos *et al.* in IEEE Transactions on Power Systems [30]. The development and maintenance of multiple prediction and optimization models results in a complex model chain spanning the pipeline from data to final decisions. For instance, the complete model chain of trading and control of the Hybrid RES system, presented above, requires:

- Two forecast models for the RES production, at day-ahead and intraday horizons, respectively.
- Two optimization models, one for trading at day-ahead stage and one for predictive control at the short-term stage.
- If market uncertainty is added to the problem, then up to 11 prediction models are needed to forecast the 11 prices associated to the joint offering problem on energy, FCR and aFRR markets.

In contrast, this section proposes an approach built upon the framework of prescriptive analytics proposed by [31]. This decision-aid model is able to tackle a variety of problems (cf. Fig 21). The overall goal is to move from the sequential model-chain (shown in black in Fig 21) to a holistic approach that jointly examines forecasting and optimization and takes into account decision-costs during learning (highlighted in green). This approach is generic and applicable to multi-objective and multi-period problems, such as the one of trading and control for a hybrid system integrating storage.

Following the framework described in [31], we deal with optimization problems with uncertain parameters y that are associated with contextual information (or explanatory variables) x. We use z to denote the decisions and $c(z,y)$ to denote the cost function. Based on a training data set $\{y_i, x_i\}$ of n observations, our goal is to develop a model that outputs decisions z as a function of x that minimize the expected costs. For this report, the uncertainty y refers to stochastic renewable production, x refers to available explanatory variables, *e.g.*, Numerical Weather Predictions, and z denotes the trading and storage control decisions. The proposed method consists of training local ML models, such as decision trees, to derive a set of weights ω and minimize a weighted Sample Average Approximation (SAA) of the original problem. In simple terms, we are searching the available training set for similar past instances and prescribe the decisions that minimize the expected cost over those instances. For an out-of-sample query $\overline{x}$, the final decisions, termed *predictive prescriptions*, are given by

$$\hat{z}(x) = \arg\min_{z \in \mathcal{Z}} \sum_{i=1}^{n} \omega_{n,i}(\overline{x}) c(z; y_i) \tag{50}$$

This project has received funding from the European Union's Horizon 2020 research and innovation programme under grant agreement No 864337

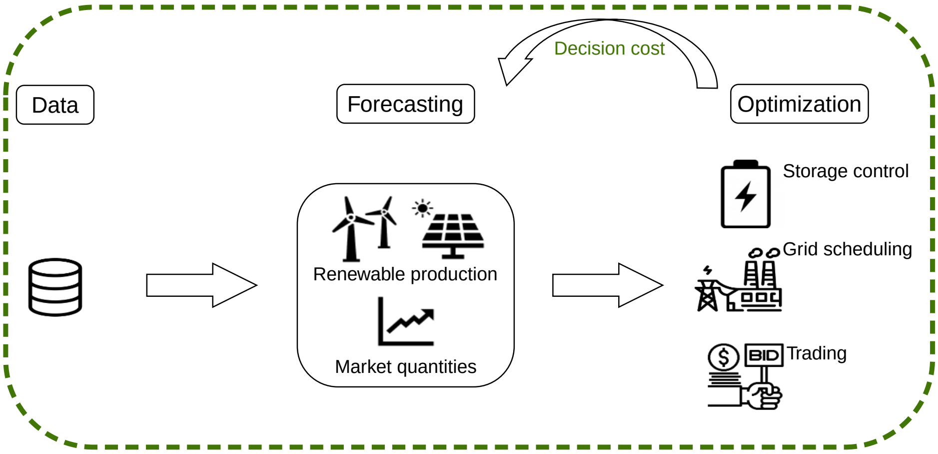

Figure 21: Prescriptive analytics for integrated forecasting and optimization considering uncertainties on RES and markets

where $\omega_{n,i}(\overline{x})$ measures the similarity of training observation i, out of the total n observations, with the new query $\overline{x}$. The various problem constraints, *e.g.*, storage technical limits, are included in the feasible set $\mathcal{Z}$. Lastly, weights $\omega_{n,i}(\overline{x})$ are non-negative and $\sum_{i=1}^{n} \omega_{n,i}(\overline{x}) = 1$. These weights can be obtained from local learning models such as nearest-neighbours or decision trees. The present work develops Prescriptive Forest based decision trees (Random Forests and Extremely Randomized Trees), due to the good performance of decision trees for prescriptive analytics [31]. Interested readers may refer to the full article [30] for the methodological details of predictive prescriptions.

The proposed approach enables us to also assess the relative impact of uncertain parameters on the downstream decision costs and weight associated features accordingly, during learning, while also exploiting possible cross-dependencies. The proposed prescriptive analytics model is evaluated on the two following use cases:

1. Multi-objective optimization of the joint participation of renewables and storage in a day-ahead energy market and the operational control policy of the storage.
2. Optimization of the joint provision of Energy and Reserve (FCR) from renewables without storage.

These two use cases are chosen because they address several challenges raised by the full problem of multi-service provision by the hybrid system investigated in the above sections, but also have a simpler structure so the benefits of the prescriptive analytics can be validated more easily. The addressed challenges are (1) the multi-objective optimization with storage integrating control policy for the first use case and (2) the joint provision of energy and ancillary service for the second use case. Results achieved on the first use case are reported in Section 7. Please refer to the full article for results on the second use case [30].

The problem posed by the first use case is now presented. The problem jointly optimizes the DA offer, considering a closed system, and the operational control policy of the storage. The aggregation participates in a DA market subject to imbalance penalties, considering a dual-price balancing mechanism. Participating in additional markets, such as intraday or offering balancing services, is not examined. Optimizing over the operational policy of the storage means that we allow recourse actions based on the realization of uncertainty. This defines a

This project has received funding from the European Union's Horizon 2020 research and innovation programme under grant agreement No 864337

multi-stage dynamic optimization problem; a tractable reformulation is provided by applying the linear decision rule (LDR) approach [32], modeling real-time decisions as an affine function of uncertainty, in this case the energy forecast error. Throughout this section, we use $\widetilde{\cdot}$ to denote decisions that depend on the realization of uncertainty. Index t is used to define a specific time period (scalar), while absence of t defines a vector over the DA horizon of length T.

Let $\xi \in \Xi \subseteq \mathbb{R}^T$ define the energy forecast error for the DA horizon, *i.e.*, a sample path of errors of length T, and Ξ define an uncertainty set. The uncertain renewable production is defined as $p^E = \widehat{p}^E + \xi$, *i.e.*, the expected value (forecast) $\widehat{p}^E \in \mathbb{R}^T$ plus the error term ξ. We define recourse actions of the storage as an affine function of uncertainty. For example, the decision vector for charging is defined $\widetilde{p}^{ch} = \widehat{p}^{ch} + D^{ch}\xi$; here, $\widehat{p}^{ch} \in \mathbb{R}^T$ denotes the scheduled DA decisions and $D^{ch} \in \mathbb{R}^{T\times T}$ is a linear coefficient matrix that determines the operational policy mapping realizations of uncertainty ξ to recourse actions. Note that the whole error history is considered; to retain non-anticipativity we require D^{ch} to be lower-triangular.

We consider a modified version of [11] and design a control policy that aims at minimizing the imbalance volume, without considering the market mechanism in the objective function. The results presented in the next paragraphs and in [30] show that this represents a realistic application for a dual-price balancing mechanism. As an objective function, we optimize over a convex combination of trading performance in the DA market and deviations from the contracted energy during real-time operation. For simplicity, we assume DA prices are known. The problem is defined as:

$$
\begin{aligned}
\min_{\mathcal{P}} \quad & \mathbb{E}\left[\sum_{t=1}^{T} -(1-k)\pi_t^{da} p_t^{offer} + k\left\| p_t^{output} - p_t^{offer}\right\|_2^2\right] && \text{(51a)}\\
\text{s.t.} \quad & p^{min} \leq p^{offer} \leq p^{max}, && \text{(51b)}\\
& p_t^{soc} = p_{t-1}^{soc} + \eta^{ch}\widetilde{p}_{t-1}^{ch} + \frac{1}{\eta^{dis}}\widetilde{p}_{t-1}^{dis} \quad \forall t \in [T], && \text{(51c)}\\
& p_1^{soc} = p_T^{soc} = p_0, && \text{(51d)}\\
& p^{output} = \widehat{p}^E + \xi + \widetilde{p}^{dis} - \widetilde{p}^{ch}, && \text{(51e)}\\
& 0 \leq \widetilde{p}^{dis} \leq c^{dis} \quad \forall \xi \in \Xi, && \text{(51f)}\\
& 0 \leq \widetilde{p}^{ch} \leq c^{ch} \quad \forall \xi \in \Xi, && \text{(51g)}\\
& 0 \leq p^{soc} \leq B^{max} \quad \forall \xi \in \Xi, && \text{(51h)}
\end{aligned}
$$

where $\mathcal{P} = \{p^{offer}, \widehat{p}^{ch}, \widehat{p}^{dis}, D^{ch}, D^{dis}\}$ is the set of decision variables, and p^{soc}, p^{output} are auxiliary variables for the induced state of charge in the storage and the actual output of the plant-storage system. The objective (51a) minimizes a convex combination of trading profit from the DA market and deviations between actual output and the contracted energy. The trade-off is controlled from parameter k. For $k = 0$ the main function of the storage is to arbitrage in the DA market, while for $k = 1$ the focus is placed on compensating deviations from the schedule during RT operation. Problem constraints include the limits for contracted energy (51b), the state transition equation of the storage (51c), initial and terminal conditions for the state of charge (51d), and technical limits of the storage (51f)-(51h). In a data-driven setting, we assume that ξ belongs to a finite set $\Xi = \{\xi_i\}_{i=1}^n$, which we use to approximate the objective (51a) (remark that the i-th observation ξ_i is a sample path of length T). Further, we employ duality theory and standard techniques from robust optimization to reformulate (51f)-(51h). For reference, constraint (51f) is reformulated as follows. First, we define a polyhedral uncertainty set $\Xi' = \{\xi \mid H\xi \leq h\}$, where $H = [I, -I]^\intercal \in \mathbb{R}^{2T\times T}$, with I defining an identity matrix, and

$h \in \mathbb{R}^{2T}$ containing the upper and lower bound for each period t. Next, we define the inner max problem

$$\max_{\xi} \left\{ \widehat{p}^{dis} + D^{dis}\xi \mid H\xi \leq h \colon \mu \right\} \leq c^{dis}, \tag{52}$$

where μ denotes the dual variables. From duality, we derive

$$\max_{\mu} \left\{ -h^{\intercal}\mu \mid H^{\intercal}\mu = D^{dis}, \mu \geq 0 \right\} \leq c^{dis} - \widehat{p}^{dis}, \tag{53}$$

which finally leads to

$$\exists \mu, \text{ with } h^{\intercal}\mu \leq c^{dis} - \widehat{p}^{dis}, H^{\intercal}\mu = D^{dis}, \mu \geq 0. \tag{54}$$

The rest of the constraints are reformulated in a similar fashion. If the uncertainty set Ξ' is too wide, no control will take place during RT operation, while if it is too tight, it is possible to get infeasible actions. During the actual implementation, we add a saturation block to ensure feasible recourse actions. Therefore, the maximum charge is set as $\min\{c^{in}, \frac{B^{max} - p^{soc}}{\eta^{ch}}\}$, while the maximum discharge is $\min\{c^{out}, p^{soc}\eta^{dis}\}$. Lastly, we note that Ξ' varies on an hourly and daily basis. To determine h we use the intervals derived from the underlying samples ξ_i. For reference, consider the example forecasts shown in Fig. 22. At 00:00 scenarios show small dispersion (*i.e.*, less uncertainty), which results in tighter upper and lower bounds in h. On the other hand, at 12:00 the derived bounds in h are wider, due to the larger dispersion of the underlying scenarios.

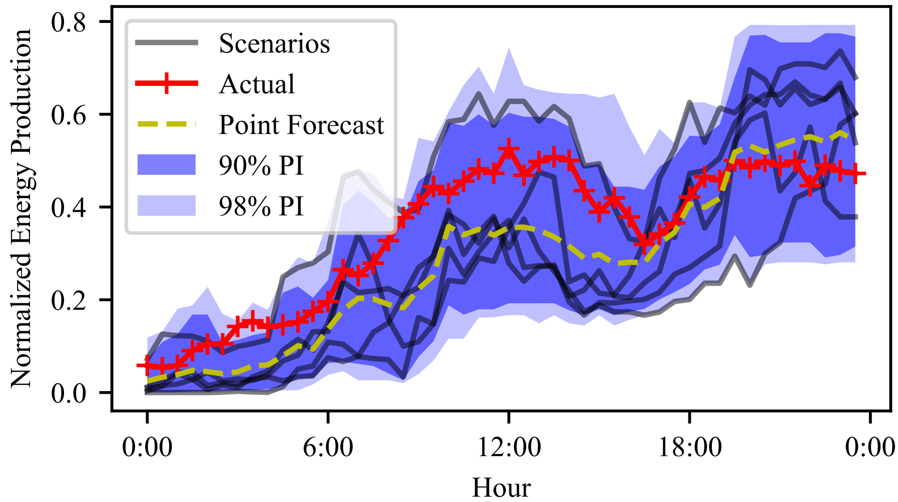

Figure 22: DA renewable energy forecasts: point forecasts, probabilistic forecasts (prediction intervals or PI), and scenarios.

This project has received funding from the European Union's Horizon 2020 research and innovation programme under grant agreement No 864337

5 Case Study of hybrid system optimization

5.1 Overview of Case of study

The model is applied to an hybrid renewable power plant, that is composed of an onshore wind farm and a stationary BESS operating under the same Grid Connection Point. The system illustrated in Fig. 23 operates in the energy market, and has the capacity to provide FCR and aFRR.

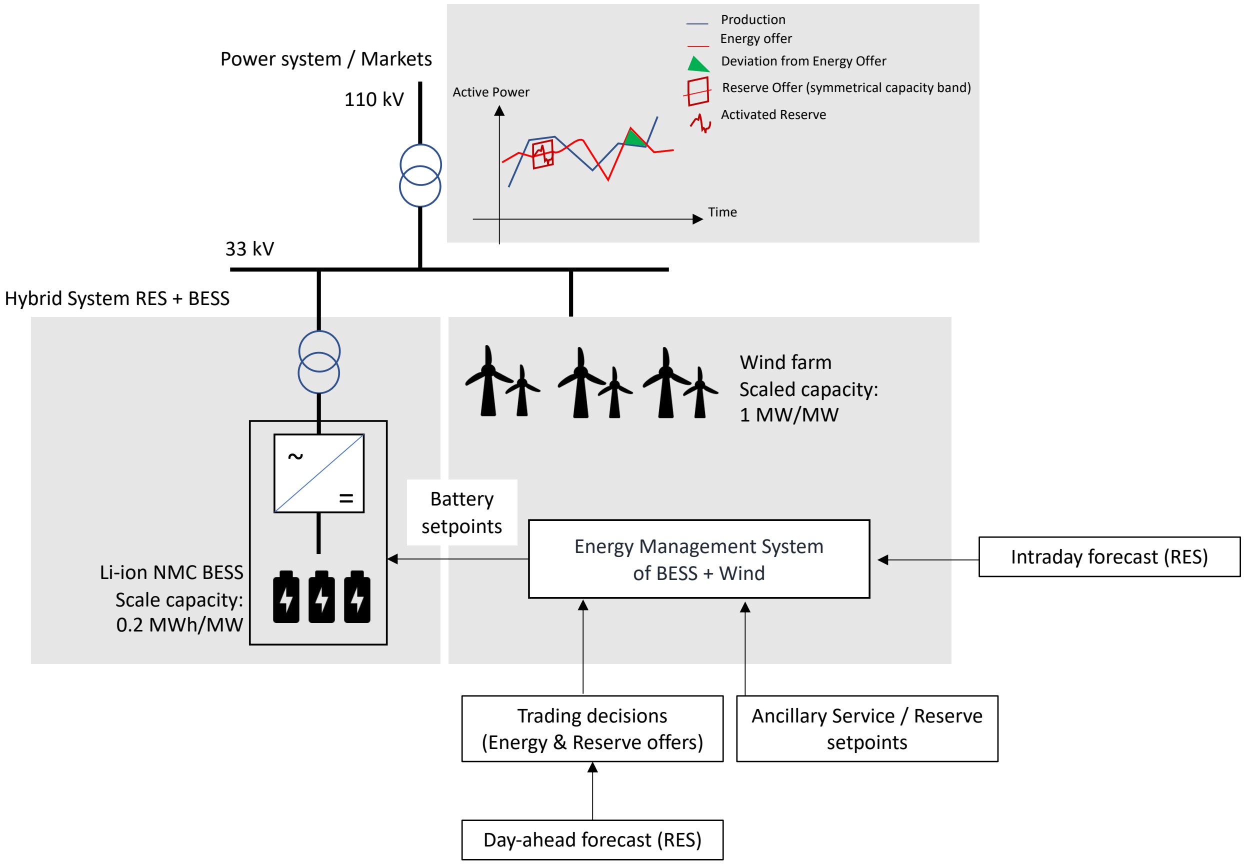

Figure 23: Configuration of the Hybrid RES+BESS power plant considered in the case study.

This case study is based on historical time-series of wind power production and the SoC of the BESS (9 months at 5-min resolution). These time series come from Dataset 7 of the Smart4RES Data Management Plan (cf. Table 1). To ensure confidentiality and replicability, the capacities of the Wind farm and of the BESS are scaled by the installed capacity of the wind farm. The capacity of the BESS is therefore considered as 0.2 MWh/0.2 MW for a 1 MW Wind farm capacity. This ratio is representative of the industrial context, where storage investment costs limits storage contribution to the total hybrid system.

The configurations of the training, validation and testing sets for the wind power forecasting model are given in Table 12. The testing set is chosen as the evaluation period for the optimization framework.

This project has received funding from the European Union's Horizon 2020 research and innovation programme under grant agreement No 864337

Dataset Index	Dataset Name	Data types used	Use in Deliverable
Dataset 7	Wind + Storage System in Romania (EDP-R)	Wind power time series BESS state-of-charge and power	RES forecasting Model validation

Table 1: Use of Smart4RES datasets

Set type	Start	End	Duration	Comments
Training set	2018-09-01	2019-02-27	6 Months	Missing data for the rest of 2019
Validation set	2020-03-01	2020-06-20	3 Months	11 missing days in June 2020
Testing set	2020-08-01	2020-10-31	3 Months	-

Table 2: Definition of training, validation, testing set of wind power forecasting

5.2 BESS Description and degradation model

The storage system is composed of 16 Ah Li-ion cells equipped with Nickel-Manganese-Cobalt (NMC) positive electrodes. The NMC oxide is a mature chemistry for BESS applications (among others like lithium-titanate) because of its high specific energy and long lifespan.

In the following sections, the proposed BESS degradation model is validated based on cycling ageing tests of the battery operating in the case study and calendar ageing tests performed by academic studies on batteries of similar chemistry (*i.e.* Li-ion NMC).

5.2.1 Cycling ageing

The modelling of cycling ageing is performed via the linear weighting of energy throughput proposed by Namor [15]. The choice to use linear modelling permits to model the entire optimization as a linear program. The performance of this linear model is discussed below.

The principle of the energy throughput modelling is illustrated below: a linear trend is found in the decrease of the BESS capacity until the EOL capacity is reached (usually 80%). The degradation is steeper with higher C-rates.
The total energy exchanged by the battery over a period T, with time steps of duration ΔT, writes following [15] as:

$$E_{exch} = \Delta T \sum_{t \in T} |w(t)B(t)| = T \sum_{t \in T} w(t)|B(t)| \tag{55}$$

where B(t) is the power exchanged by the battery at time step t. The absolute power exchange is modelled in the present study as the absolute difference of the battery state between two consecutive time steps $|x_t - x_{t-1}|$. In order to simplify the optimization model, a constant cycling weight w_2 replaces the variable $w(t)$:

$$E_{exch} = \Delta T w_2^* \sum_{t \in T} |x_t - x_{t-1}| \tag{56}$$

The value of w_2^* is estimated as the affine parameter of a linear function $w_2^*(\textit{C-rate})$ [15]. This function is obtained from cycling tests at different C-rates in Fig. 24. It is considered that the normalizing weight value $w_2^* = 1$ is reached at maximum C-rate $\textit{C-rate}_{max}$, 3C in the present

This project has received funding from the European Union's Horizon 2020 research and innovation programme under grant agreement No 864337

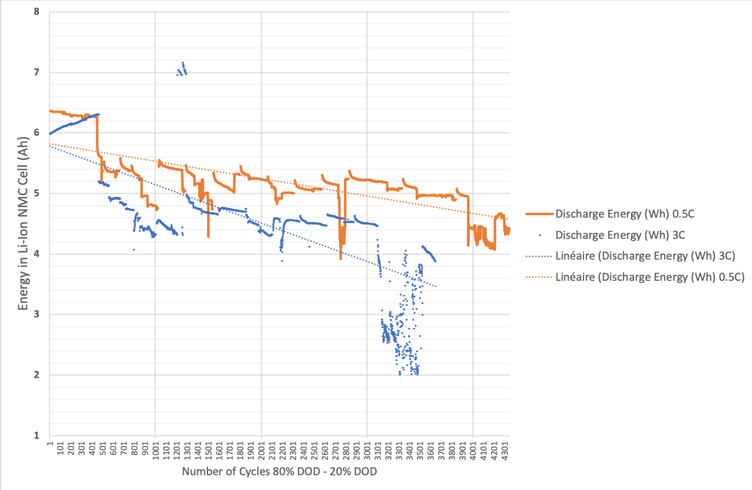

Figure 24: Degradation of a Li-ion NMC battery cycling test 60 % DOD, 25 °C.

system. The effect of C-Rate is similar to the values found by [15], even if the battery chemistry is different (Lithium titanate vs Lithium NMC).

$$w_2^*(C\text{-}rate) = 0.7 + 0.09C\text{-}rate$$

Finally, the capacity retention over the period T for the linear model of cycling degradation $\Delta C_T^{cyc,lin}$ is derived as the ratio between the equivalent number of cycles associated with the energy exchanged over the rated number of full cycles before End of Life n_{EOL}^{100}.

$$\Delta C_T^{cyc,lin} = \frac{\frac{E_{exch}}{2x^{max}}}{n_{EOL}^{100}} = \frac{\frac{\Delta T w_2^*}{2x^{max}} \sum_{t \in T} |x_t - x_{t-1}|}{n_{EOL}^{100}} \tag{57}$$

So the scaled weight to be used in the optimization problem is:

$$w_2 = \frac{\Delta T w_2^*}{2x^{max} n_{EOL}^{100}} \tag{58}$$

As a benchmark, a non-linear degradation model (Rainflow Counting Algorithm) is employed to detect cycles of different DoD. The corresponding capacity retention $\Delta C_T^{cyc,nonlin}$ is obtained by summing the counts of cycle at different DoD intervals $d_s, s \in S$ and affecting them the exponential relationship between DoD and number of cycles until EoL at this DoD, parameterized by an exponent k_p derived by an exponential fitting of the curve of full number of cycles versus DoD [7].

$$\Delta C_T^{cyc,nonlin} = \frac{\sum_{s \in S, t \in T} 1_{d_t \in d_s} d_s^{k_p}}{n_{EOL}^{100}} \tag{59}$$

In what follows, a sensitivity analysis is performed to know how w_2^* parameters influence the degradation and which parameters' values minimize the difference to the benchmark non-linear degradation model.

The cycling models are applied first to a sinusoidal state signal, simulating 4500 cycles of varying DoD (20% to 80% DoD). Results in Fig. 25 show that the linear model with smallest deviation from the exponential model is $w_2^* = 1.1 + 0.09$ C-rate. This is confirmed by the computation of the Mean Squared Error over the DoD range. To simplify the degradation model,

This project has received funding from the European Union's Horizon 2020 research and innovation programme under grant agreement No 864337

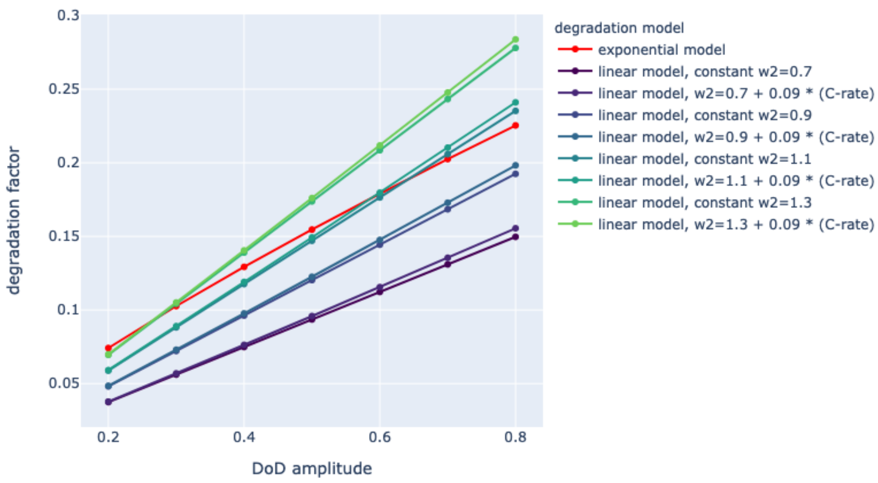

Figure 25: Results of cycling degradation analysis on sinusoidal data. Yearly degradation factor of the capacity retention [%/year] for the exponential degradation model and linear degradation model, as a function of the DoD of a sinusoidal battery charging signal. The linear degradation model is tested with constant weight and weight depending on the C-Rate.

only the constant part is used, *i.e.* $w_2^* = 1.1$ as C-Rate dependency has an impact below 10% on the total capacity retention.

Finally, the linear degradation model and exponential model are applied to the 9-month SoC signal of the BESS in the case study presented in Fig. 26. The linear degradation model gives a 3.3% capacity retention if the C-rate is included, 2.6 % otherwise, for 3.4 % degradation for the exponential model. We conclude that the linear model of cycling ageing with a coefficient w_2 not depending on C-rate is sufficient for the purpose of the study, as the difference in capacity retention with the more detailed non-linear model is limited to 0.8% over the entire evaluation period. Further developments could consider a w_2 dependent on C-rate.

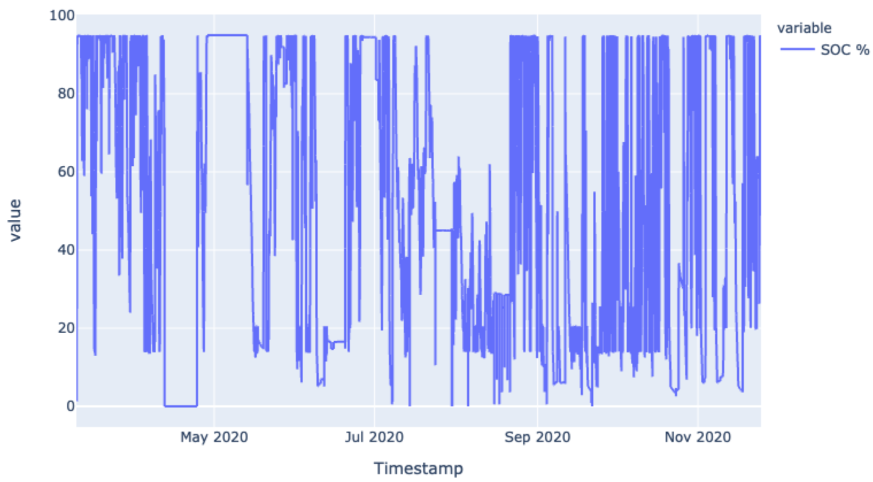

Figure 26: Cycles of BESS, 9 month data interpolated at 5min resolution. A few idle periods correspond to missing/erroneous data.

This project has received funding from the European Union's Horizon 2020 research and innovation programme under grant agreement No 864337

5.2.2 Calendar ageing

Calendar ageing is evaluated in two steps:

1. Define an average cell temperature by confronting to existing literature and looking for a cost balance between air conditioning of the BESS and cost of degradation.
2. Use laboratory tests to define the degradation coefficient w_1 associated with SoC.

Low temperatures (below 15℃) are known to foster reactions between lithium and the electrolyte and increase the impedance of the battery. High temperatures degrade the battery according to the Arrhenius law (dependence of chemical reaction on temperature). Here we assume that an EOL due to calendar ageing of 10 years can be attained and look for the corresponding average cell temperature. Available data for Li-ion cells situate this average cell temperature at 25℃ (10% capacity retention in 5 years, see Fig. 27). An energy balance simulation with time series of exterior temperature and solar radiation on a typical container equipped with HVAC on the site of case study confirmed that a standard HVAC (COP 150%) set at 25℃ ambient temperature (assumed same temperature for the cell) is able to limit the degradation due to temperature to 2% / year. Therefore a constant cell temperature of 25℃ is retained for the degradation study.

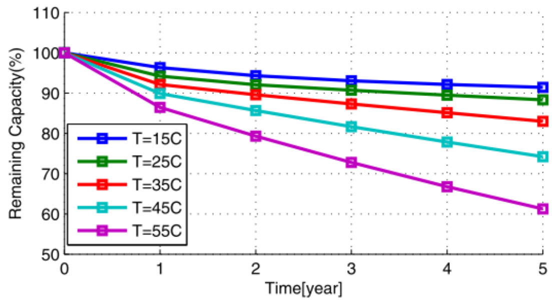

(a) Calendar aging with varying temperature at 50% SoC.

Figure 27: Degradation of Li-ion with temperature.

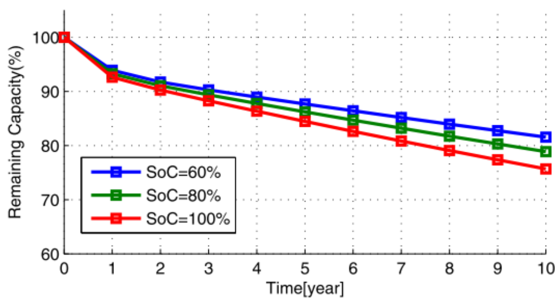

(b) Calendar aging with varying SoC at $25°C$.

Figure 28: Degradation of Li-ion with SoC, constant 25℃ Temperature.

The calendar ageing weight is derived as the linear coefficient of capacity retention with time until tested end of life T^{cal}_{EOL}, multiplied by the reference state level, *i.e.*, the average state for which the degradation takes place.

$$w_1 = \frac{1}{T^{cal}_{EOL} x^{ref}} \tag{60}$$

This project has received funding from the European Union's Horizon 2020 research and innovation programme under grant agreement No 864337

Considering that calendar ageing is significant for high SoCs, the reference state level is taken at 80% SoC. The minimum threshold on the state is defined in order to ensure system integrity, therefore it is modelled as a hard constraint in the optimization problem.

5.3 Parameters

This section presents all the numerical parameters used to obtain the simulation results presented in the next Section.

Prices and volumes on the energy and AS markets correspond to historical observations on the Romanian market, retrieved from ENTSOE's Transparency Platform. The penalty price for reserve deficit is assumed to equal 5 times the reserve capacity for both FCR and aFRR. This assumption is inspired by current rules in France however it should be clear that prices for reserve deficits are likely to be defined more precisely in the next years for variable RES-based reserve offers, more likely to show deficit than reserve offers from dispatchable plants.

$$\pi_{\delta,R,t} = 5 \cdot \pi_t^{R,DA} \tag{61}$$

The marginal cost for battery degradation $\pi^B = 20$ RON/MWh, under the assumption of a CAPEX of 200 kEuro/MWh for the BESS system. Different values of weights for the multiple objectives in the trading or control problem are considered in order to verify possible trade-offs and are specified as needed when presenting results.

The CCT degradation model for the BESS is defined by two weighting parameters for the calendar ageing cost and cycling ageing cost respectively. As a consequence of the reasoning presented in the previous section, these weights assume the numerical values presented in Tab. 3. The sizing of the BESS and parameters of the degradation model are as follows:

- Initial state $x^i = 0.1\ MWh$.
- Maximum threshold $x^{thr,max} = 0.14\ MWh$.
- Minimum capacity $x^{min} = 0.04\ MWh$.
- Maximum capacity $x^{max} = 0.2\ MWh$.

CCT SIMULATION WEIGHTS		
name	**symbol**	**value**
calendar ageing weight	w_1	0.79
cycling ageing weight	w_2	2.75

Table 3: Weight values and meaning in the CCT BESS degradation model.

The evaluation period consists of a 3-month period from 01/08/2020 to 30/10/2020. The horizons and temporal resolution of the optimization problems are the following:

- DA trading: $24h - 48h$ horizon, $1h$ temporal resolution which corresponds to the energy market time interval and validity period of reserve offers.
- ST control: $5min - 6h$ horizon, $5min$ temporal resolution
- Rolling period for the estimation of AS activation: $1month$ in the DA problem, 15 min in the ST problem

This project has received funding from the European Union's Horizon 2020 research and innovation programme under grant agreement No 864337

The number of scenarios of RES production is set to 10 after scenario reduction from an initial ensemble of 50 trajectories [33].

This project has received funding from the European Union's Horizon 2020 research and innovation programme under grant agreement No 864337

6 Evaluation of hybrid system optimization

The framework is evaluated in terms of trading and control performances, and finally via an *ex-post evaluation* where trading and control decisions are evaluated and compared to the actual observations of RES production. The following *evaluation metrics* are used to evaluated the framework:

- Average values of ex-post revenue, BESS degradation, upward and downward deviations. Example for the ex-post revenue (REV) of the DE-MPC:

$$\frac{1}{T}\sum_{t=0}^{T} REV_t^{DE-MPC,RT} \tag{62}$$

- Net differences (normalized on DRT-MPC) of ex-post revenue, BESS degradation, upward and downward deviations. Example for the ex-post revenue of the DE-MPC:

$$\sum_{t=0}^{T} \frac{REV_t^{DE-MPC,real} - REV_t^{DRT-MPC,real}}{REV_t^{DRT-MPC,real}} \tag{63}$$

- Relative differences (% DRT-MPC) of ex-post revenue, BESS degradation, upward and downward deviations. Example for the ex-post revenue of the DE-MPC:

$$100 \cdot \sum_{t=0}^{T} \frac{REV_t^{DE-MPC,real} - REV_t^{DRT-MPC,real}}{REV_t^{DRT-MPC,real}} \tag{64}$$

All these scores are presented in tables and diagrams. The actual obtained results for the case of study proposed in this work are presented in the following chapter.

Finally, hereafter are the KPIs designed to evaluate the performance of the proposed approach.

The first is a Smart4RES KPI defined in Deliverable D1.1. $KPI_{1.3.d}$ evaluates the increase of revenue when offering AS + energy compared to only energy for hybrid RES systems, or more generally RES operating jointly with storage.

$$KPI_{1.3.d} = \frac{\text{Revenue}_{\text{Energy+AS}} - \text{Revenue}_{\text{Energy}}}{\text{Revenue}_{\text{Energy}}} \geq 10 - 15\% \tag{65}$$

The second KPI is a KPI specific for this work that enables to assess storage degradation when offering multiple ancillary services:

$$KPI_{degradation} = \frac{\text{Total BESS Degradation}_{\text{framework}} - \text{Total BESS Degradation}_{\text{ref}}}{\text{Total BESS Degradation}_{\text{ref}}} \geq 0\% \tag{66}$$

This project has received funding from the European Union's Horizon 2020 research and innovation programme under grant agreement No 864337

7 Results of hybrid system optimization

7.1 Day-Ahead (DA) Evaluation

This section is devoted to an analysis of the results obtained in the DA stage of the problem, thus the solutions computed for the optimization problems presented in Section 4.3, which will then be used as inputs for the ST stage.

An important point of the proposed formulation is the multi-objective nature of the optimization problems between market cost weight w_M and battery degradation cost w_B. In order to investigate the behavior of the solution when varying the market weight w_M (and correspondingly w_B), different simulations have been performed for both cases of provision of energy only and provision of energy+FCR AS. For the sake of simplicity, provision of aFRR is discarded and results are shown for the deterministic optimization. Fig. 29 and Fig. 30 show the total revenue and BESS degradation obtained when varying w_M, respectively in the energy only and energy+FCR cases, over the 3-month simulation period (from August to October). The results presented in these figures are expected. In both case it is possible to see that, when increasing the market weight w_M, the revenue increases hand in hand with the BESS degradation. A comparison between the curves obtained in the energy only and energy+FCR cases is shown in Fig. 31. Here it is possible to observe that the degradation of the BESS is comparable in the energy and energy+FCR case, but the obtained revenue is higher in the latter case. This is due to the presence of the additional service provided on the market. This service can be exploited to substitute the energy offer with the FCR offer when the FCR price is higher than the energy offer price. Thus, the presence of this AS can be exploited to increase the revenue by bidding more on the AS market (thus less on the energy market) when the AS price is more favourable than the energy offer price. It is then possible to conclude that taking into account the AS instead of energy only gives an advantage from a market point of view, under these assumptions for the prices. These results indicate that the Smart4RES KPI 1.3.d defined in (65) relative to the increase of electricity market revenue, is attained. Under the assumptions stated above, the KPI value when trading energy + AS compared energy only is in the range of 20%, above the target value of 10-15%. This Deliverable is however not focused on trading performance but rather on the technico-economic feasibility of multiple service provision. The interest here is to identify how the different modelling options impact decisions and results at delivery.

Besides the revenue, it is important to analyse the BESS state schedule obtained when using the CCT degradation model. This is shown in Fig.32, which shows the distribution of the BESS state over the simulation period. Fig.32 shows that the storage system is either not used (*i.e.* the BESS state is kept to the initial value) to minimize the BESS degradation, or it is charged up to its maximum threshold value (not above to avoid calendar ageing penalization in the model), to be then completely discharged to its minimum capacity value. In special cases, as shown in the previous results, very favourable energy offer prices can bring to the full charge of the BESS up to its maximum capacity value.
To conclude the analysis of the DA stage, it is important to evaluate the advantages of considering stochastic programming instead of a simple deterministic approach. This can be evaluated using the Value of the Stochastic Solution (VSS), which measures the advantage of the stochastic approach with respect to the deterministic one [7]. Tab.4 presents the obtained VSS for the case of provision of energy only and the case of provision of energy and FCR. In the table, the *Stochastic Objective* is the value of the stochastic objective function at the optimal solution, while the 2^{nd} *Stage Objective* is the value of second stage problem objective function

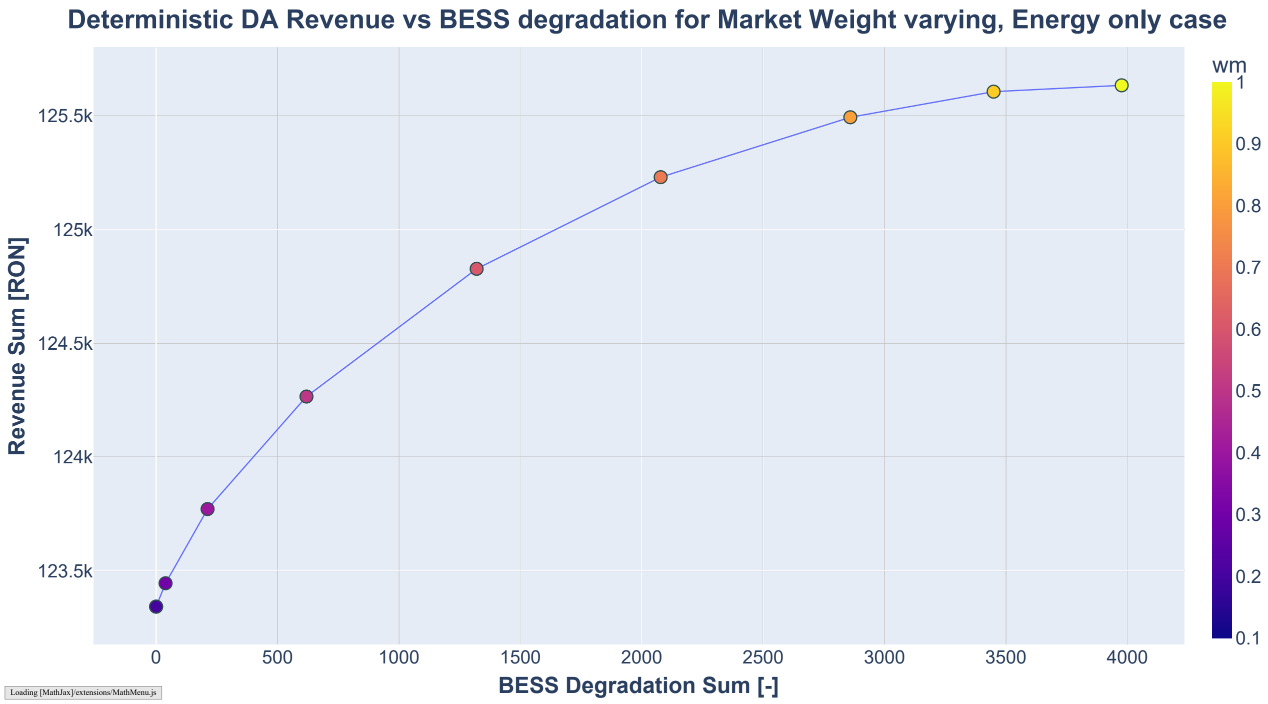

Figure 29: Deterministic DA Total Revenue vs Total BESS Degradation for w_M varying, for the problem of energy provisioning.

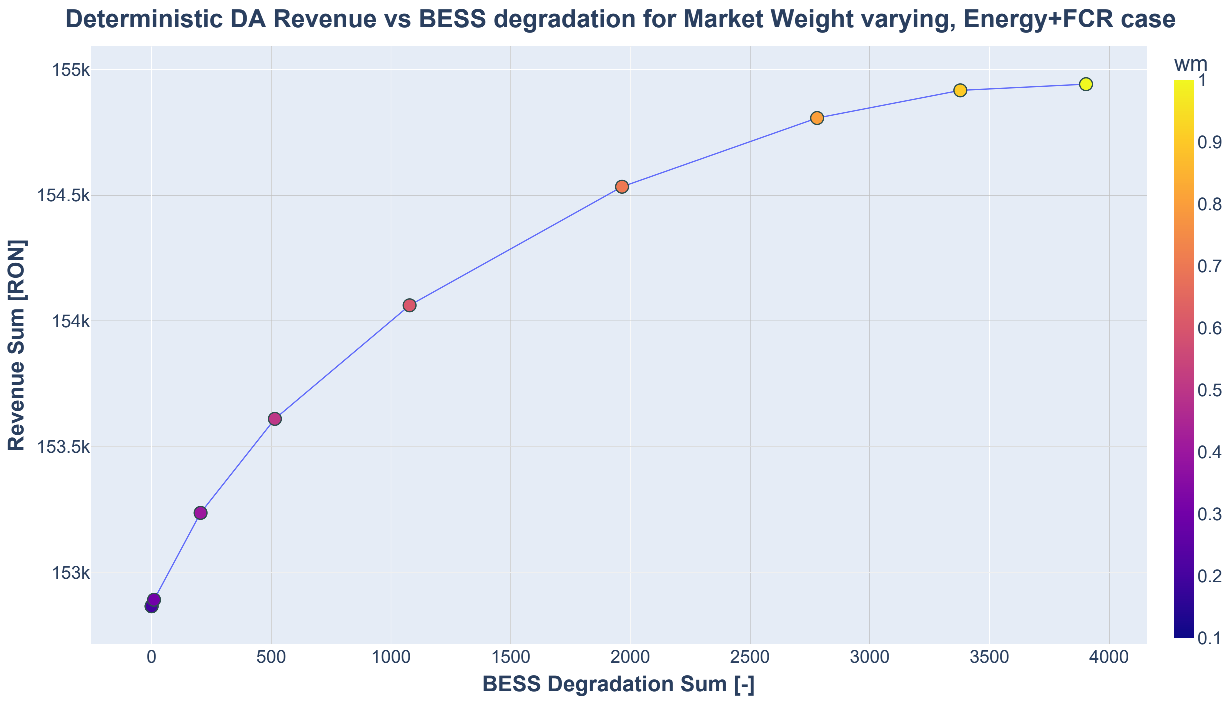

Figure 30: Deterministic DA Total Revenue vs Total BESS Degradation for w_M varying, for the problem of energy+FCR provisioning.

at the optimal solution. This second stage problem is obtained as a simplified version of the stochastic problem, where the first stage variables are fixed to the optimal values computed solving the corresponding deterministic problem. Moreover, since the optimization problems presented at this stage are solved in batches, the values presented in the table are computed

This project has received funding from the European Union's Horizon 2020 research and innovation programme under grant agreement No 864337

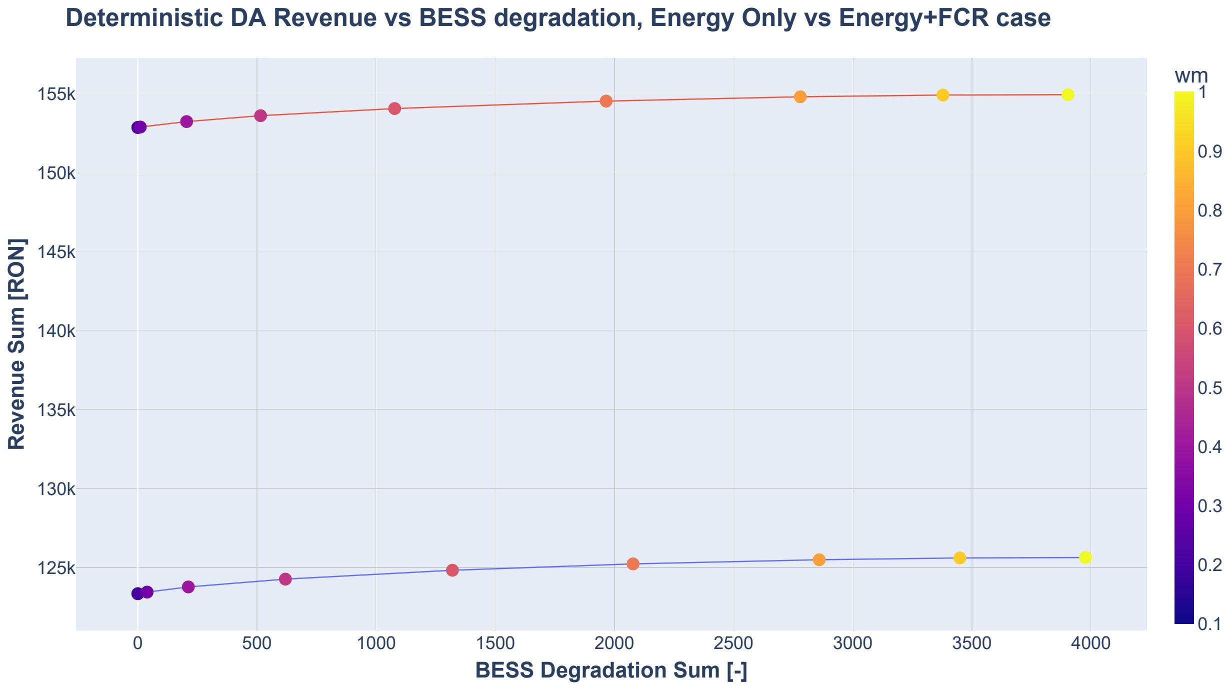

Figure 31: Deterministic DA Total Revenue vs Total BESS Degradation for w_M varying. Comparison between the problem of energy (red line) provisioning and the problem of energy+FCR (blue line) provisioning.

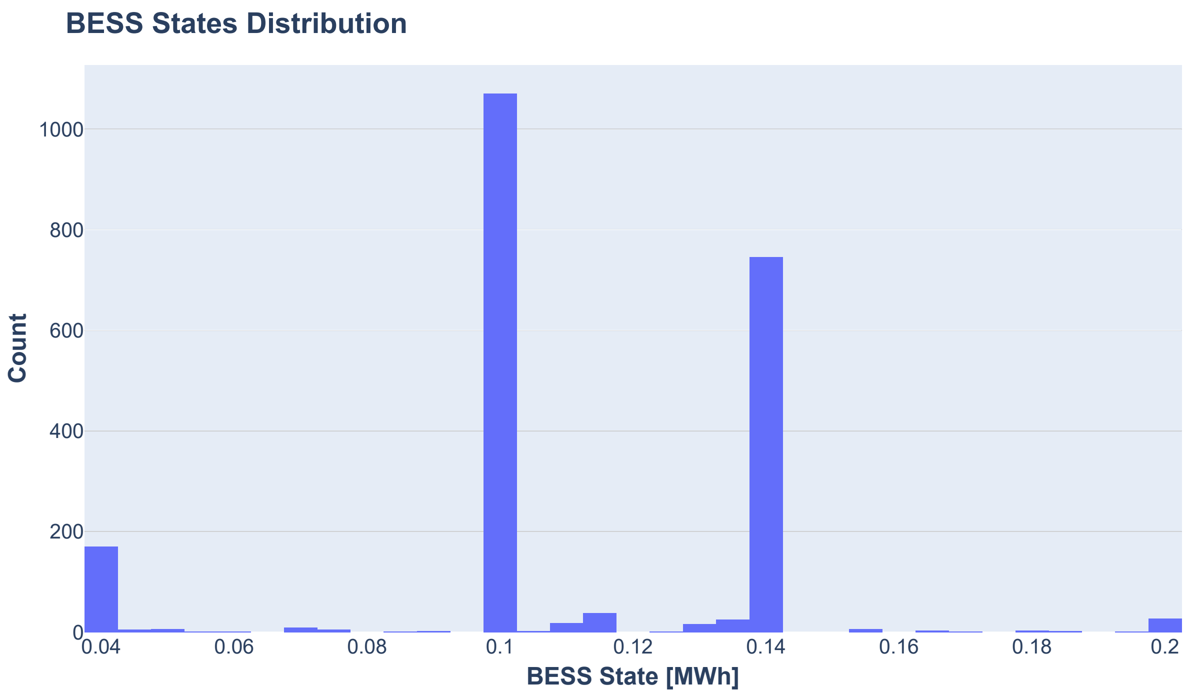

Figure 32: Distribution of the BESS state with the CCT degradation model

as averages over all batches. Looking at the VSS values, computed as the difference between *Stochastic Objective* and 2^{nd} *Stage Objective*, it is possible to conclude that in both cases the stochastic solution is able to find a better solution with respect to the deterministic case. In particular, the stochastic approach is able to provide a 6.5% of decrease in the objective value of

This project has received funding from the European Union's Horizon 2020 research and innovation programme under grant agreement No 864337

the 2^{nd} stage problem in the provision of energy case and a decrease of 15.1% in the provision of energy and AS case.

Value of Stochastic Solution (VSS)			
Problem	**Stochastic Objective**	2^{nd} **Stage Objective**	**VSS**
Provision of energy	-632.8	-594.2	-38.6
Provision of energy + FCR	-873.7	-759.3	-114.4

Table 4: Value of the Stochastic Solution for the provision of energy and provision of energy + FCR cases.

7.2 Short-Term (ST) Evaluation

Moving to the ST stage of the framework, it is possible to investigate the performances of the different MPC strategies that have been implemented, in both cases of provision of energy only and provision of energy+FCR. Starting from the DRT-MPC, it should be kept in mind that the aim of this approach is to minimize the DA-ST error in the energy delivery and the DA-ST error in the BESS state. Using a neutral weight $w_e = 0.5$ in the optimization problem (38), some simulations have been performed to investigate the behavior of the DRT-MPC controller. To this aim, Fig. 33 shows, for an example period of 3 days, the difference between the energy delivery error and the BESS state error. It is easy to understand qualitatively that the major contribution to the MPC error is given by the energy delivery term. A quantitative measure of this can be easily obtained by computing the average error over a simulation period of ~ 1 month:

- The average weighted quadratic energy delivery error is 0.795.
- The average weighted quadratic BESS state error is 0.007.

Thus, one may ask the reason of such a large energy delivery error. This can be related to the so called *RES forecast difference*, defined as the difference between the DA RES forecast and the intraday RES forecast. Since the intraday RES forecast used in the MPC changes at each iteration of the controller for the prediction horizon $N = 6h$, this difference is computed as the average difference between the $6h$ DA RES forecast and the $6h$ intraday RES forecast over all iterations of the MPC controller. For an example period of 3 days, Fig.34 shows the absolute average RES forecast difference (in red) and the weighted quadratic energy delivery error (in blue). Already from a qualitative analysis of this plot it is possible to guess that there exist a strong correlation between this RES forecast difference and the energy delivery quadratic error term in the DRT-MPC. A quantification of this similarity can be given by means of the Cross-Correlation of the two signals, which is a measure of similarity of the two series as a function of the displacement of one relative to the other. Among the various definitions of this measure, here the following one has been used:

$$(f \star g)[n] = \sum_{n} f^*[m] g[m+n], \tag{67}$$

where f and g are discrete functions and $f^*[m]$ denotes the complex conjugate of $f[m]$.
For the purposes of this evaluation, the two signals have been first normalized, in order to have zero mean and unitary standard deviation, to compute then their normalized Cross-Correlation. Given a series $f[n]$ with mean μ_f and standard deviation σ_f, this normalization is performed as:

$$\bar{f}[n] = \frac{f[n] - \mu_f}{\sigma_f}, \tag{68}$$

This project has received funding from the European Union's Horizon 2020 research and innovation programme under grant agreement No 864337

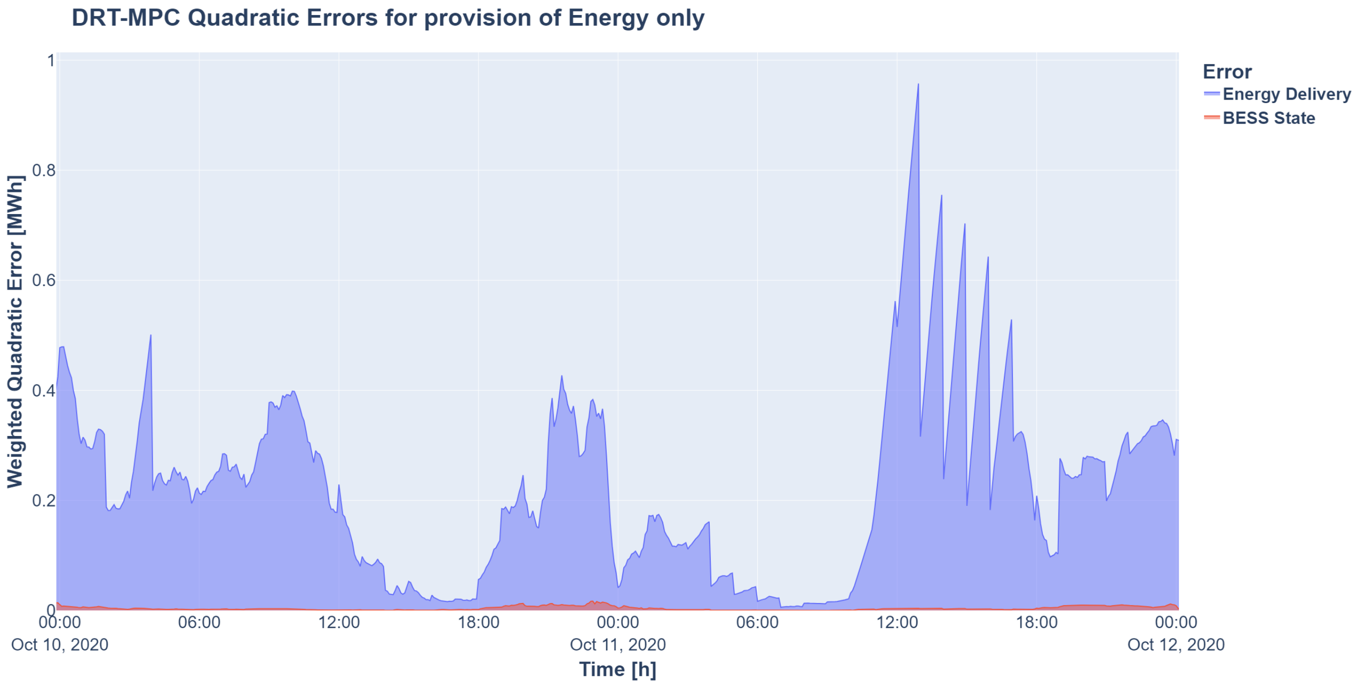

Figure 33: Comparison between the DRT-MPC weighted quadratic errors (energy delivery error and BESS state error) in the provision of energy only case. Large part of the DRT-MPC error is due to the energy delivery.

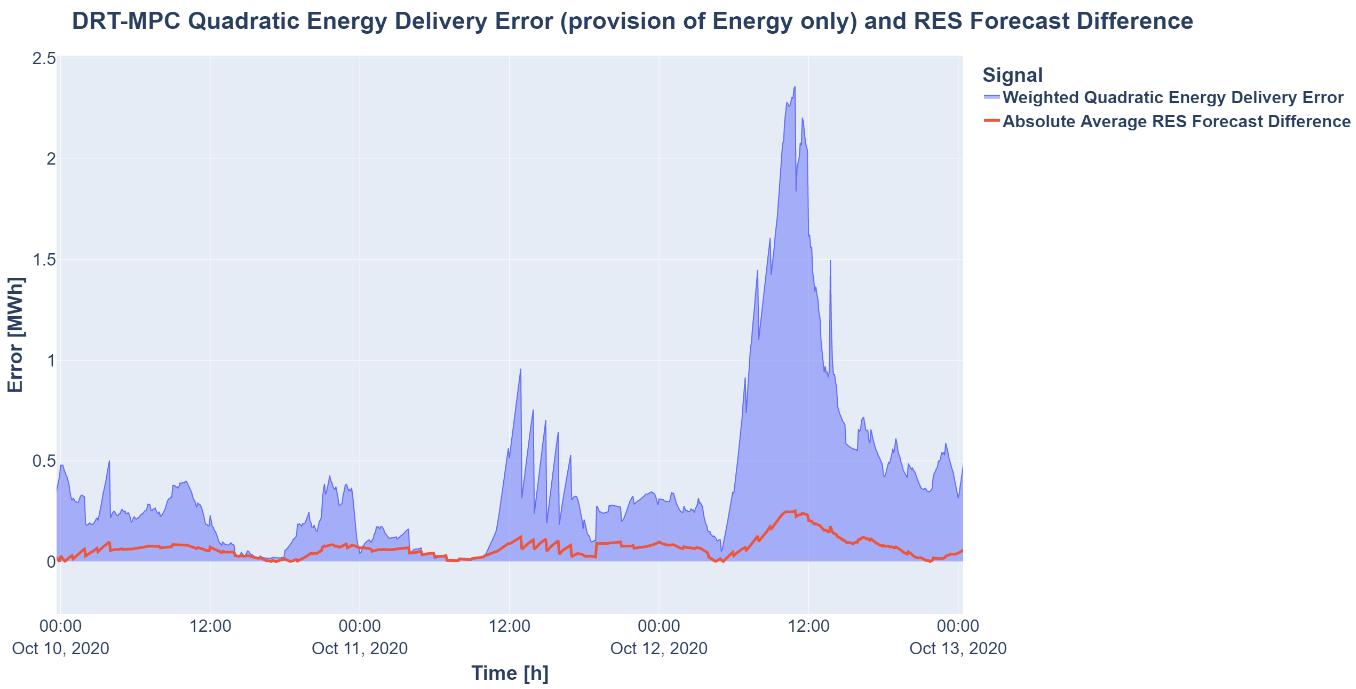

Figure 34: Comparison, for a period of 3 days, between the DRT-MPC weighted quadratic energy delivery error and the absolute average RES forecast difference between DA and intraday.

where $\bar{f}[n]$ is the normalized signal.

As a result of these computations, Fig.35 shows the normalized Cross-Correlation between the DRT-MPC weighted quadratic energy delivery error and the RES forecast difference. It is possible to conclude that a strong correlation exists between these two signals. Thus, to summarize

This project has received funding from the European Union's Horizon 2020 research and innovation programme under grant agreement No 864337

the previous analysis, the error in the DRT-MPC strategy is mostly due to the energy delivery term. Moreover, this error is found to be strictly related to the difference between the DA and intraday RES forecast, which is the only source of uncertainty in the system.

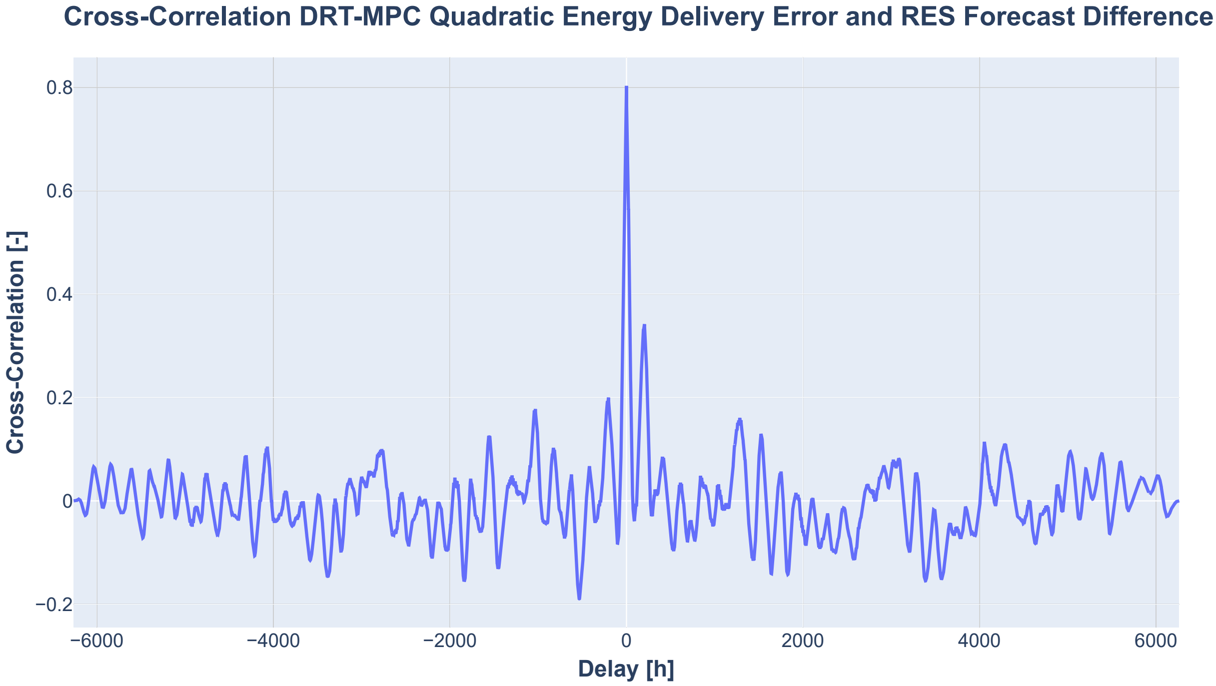

Figure 35: Normalized Cross-Correlation between the DRT-MPC weighted quadratic energy delivery error and the RES forecast difference.

Fig.36 shows the evolution of the sum of the weighted quadratic tracking errors in the DRT-MPC controller, for the problem of provision of energy only, when using the DA RES forecast affected by Gaussian noise with increasing standard deviation. Five points are computed (for standard deviation values $\sigma = 0, 0.05, 0.1, 0.15, 0.2$) and interpolated in the plot. The figure shows that the sum of the weighted errors (*i.e.*, the objective) increases exponentially with the standard deviation. The major contribution is given by the quadratic error in the energy delivery, but also the error on the BESS scheduling tracking becomes more significant the more the RES forecast is perturbed.

Using the same reasoning in the generation of the intraday forecast as a perturbed version of the DA one, Fig.37 shows a comparison in the objective sum (weighted sum of the tracking errors) between the two problems of provision of energy and energy+FCR. The evolution is shown to be the same but, as expected, a huge degradation in performances is observed when considering also the AS (from values of the objective in between $[1000, 4000]$ to values in $[47000, 50000]$).

The same sensitivity analysis has been performed for the economic-oriented strategies, which have proven to be much less sensitive to perturbations in the RES forecast. Fig. 38 shows a similar plot of Fig. 37, now for the DE-MPC instead of the DRT-MPC. The first important difference that can be found between the DRT-MPC case and the DE-MPC approach, is that with the latter one, the AS can be exploited to obtain a higher revenue (*i.e.*, a lower objective function, which in this case represents costs in [RON]), while with the DRT-MPC a degradation in performance was obtained when considering also the presence of the AS. Moreover, the difference between the objective function values obtained when considering the provision of energy problem or the provision of energy+FCR is much less significant than the one observed for the DRT-MPC case. Thus it is possible to conclude that an economic-oriented MPC approach

This project has received funding from the European Union's Horizon 2020 research and innovation programme under grant agreement No 864337

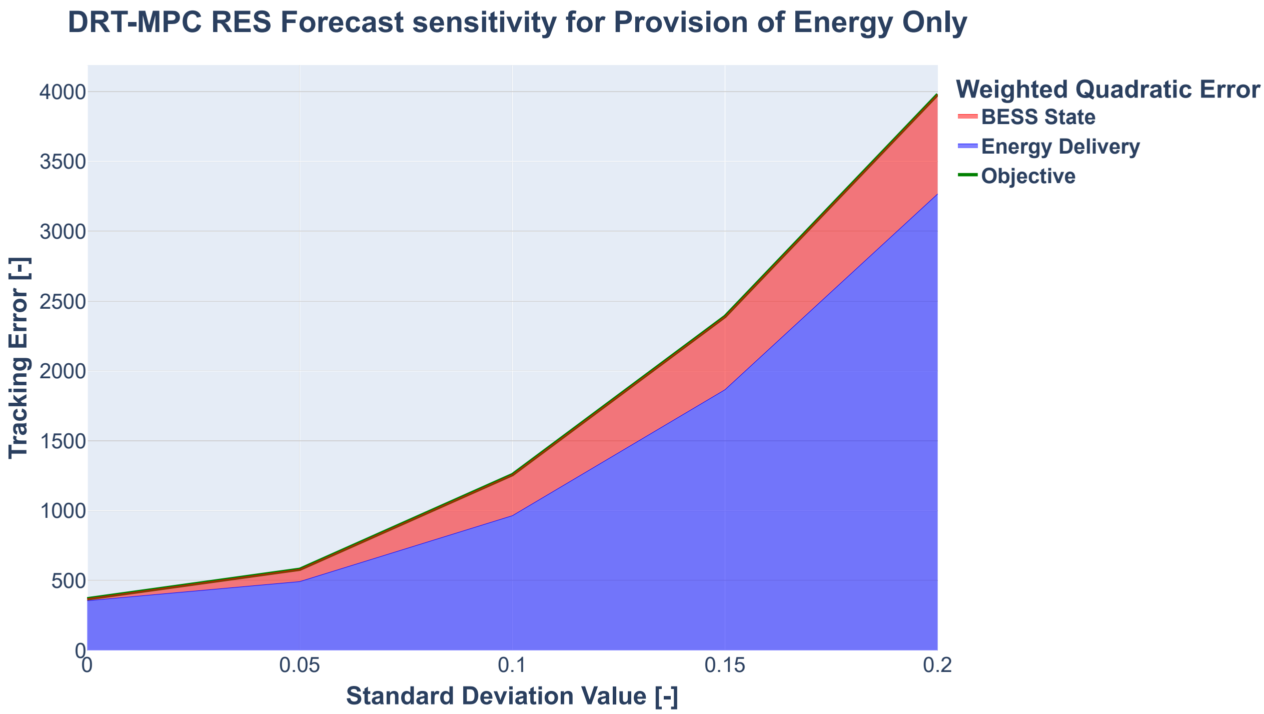

Figure 36: Tracking errors sensitivity to the RES forecast in the DRT-MPC optimization problem, for provision of energy only.

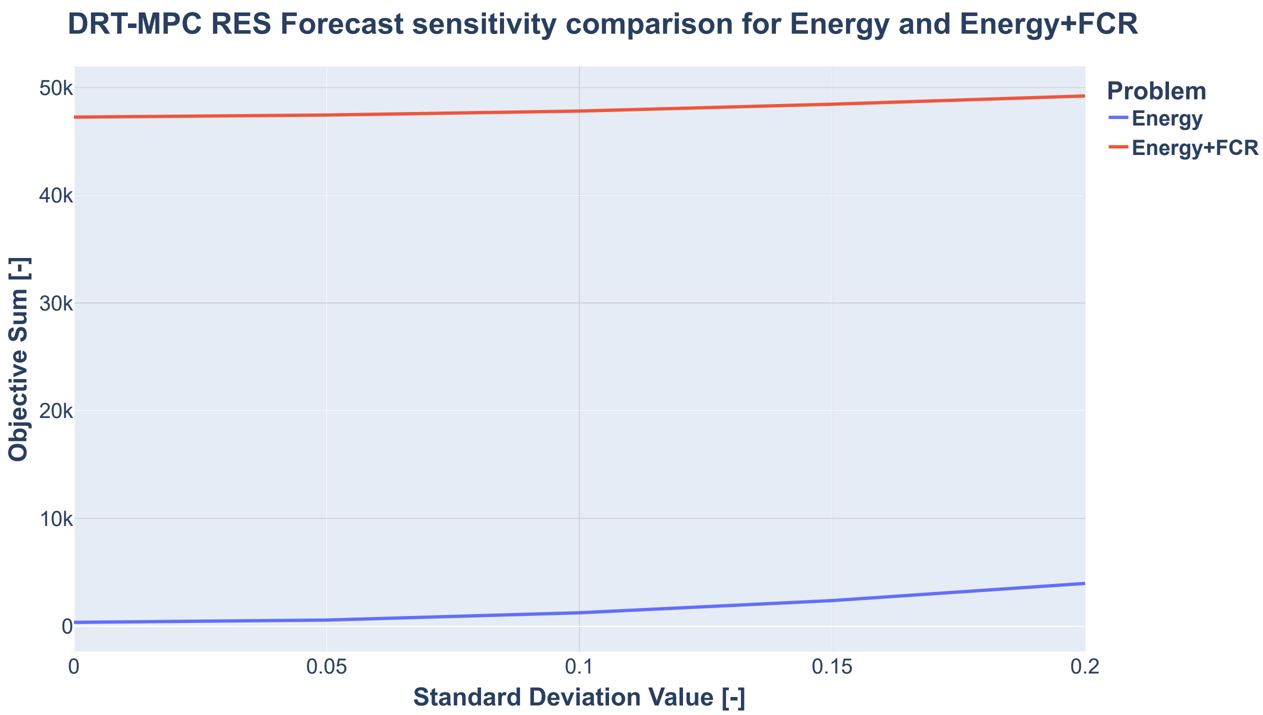

Figure 37: DRT-MPC forecast sensitivity comparison between the problem of provision of energy and provision of energy+FCR.

results to be much less sensitive to errors in the RES forecast, with respect to a canonical reference tracking MPC strategy.

This project has received funding from the European Union's Horizon 2020 research and innovation programme under grant agreement No 864337

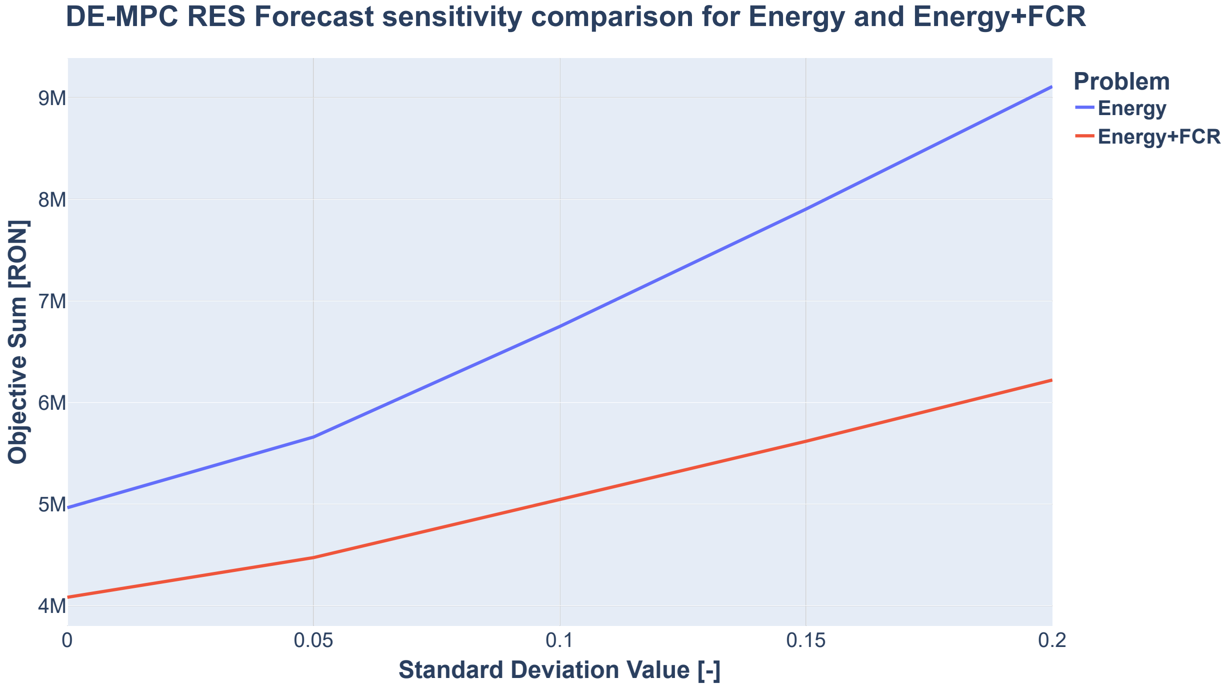

Figure 38: DE-MPC forecast sensitivity comparison between the problem of provision of energy and provision of energy+FCR.

7.3 Ex-Post Evaluation

Table 5 shows a comparison between the three proposed strategies, in terms of total revenue obtained on the energy and AS markets and the BESS degradation obtained via the CCT degradation model (5). In the table we report the mean and standard deviation values over the trading period of interest. The obtained results show that the economic-oriented approaches (DDA+DEMPC and SDA+SEMPC) are able to significantly overcome the traditional DDA+DRTMPC approach on both scores. Compared with this traditional approach, the DDA+DEMPC and SDA+SEMPC show an increase of 12% and 13%, respectively, on the average markets revenue and a decrease of 25% and 23%, respectively, on the average BESS degradation. The results obtained with the economic-oriented strategies are quite similar, but the stochastic approach shows a small reduction in the standard deviation of both scores. This is a first indication of the higher robustness of the stochastic approach with respect to system uncertainties.

To complete this analysis, in Table 6 we report the ex-post energy deviations and AS deficits. Both the economic-oriented approaches are able to avoid AS deficits on average, which implies a higher reliability of the BSP. In order to obtain this without increasing significantly the storage degradation, the latter approaches perform larger deviations, on average, from the DA energy offer, compared to those of DDA+DRTMPC. This choice is motivated by the fact that, in the available price data, AS deficits are much more penalized than energy deviations. This is expected to have a small impact on the traditional DDA+DRTMPC approach, whose control strategy is insensible to prices, while it is expected to have a significant impact on the economic-oriented approaches. Indeed, a traditional approach will tend to distribute the deviations among all the services, while an economic-oriented strategy will tend to concentrate them just on the less profitable markets. Thus, under these price conditions, when choosing DDA+DEMPC or SDA+SEMPC instead of DDA+DRTMPC, a reduction in the revenue obtained from the energy market is expected, in exchange for a large increase in the revenue on the AS markets and a

This project has received funding from the European Union's Horizon 2020 research and innovation programme under grant agreement No 864337

significant decrease in the storage degradation.

Table 5: Ex-post markets revenue (total revenue from energy and ASs markets) and BESS degradation with the proposed approaches for trading and control. For the trading period, the table shows for each approach: hourly mean (standard deviation).

Score [RON]	**DDA + DRTMPC**	**DDA + DEMPC**	**SDA + SEMPC**
Markets Revenue	440.2 (123.2)	494.7 (110.6)	497.5 (109.2)
BESS Degradation	1.3 (1.4)	0.97 (1.4)	1 (1.3)

Table 6: Ex-post energy imbalances and ASs deficits with the proposed approaches for trading and control. For the trading period, the table shows for each approach: hourly mean (standard deviation).

Score [MWh]	**DDA + DRTMPC**	**DDA + DEMPC**	**SDA + SEMPC**
$E^{\uparrow}$	0.06 (0.13)	0.07 (0.16)	0.06 (0.16)
$E^{\downarrow}$	0.37 (0.36)	0.44 (0.44)	0.45 (0.44)
δ^{FCR}	0.003 (0.01)	0 (0.0)	0 (0.0)
$\delta^{aFRR,\uparrow}$	0.03 (0.08)	0 (0.0)	0 (0.0)
$\delta^{aFRR,\downarrow}$	0.12 (0.15)	0 (0.0)	0 (0.0)

Fig. 39 reports a one day comparison of the typical BESS scheduling computed via the traditional approach and the stochastic economic-oriented approach. During this day there is no activation of FCR and the aFRR prices are constant. Thus, the storage commands are affected mostly by energy prices and aFRR activation signals. Then, we can relate the storage SoC evolution to three main events: energy peak price periods (indicated as P), large aFRR activation times in the positive and negative directions (indicated in as R^{+} and R^{-} respectively). Two energy peak price periods occur during the day, first in the morning, than in the late evening. Since the prices are assumed to be know already at DA, both strategies are able to identify these events and discharge the storage to capitalize this favourable market condition. On the contrary, when large activation of aFRR occurs, the traditional strategy is not always able to respond properly. This is as consequence of the fact that the DRTMPC strategy aims to track the BESS scheduling computed at DA, when it is almost impossible to predict the exact times and volumes of activated reserves. Thus, when a first R^{+} period occur (approximately at 4 a.m.) the storage is charged with the traditional approach instead of being discharged as expected. When a second positive aFRR activation occurs (approximately at 5 p.m.) the economic-oriented approach fully discharge the BESS, while the traditional control approach shows only a very small discharge, probably resulting in large deviations from DA offers. Moreover, at R^{-} (approximately at 8 p.m.), when the storage is expected to charge to compensate for a negative aFRR activation, the traditional strategy shows just a minor charge, since again the DA BESS scheduling to be tracked was unable to identify this major event. As a final consideration, Fig. 39 clearly shows the drawbacks of the non-inclusion of the BESS degradation model in the traditional MPC approach. Indeed, compared to the SEMPC strategy, with DRTMPC the storage performs many more smaller charge/discharge cycles, resulting in an higher cycling ageing, and it is kept above the $x^{thr,max}$ (80% SoC in this case) for much longer periods, resulting in an higher calendar ageing as well.

As should be evident from the previous analysis, the deterministic and stochastic economic-oriented approaches show very similar results in terms of average scores, energy imbalances

This project has received funding from the European Union's Horizon 2020 research and innovation programme under grant agreement No 864337

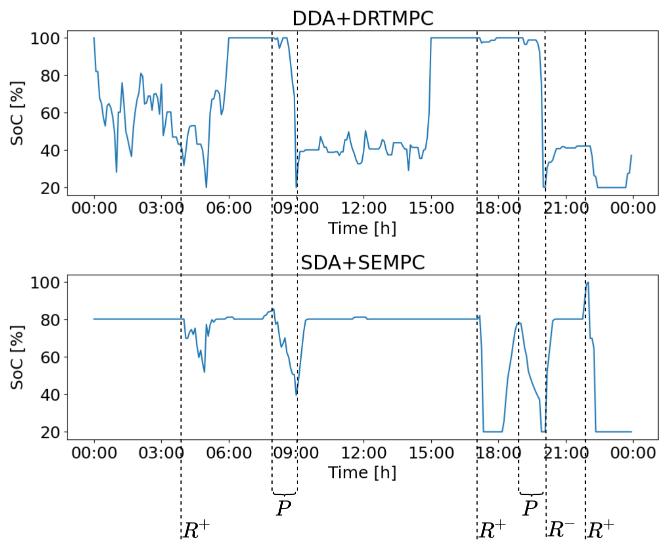

Figure 39: One day BESS scheduling comparison between DDA+DRTMPC (top) and SDA+SEMPC (bottom). P identifies energy peak price periods, while R^+ and R^- identify large aFRR activations in the positive and negative direction respectively.

and AS deficits. Thus, the higher effort required to implement the stochastic strategy may appear to be unjustified. To show the advantages of a stochastic solution of the problem, we propose an analysis of the economic-oriented approaches in terms of robustness with respect to errors in the forecast of system uncertainties. Call intraday forecast error the difference between the average intraday renewable production forecast over all scenarios and the actual observation of renewable production. Then, Fig. 40 shows the objective function (difference between markets revenue and BESS degradation) mean and standard deviation values over the trading period, for the DDA+DEMPC and the SDA+SEMPC approaches, as a function of increasing values of intraday forecast error. The figure clearly shows that the stochastic ap-

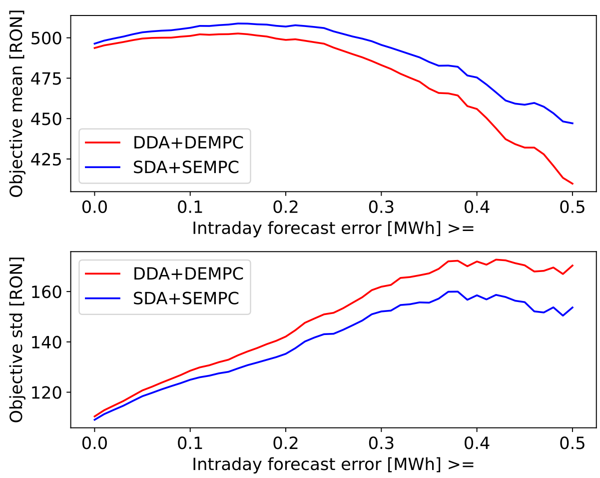

Figure 40: Objective (difference between markets revenue and BESS degradation) mean (top) and standard deviation (bottom) values over the trading period, with the DDA+DEMPC approach (in red) and SDA+SEMPC approach (in blue), as a function of the intraday renewable production forecast error.

proach is able to give significantly more robust results. Indeed, the objective mean value is always higher in the stochastic approach with respect to the deterministic case and conversely

This project has received funding from the European Union's Horizon 2020 research and innovation programme under grant agreement No 864337

the standard deviation is always lower. In addition to this, this difference is shown to increase the more the prediction error increases. Thus, prediction errors are expected to have a smaller impact on the stochastic framework compared to the deterministic approach.

7.4 Evaluation of the Machine Learning alternative

This subsection concludes the presentation of results with an evaluation of the Machine Learning alternative for the trading and control developed in Section 4.8. The case study considered here is a generic storage device that operates with an aggregation of renewable plants presented in [30]. This hybrid system follows two objectives, namely trading on the DA energy market and control its output so as to minimize the deviation between trading decision and actual power output.

The approach is tested on an aggregation of 3 Wind Power Plants (WPPs) and 1 PV plant, with a total capacity of 49 MW (16% PV share), respectively located in northern and southern France. The parameters of the BESS are shown in Table 7. Explanatory variables include NWP and energy market prices and quantities. wind speed, wind direction, temperature, cloud coverage, and solar radiation forecasts for each plant location. Models are trained on one year of historical data spanning 2019 and evaluated on the first 4 months of 2020. Lastly, a half-hour settlement period is assumed for the energy market (DA and balancing stage).

Table 7: Storage parameters (normalized).

Parameter	Value
B^{max}	0.5
c^{ch}	$0.5B^{max}$
c^{dis}	$0.2B^{max}$
η^{ch}	0.8
η^{dis}	0.9

Contextual information x comprises features typically used as input in forecasting applications. A forecast horizon of 12-36 hours ahead is considered. In order to deal with possible temporal correlations, we conduct a preliminary analysis by examining the partial autocorrelation function (PACF) of target variables (energy and prices) and include relevant lags as additional features in x. By sufficiently enlarging the feature space x with historical lags, we treat training data (y_i, x_i) as i.i.d.

Regarding renewable production, the feature vector x^E comprises weather forecasts from a numerical weather predictions (NWP) model, namely wind speed, wind direction, temperature, cloud coverage, and solar radiation forecasts for each plant location. The NWP forecasts are issued at 00:00 on day D-1 spanning a horizon of 24-48 hours ahead. Examining the PACF did not reveal any lags to be important, thus we do not include any in x^E; this result is standard in renewable forecasting for horizons larger than a couple of hours ahead.

Regarding market data, we employ data from the French electricity market for the same period, downloaded from ENTSOE Transparency Platform. Market-related contextual information x^{market} include historical lags (as indicated from the PACF) for DA prices (one day and one week prior), historical lags for system imbalance volumes (two days prior), and DA forecasts for available thermal generation, electricity demand, and renewable generation at transmission level.

This project has received funding from the European Union's Horizon 2020 research and innovation programme under grant agreement No 864337

The system-wide forecasts issued from the operator are processed to determine a net load series, by subtracting the expected renewable production from the expected electricity demand, and a system margin series, defined as the ratio of net load to available thermal generation. In addition, we include categorical variables for the calendar effect, namely day of the week and hour of the day. For the tree algorithm, feature vectors x^E and x^{market} are concatenated, resulting in a total of $d_x = 20$ features.

Our goal is to showcase the ability of the proposed approach to provide informed decisions under different objectives using a single data-driven model, without the need to deploy multiple forecasting models. The following approaches are compared:

- *FO*: The standard sequential modeling approach. This involves 1) deriving probabilistic energy forecasts using the classical Quantile Regression Forest (QRF) model, 2) forecasting the unit regulation costs with exponential smoothing, and 3) solving a stochastic optimization problem.
- *PF*: Predictive prescriptions with weights derived from a prescriptive forest with random splits.

For the sake of comparison, the naive SAA solution and the perfect-foresight solution are also estimated. Optimization problems are solved either analytically, when applicable, or numerically. As mentioned, different values of design parameter k define different objectives; thus, a different prescriptive forest is trained for each value of k. Note that we consider offline (batch) learning, thus we implicitly assume stationarity. If the underlying processes are non-stationary, then offline learning will not suffice and online learning should be considered. This is outside the scope of the current work but presents an interesting research direction.

The proposed approaches are examined in terms of out-of-sample prescriptive performance and trading results. For the former, we employ the coefficient of prescriptiveness P [31], a unitless metric that measures relative optimization performance against a naive Sample Average Approximation (SAA) and the perfect-foresight solution. Specifically, for each i in $\{FO, PF\}$ and different values of design parameter k the coefficient P is estimated as:

$$P_{i,k} = 1 - \frac{\widehat{v}_k^i - \widehat{v}_k^*}{\widehat{v}_k^{SAA} - \widehat{v}_k^*}, \tag{69}$$

where $\widehat{v}_k^i, \widehat{v}_k^{SAA}, \widehat{v}_k^*$ are the aggregated cost over the test set under the i, SAA, and perfect-foresight method. Note that the SAA approach optimizes over the empirical distributions without leveraging contextual information. The coefficient P is bounded above by one, while negative values indicate a failure to outperform the SAA. Regarding trading results, we estimate aggregated profit and risk. The conditional value at risk at 5% level ($CVaR_{5\%}$) is used as a proxy for trading risk, defined as the expected profit over the 5% worst returns.

As shown in [30] in practice there is no significant difference between the optimal offering strategy and offering the expected energy production under a dual-price imbalance setting for the energy market. Therefore, the operational control policy implemented, *i.e.*, using storage to minimize deviations from the submitted schedule, also makes sense from an economic perspective.

Table 8 shows results for a value of $k = 0.75$. In terms of trading performance, the proposed method attains a 3.07% profit increase, accompanied with a decrease in $CVaR_{5\%}$. The prescriptive performance is also improved as evident by the increased value of coefficient P. Values attained are also higher than a case study without storage, presented in the full article. In conclusion, results of this use case show that the proposed approach based on prescriptive

This project has received funding from the European Union's Horizon 2020 research and innovation programme under grant agreement No 864337

analytics achieves a similar profit to the complex 'Forecast-Then-Optimize' complex approach, with even lower risk of worst returns. Finally, it is shown in the full article [30] that an analysis of the prescriptiveness enables to quantify the impact of all explanatory variables in the feature set x on the decision cost.

Table 8: Results-Storage ($k = 0.75$)

Method	FO	PF
Total Profit (10^3 EUR)	1 628	1 678
$CVaR_{5\%}$ (EUR)	-8.88	-6.12
Coefficient P	0.89	0.92

This project has received funding from the European Union's Horizon 2020 research and innovation programme under grant agreement No 864337

8 Advanced ancillary services in isolated power systems with high RES penetration

8.1 Overview of Non Interconnected islands with high renewable penetration

This chapter is devoted to describe the characteristics of non interconnected islands (NII), evaluate the services required by a BESS unit to safely reach high RES penetration levels and propose a framework to include this services in the economic dispatch of the system. In Fig.41 the scheme of a NII operating in high RES penetration levels is presented.

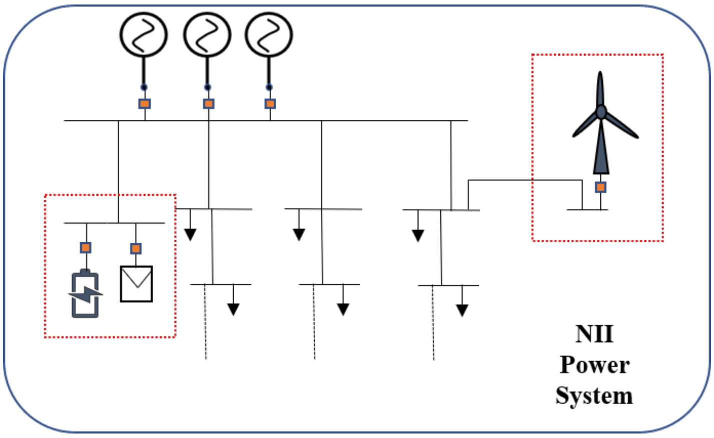

Figure 41: Non-interconnected island system scheme.

To reach that target RES plants, *i.e.* Photovoltaic (PV) and Wind Turbine (WT) plants, are installed in the system additional to the existing diesel generators. The installation of a BESS unit is also necessary for the provision of ancillary services crucial to the system operation. The characteristics of those services, however, could differ from the existing services provided by the diesel generators. It will be explained in the following sections that the different nature of these services should be considered also in the economic dispatch of the generating units to ensure the security of power supply.

In this chapter, the necessary services of the BESS unit will be described, trying to find possible gaps of the existing greek NII network code. Then, a methodology will be presented to extract linear constraints for the economic dispatch that include the different characteristics of crucial BESS ancillary service, *i.e.* synthetic inertia, FCR. Finally, the formulation of a stochastic economic dispatch with frequency constraints is presented that receives probabilistic forecast inputs from the forecast algorithms proposed in WP3 (ref).

8.2 Battery storage ancillary services in small isolated island systems

NII are small electrical systems with a limited number of thermal generators. Maintain security in the island's operation is a demanding task, which becomes more challenging as RES penetration increases. In such systems the provision of ancillary services by a BESS unit is important. Several AS have been introduced in grid codes or proposed in research to address the challenges that rise under those circumstances. Nevertheless, it is not clear if the services described in the greek NII code are sufficient to ensure proper operation. Therefore, it is necessary to evaluate the different services, find possible gaps and propose what AS must be provided by the BESS unit.

8.2.1 Frequency containment reserves

Several grid codes have proposed the provision of FCR by the BESS unit to assist in frequency control. This service is provided dynamically according to the deviation of frequency as presented in Fig.42. Around the nominal value of frequency a deadband is usually consider to avoid deployment of reserves for small frequency transients. The upward FCR are deployed in underfrequency events proportionally to the deviation of frequency, similar to the concept of droop controllers in thermal generators. The same holds true for downward FCR that are deployed in overfrequency events. Downward FCR can be also deployed by RES units by curtailing their output power according to the frequency. RES plants can only provide upward FCR if they are curtailed from their maximum power prior to the frequency event.

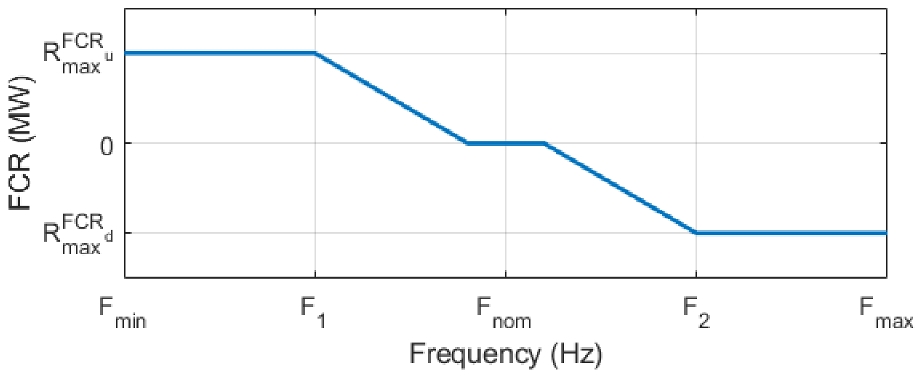

Figure 42: BESS FCR service.

FCR are deployed to stop the decay (or rise) of frequency after a power imbalance in the system. In order to stabilize the frequency to a new point the total FCR levels of the generating units providing this service must be greater than the disturbance expected. In high RES penetration levels a limited number of thermal generatrs operate thus the FCR will be mainly deployed by the BESS unit. Another important factor is the response speed for the provision of reserves. BESS units are interfaced to the grid through power electronics allowing them a faster response in the FCR provision. In Great Britain this ability is highlighted considering a different AS product, *i.e.* fast FCR, that requires the full deployment of the reserves in less than a second. This is important since the physical inertia are limited therfore fast frequency decays of frequency and high ROCOF events are expected.

To evaluate the services a dynamic model of Astypalea power system was implemented in DIgsilent Powerfactory. The characteristics of this island are presented in detail in the next chapter. A scenario of 2MW demand was simulated with the diesel generator operating at 0.4MW and the WT at 1.2MW and the BESS unit discharging at 0.4MW, resulting in 80% inverter resources penetration.This scenario can be critical for security since it has the limited amount of inertia (1 synchronous unit operates) and limited amount of FCR levels by the BESS since it discharge power. The disconnection of the WT was the contingency performed. Different time responses were simulated for the provision of FCR by the BESS unit (Fig.43). The

This project has received funding from the European Union's Horizon 2020 research and innovation programme under grant agreement No 864337

impact of the speed response on the frequency and ROCOF transients are presented in Fig.44 and Fig.45 respectively.

As expected the faster response results in less severe transients. However, with the response of 1s that is usually described in most grid codes the frequency transient can be severe surpassing the Under Frequency Load Shedding (UFLS) relays settings, which can result in load curtailment despite the presence of adequate levels of FCR. The load curtailment could be probably avoided with a faster response, *i.e.* of 0.5s. Nevertheless, even with the faster provision of FCR the transient in ROCOF remain critical and surpasses the threshold of 1Hz/s, imposed by the greek NII code, that allows the generating units disconnection. Furthermore, islanding detection relays in the generating units, that usually detect the island through ROCOF using thresholds of 1HZ/s, could be also tripped. Thus, despite the faster provision this significant ROCOF events can cause a cascaded outage of generation units resulting in total system outage. This issue has been observed in the island of Cyprus when a severe frequency transient exceeded the islanding protection settings leading to the disconnection of 68 MW of wind power [34].

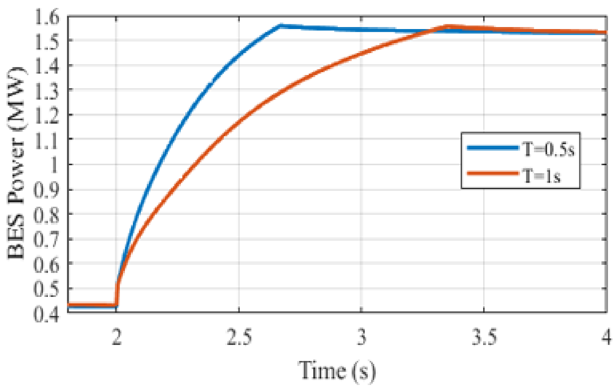

Figure 43: BESS deployment of reserves in different time frames

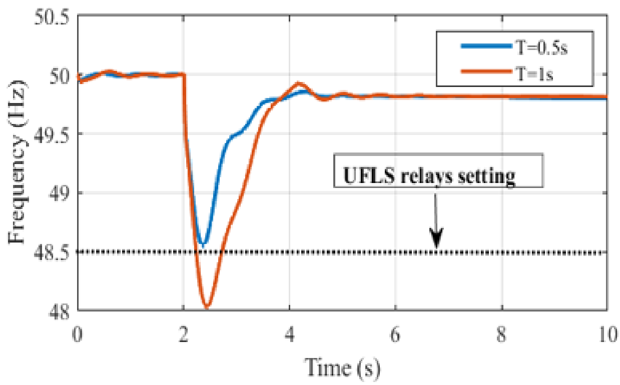

Figure 44: Frequency transient comparison for different time responses of the BESS unit

The reason of the high ROCOF transients is the limited inertia provided by the remaining thermal unit operating in the system. To mitigate this effect, in a power system dominated by power electronics based generation, the provision of a synthetic (or virtual) inertia service has been proposed in research.

This project has received funding from the European Union's Horizon 2020 research and innovation programme under grant agreement No 864337

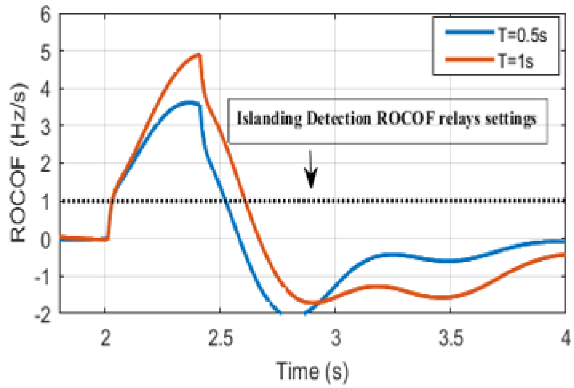

Figure 45: ROCOF transient comparison for different time responses of the BESS unit

8.2.2 Synthetic Inertia

The synthetic inertia service is incorporated in the control of the BESS unit to emulate the mechanical inertia, *e.g.*, mimic the behavior of a synchronous machine. This service can be provided by when the BESS units operates in grid forming control and in grid following. In grid following control the power output modified according to the measured in ROCOF. In grid forming control the BESS unit in a virtual synchronous machine control mimicking the swing equation of a synchronous generator. In both control modes the goal is to modify the power at the beginning of the transient where the ROCOF has its higher values in order to mitigate it.

For the same scenario presented in the previous section, a synthetic (or virtual) inertia services is incorporated to the BESS unit and it is compared with a case where it provides only FCR service. Through the synthetic (virtual - VI) inertia service the BESS unit has a much faster response as presented in Fig.46). This leads to a less severe transient in frequency (Fig.47) as well as in the ROCOF (Fig.48).

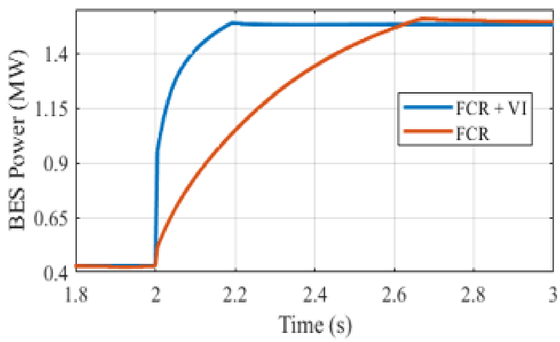

Figure 46: BESS power response comparison with and without synthetic inertia

Thus, apart from a fast FCR service the synthetic inertia service could be required in NII operating in high RES penetration levels. Based on the simulation results the frequency and ROCOF transients, when the BESS unit provides synthetic inertia, are significantly mitigated and do not exceed critical thresholds imposed by the greek NII network code or the protection devices in the NII considered (Astypalea).

In contrast to the synchronous generators that are able to provide multiple times their nomi-

This project has received funding from the European Union's Horizon 2020 research and innovation programme under grant agreement No 864337

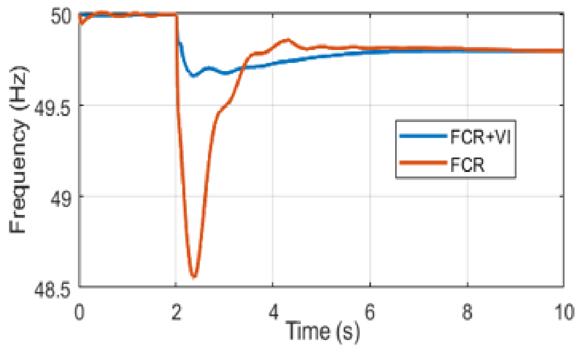

Figure 47: Frequency transient comparison with and without synthetic inertia

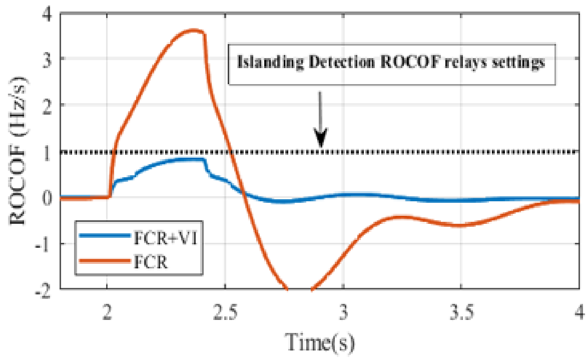

Figure 48: ROCOF transient comparison with and without synthetic inertia

nal current in transients, the BESS limit their current contribution to values close to nominal. Thus, during SI provision this limitation can restrict the unit response, hence despite the BESS controller design to provide SI, its resulting contribution will be limited.

To further illustrate this concern a second scenario was simulated that additional 0.5MW more demand that is covered with additional 0.5MW power discharge from the BESS unit. The power limit was considered at 1.8MW. In both scenarios the WT disconnection was considered as outage. The transient in the BESS power is presented in Fig.49. It is clear that the 1.2MW disturbance can not be compensated entirely in the second scenario since there isn't sufficient power resulting in power limitation. On the other hand, in the initial scenario there is sufficient levels of active power available that allow the power deployment according to the designed SI service.

The power limitation can affect significantly the ROCOF and frequency transients as presented in Fig.50 and Fig.51 respectively. Thus, constraints that consider the aforementioned concern will be modelled and included in the frequency dynamic economic dispatch model proposed in this chapter.

8.2.3 Automatic Frequency Restoration Reserves

In small NII the frequency restoration is performed through an isochronous control that regulates the power setpoints of the thermal units. Their setpoints is usually computed through an integration that is performed to the frequency error. Thus, currently only the diesel generators provide aFRR.

This project has received funding from the European Union's Horizon 2020 research and innovation programme under grant agreement No 864337

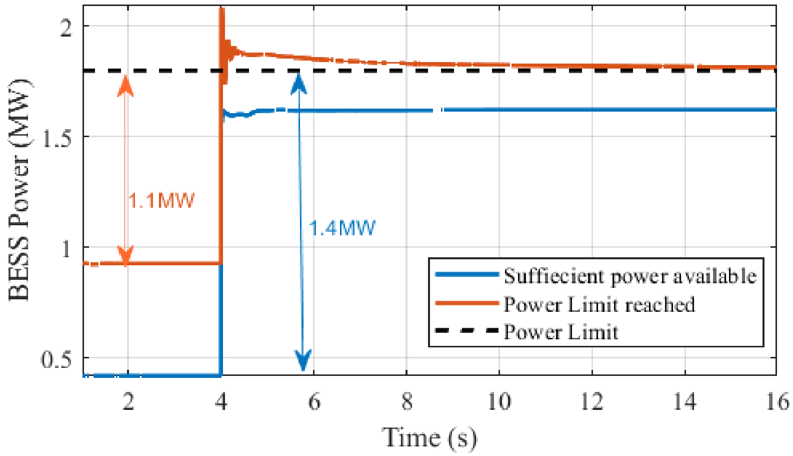

Figure 49: Power output transient comparison in the two scenarios

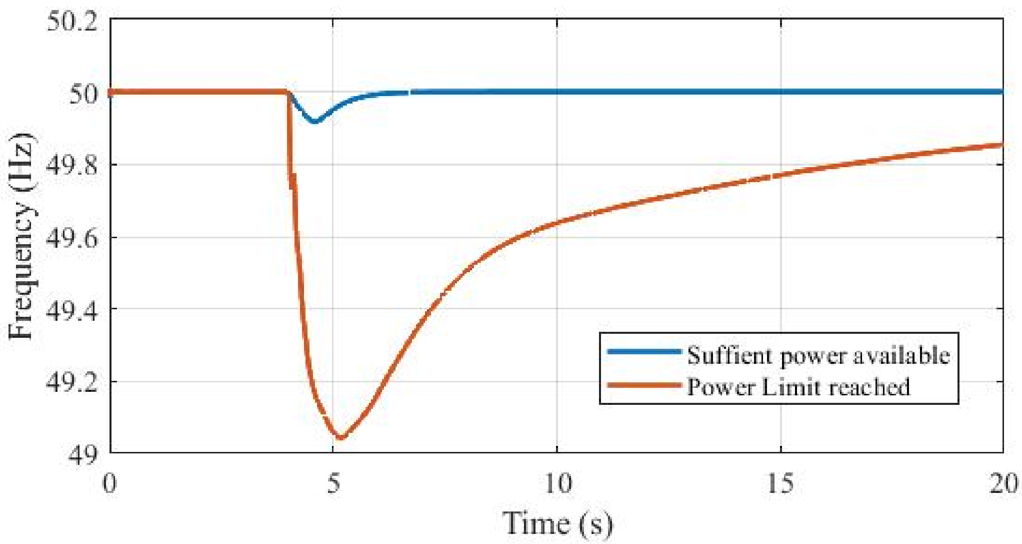

Figure 50: Frequency transient comparison in the two scenarios

Under high RES penetration levels the operating diesel units and their cumulative aFFR are reduced. This can lead to insufficient levels of aFFR to restore the frequency to its nominal value resulting also in overloading of the operating diesel generators. Therefore, the automatic frequency restoration should include also aFRR provided by the BESS unit. To present their impact an automatic frequency restoration is included in the previous example. Two cases were considered. In the first the BESS unit does not provide aFRR and in the second its aFRR are deployed through the central control. In that case 0.8MW of FRR were considered in the diesel unit.

In Fig.**??** the frequency transients are compared. Since the disturbance (WT disconnection results in loss of 1.2MW of production) is greater than the aFRR available in the diesel generator the frequency can not be restored. The provision of aFRR by the BESS unit can compansate the lost generation allowing the frequency restoration to take place. The power transients of the BESS unit and the diesel generator are presented in Fig.**??** and Fig.**??** respectively. As expected the absence of aFRR in the BESS unit results in overload of the diesel generator,

This project has received funding from the European Union's Horizon 2020 research and innovation programme under grant agreement No 864337

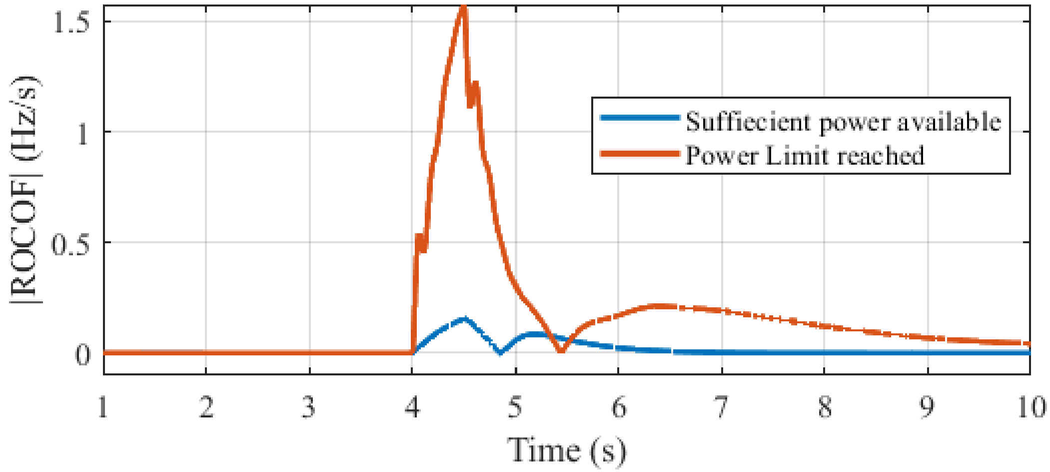

Figure 51: ROCOF transient comparison in the two scenarios

while aFRR provision by the BESS results in better power sharing between the diesel generator and the BESS.

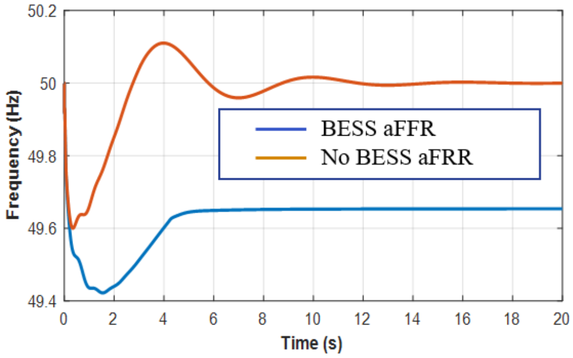

Figure 52: Frequency transient during aFRR response with and without aFRR form the BESS

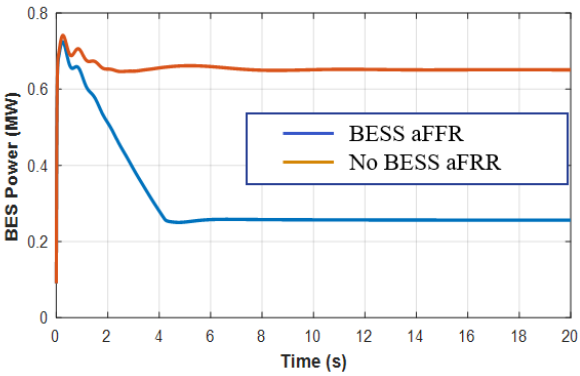

Figure 53: BESS power output power during aFRR response with and without aFRR form the BESS

The aFRR are deployed to restore the adequate FCR levels in the system. However, according to the greek NII code this service have to be maintained for at least 20 minutes. Therefore, it is important to ensure that the BESS unit has sufficient energy stored to supply the aFRR for this time interval without reaching states of charge that can severe impact on the degradation

This project has received funding from the European Union's Horizon 2020 research and innovation programme under grant agreement No 864337

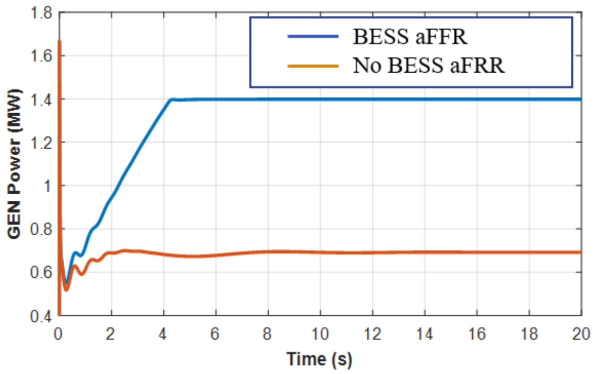

Figure 54: Diesel generator power output power during aFRR response with and without aFRR form the BESS

of the batteries.

In the economic dispatch algorithms the frequency security is ensured through the fulfillment of certain levels of FCR and aFRR. In our formulation the provision of synthetic inertia will be considered too. Both FCR and synthetic inertia will be linked with specific frequency metrics. Nevertheless, there additional services that should be provided by the BESS unit that are crucial for the safe operation of the NII. To present a more broad overview, these services will be also presented even if they are not linked with the economic operation of the system or RES and demand forecast.

8.2.4 Fault Ride Through

When a fault occurs somewhere in the electric network, the voltage drops to lower levels until protection devices detect the faulty area and isolate it. During the fault, generators in close proximity to it experience significant voltage sags at their terminals. In small NII that have limited geographical size and lengths of electrical lines all generating units will experience significant voltage drops.

The disconnection of crucial generators to the NII operation and the loss of significant portion of production during a fault can lead to the interruption of power supply in the island. Modern grid codes and the greek NII code specify the requirements that request uninterrupted operation during faults according to given voltage–time profiles. These requirements are usually referred to as fault ride through (FRT) capability. In Fig.55 the requirements of the controlled plants (diesel and BESS unit) and of RES plants are presented. The units must remain connected for operating conditions that lay above their specific curves. The FRT presented for WT and PV is specified in the code only for Wind power plants but since in small NII large PV plants are considered it is assumed that those plants must have similar requirements.

The limited lengths of the lines in small NII will result in significant voltage sags. At the same time, the replacement of synchronous generators with power electronics interfaced generation will result in a reduction of short circuit current since the later have limited short circuit current contribution (up to 1-1.5 times their nominal current). As a result protection equipment could require higher times to detect and clear a fault. If the fault detection surpasses the time that the FRT requirements allow for the units to remain connected the generation units can be disconnected. Using the existing protection settings in the Astypalea system and performing the a three phase fault in the previous operating scenario the FRT requirements of the generators

This project has received funding from the European Union's Horizon 2020 research and innovation programme under grant agreement No 864337

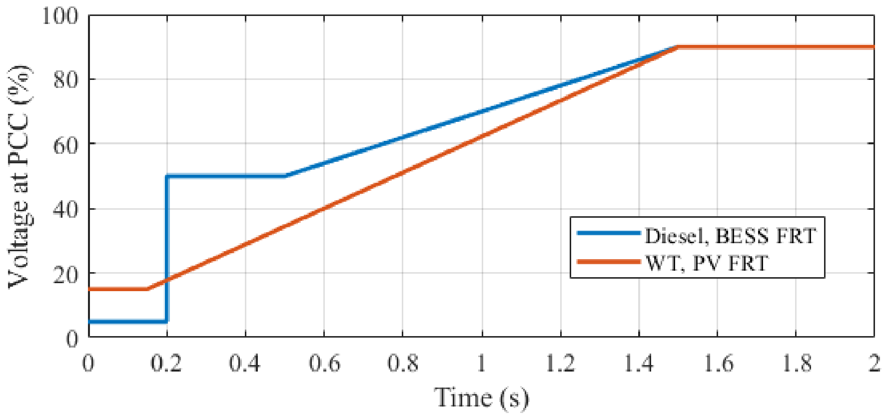

Figure 55: Fault Ride Through requirements according to the greek NII code

are exceeded and are disconnected prior to the fault clearance as presented in Fig.56.

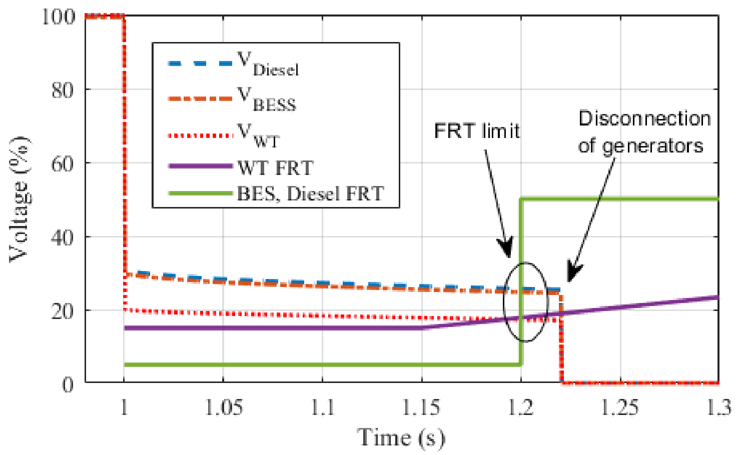

Figure 56: FRT and fault detection coordination concern in a simulation of Astypalea island

To avoid this, more strict FRT requirements can be applied, especially for the BESS unit which is critical to the NII operation. The FRT of the German code or the Australian grid code, which have more strict requirements, are presented in the following figure in comparison to the greek NII code requirements.

Furthermore, the BESS and the rest power electronic based resources should provide short circuit currents during faults both to support the voltage at their PCC and to increase short circuit currents facilitating in a faster fault detection. The current contribution of the Wind power plants is specified in the greek NII code. According to Fig. 58 W should provide reactive current proportionally to the voltage sag. Similar requirements can be included also for the BESS unit. More advanced specifications (*e.g.* current contribution in asymmetrical faults) have not been included in grid codes yet. To increase further the short circuit currents, especially at 100% RES penetration the BESS unit is oversized (ref azores) or a synchronous condenser (ref giglio) is installed. To avoid BESS oversize or the installation of synchronous condensers the adaptive protection scheme has been also proposed in research to address the different short circuit current levels (ref PE).

This project has received funding from the European Union's Horizon 2020 research and innovation programme under grant agreement No 864337

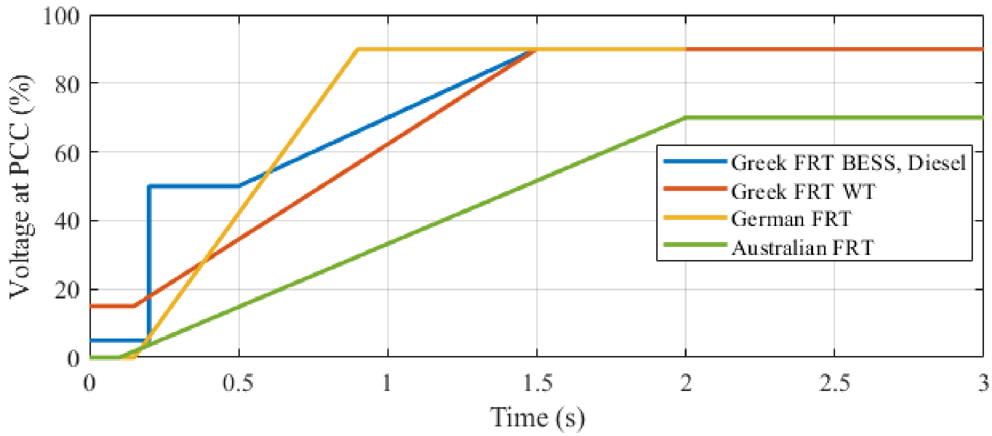

Figure 57: Comparison of FRT in different grid codes.

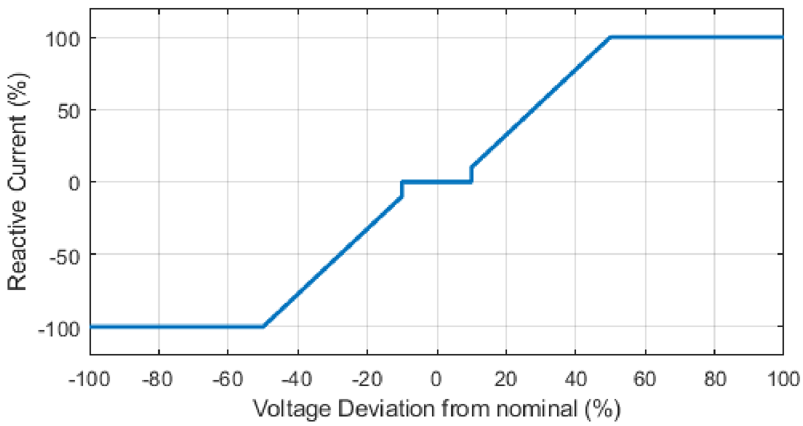

Figure 58: Reactive current provision during faults from WT in the greek NII code

8.2.5 Voltage support

Voltage control in small NII is less complicated than voltage control in large power systems. The small lenght of lines results in less severe voltage rise (at high RES production) or drop (during periods of high demand). Therefore, the voltage control in NII is maintained by having the adequate levels of reactive power reserves. The diesel generators are providing reactive power for voltage control in the NII.

In the NII code it is specified that the BESS unit as well as the rest RES can participate in the voltage control through a Q(V) characteristic (Fig. 59).

Apart from this characteristic the BESS and RES unit can be remotely controlled to operate at specific levels reactive power setpoints or power factor. Thus, even with the disconnection of diesel generators the operating power electronics' interfaced units are able to provide the necessary reactive power to the system.

This project has received funding from the European Union's Horizon 2020 research and innovation programme under grant agreement No 864337

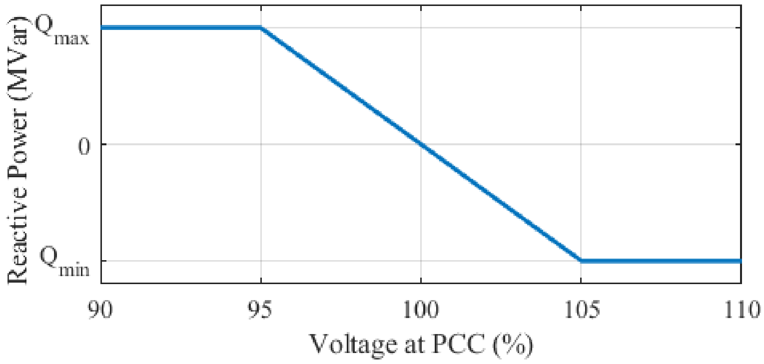

Figure 59: Reactive power to voltage curve in the greek NII code

8.2.6 Grid forming service

To meet the target of high RES penetration (>60%) in small NII, the system should be able to operate in certain periods at 100% RES penetration. Under those circumstances, the diesel generator switch off and only power electronics interfaced units operate in the island. In these periods the BESS unit is the only unit that can direcly control the voltage and frequency in the system. The grid forming ability on a BESS unit allows the direct control of voltage and frequency and is performed usully through a virtual generator control. During black start the same ability of the BESS unit permit the forming of the grid locally and then a sequential connection of the other part of the system. During black start a gradual increase in the voltage amplitude during the re-energization has been proposed to reduce the initial currents that occur during the re connection of transformers aand load.

Grid forming operation can be provided by the BESS unit even with the diesel generators present. In terms of FCR and synthetic inertia provision the grid forming operation can have a faster response compared to grid following, but though proper controller tuning both of the approaches can result in adequate response for those services provision.

The main advantage of grid forming control is its ability to seamlessly transit to operating states of 100% RES penetration without the need of islanding detection techniques or communication signals. A conventional controller of a BESS unit would operate in grid following mode when another grid forming source is present (diesel generator). When that grid forming unit is disconnected the BESS unit switch its control to grid forming. The identification of the diesel unit disconnection can be transmitted through high bandwidth communication, identified through an islanding detection protection or through an islanding detection module of the BESS controller.

All of those options (presented in Fig. 60) have a slight delay until the transition of the control to grid forming, *e.g.* due to communication delays or until the islanding condition is identified. Under this time interval the NII might lack proper voltage and frequency control due to the absence of a grid forming unit. This is avoided by using under all conditions a grid forming control in the BESS unit that emulates a synchronous generator, thus can operate in parallel with the other grid forming units.

In the scenario described in the previous sections the diesel generator outage was considered as contingency. Two control modes were considered. In the first a Grid Forming (GFM) control emulating a synchronous generator and a grid following control (GFL) that measures ROCOF and if it surpasses the threshold of 0.8Hz/s it switch its control to GFM similar to what is pre-

This project has received funding from the European Union's Horizon 2020 research and innovation programme under grant agreement No 864337

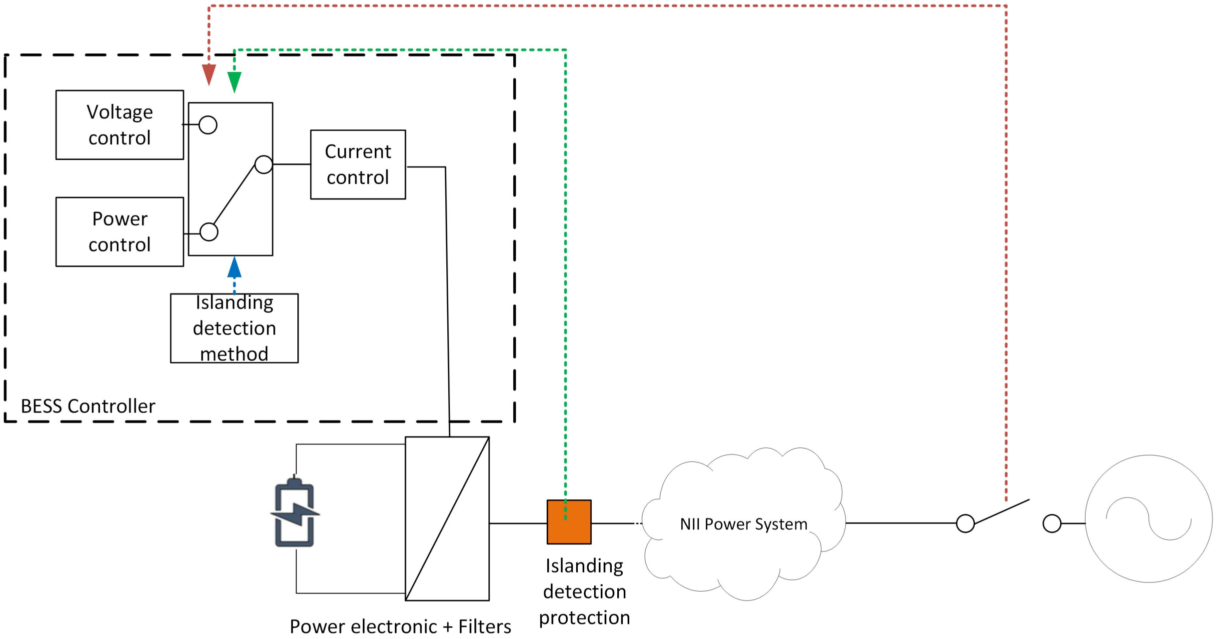

Figure 60: Transition of grid following control to grid forming

sented in Fig. 60). The frequency and ROCOF transients were measured in both modes and presented in Fig. 61) and in Fig. 62), respectively. After the diesel outage a higher frequency transient occurs in the GFL control unit it detect the island and switch its mode. The high ROCOF transient in that case result in the disconnection of the WT and a higher loading of the BESS unit, thus a higer frequency deviation. In the GFM case the diesel outage affects its operation as any other transient resulting in less severe frequency and ROCOF events.

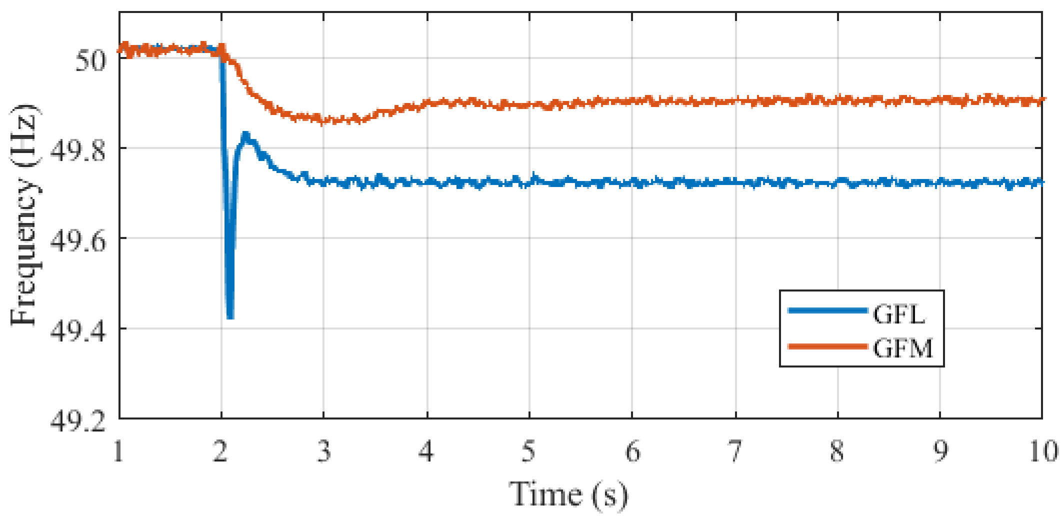

Figure 61: Frequency transients at diesel generator disconnection in different control modes.

sum up, the BESS unit is able to offer multiple services in a NII operating in high RES penetration. In the frequency control frame synthetic inertia provision and fast deployment of FCR are both crucial to avoid critical frequency nadirs and ROCOF transients. aFRR should be provided too especially in high RES penetration levels to restore effectivelly the frequency to its

This project has received funding from the European Union's Horizon 2020 research and innovation programme under grant agreement No 864337

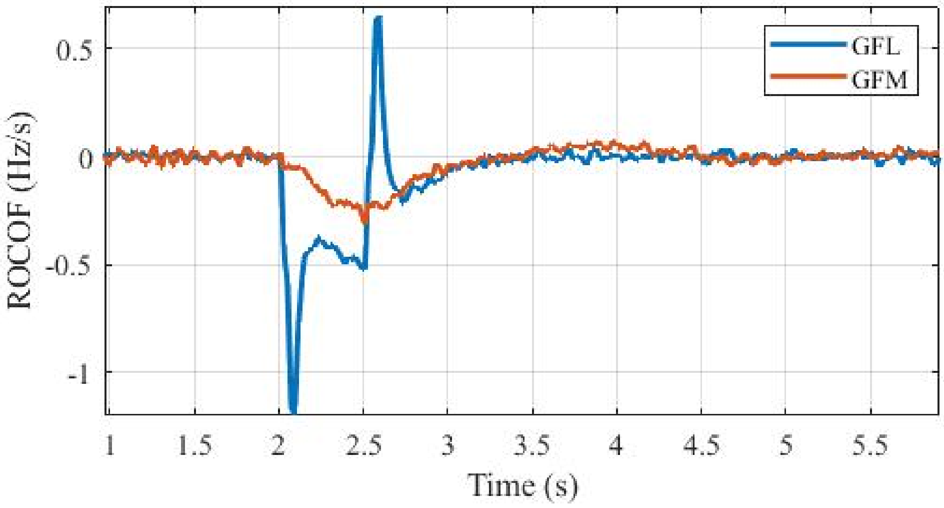

Figure 62: ROCOF transients at diesel generator disconnection in different control modes.

nominal value. All of these services should be incorporated in the economic operation of the system.

Additional services such as FRT and grid forming control are also crucial to security to address the threats that rise during faults and in the transitions of the system states. Finally, through a voltage control service the BESS unit, as well as the RES units, can provide reactive power to ensure proper voltage control in the system and adequate reactive power sharing between the units.

8.3 Stochastic Frequency Secure Economic Dispatch

This section is devoted to present a stochastic economic dispatch formulation for small non-interconnected islands with high RES penetration.

The problem developed here will be a Mixed Integer Linear Programming optimization problem that aims to compute the optimal dispatch and commitment of thermal units taking into account generation costs, RES production and the operation of the central BESS unit (charge/discharge levels and ancillary services provided) to ensure security regarding certain frequency metrics.

The stochastic formulation is adopted, instead of a deterministic approach, in order to address the uncertainty in RES production and demand in the considered horizon T. This uncertainty could affect not only the expected costs but also the ancillary services (synthetic inertia, FCR, FRR) levels that ensure secure operation deployed.

In the following, it will be explained the meaning only of the symbols that have not been previously introduced. For a complete description of them, please refer to the Notation section.

8.3.1 Modelling of BESS ancillary services in an optimization problem

Economic dispatch algorithms in small isolated systems usually consider the production costs, power balance and the adequate FCR and FRR levels for proper frequency control. The provi-

This project has received funding from the European Union's Horizon 2020 research and innovation programme under grant agreement No 864337

sion of ancillary services by a BESS unit is essential to ensure security in high RES penetration levels.

The formulation that is usually proposed for such system considers the FCR and aFRR requirements of the BESS similar to the reserves of thermal units [20]. This approach, however, fails to capture the different dynamics of the BESS unit FCR. As presented in the simulations of the dynamic model of Astypalea island at the previous section, FCR of the BESS have a more critical impact on the system frequency security compared to the thermal generators, due to its faster acting response. Apart form that its synthetic inertia service is also important to ensure the security and it can be deployed properly only if the proper headroom in BESS active power exists.

The aim of the selection of adequate FCR, physical and synthetic inertia levels is to ensure proper security control. Thus, they have to be correlated with specific frequency metrics. As already presented, ROCOF and F_{nadir} are the critical measures of frequency security. On the other hand, introducing all the components affecting the frequency dynamics (inertia, generator governors, BESS controller, grid dynamics, etc.) analytically into linear constraints used in an economic dispatch formulation is impossible. The approach used here uses a simple representation of frequency dynamics based on the swing equation:

$$\frac{2 \cdot (H_{phys} + H_{syn})}{f_{nom}} \cdot \frac{d\Delta F(t)}{dt} = R^{G,FCR}(t) + R^{B,FCR}(t) - P^{DIS} \tag{70}$$

Usually in 70 another term is introduced that represents the load damping effect. Due to the small overall demand in small isolated islands this term is neglected, which makes the 70 slightly more conservative compared to a formulation that considers also the load damping. In 70, the deployment of the FCR of the thermal and BES units are modelled as ramps, 71 and 72 respectively, with a faster time constant for the BESS units (T_s) compared to the thermal units (T_g). Finally, P^{DIS} represents the magnitude of the contingency.

$$R^{G,FCR}(t) = \begin{cases} \frac{R^{G,FCR}_{max} \cdot t}{T_g}, & \text{if } t \leq T_g. \\ R^{G,FCR}_{max}, & \text{otherwise.} \end{cases} \tag{71}$$

$$R^{B,FCR}(t) = \begin{cases} \frac{R^{B,FCR}_{max} \cdot t}{T_s}, & \text{if } t \leq T_s. \\ R^{B,FCR}_{max}, & \text{otherwise.} \end{cases} \tag{72}$$

The largest ROCOF is considered at the beginning of the transient. Considering t=0 in 70 the following expression for ROCOF is deducted:

$$|ROCOF| = |\frac{d\Delta F(t)}{dt}| = \frac{f_{nom} \cdot P^{DIS}}{2 \cdot (H_{phys} + H_{syn})} \tag{73}$$

Equation 73 reveals that the magnitude of the disturbance and the physical and synthetic inertia affect the ROCOF levels. First of all, since the island is dominated at high RES penetration levels, it is probable that the largest power in-feed is the output of RES plant. Therefore, the magnitude of the disturbance is of uncertain nature. Nevertheless, in Greek island code it is pointed out that through the economic dispatch the setpoint for the maximum operating point of a RES power plant is determined. Thus, the largest power in-feed can be restricted.

This project has received funding from the European Union's Horizon 2020 research and innovation programme under grant agreement No 864337

According to the greek NII network code the ROCOF threshold excess of which permits the generating units disconnection is 1Hz/s. To check if the ROCOF is maintained in the desired thresholds, let us consider initially the 100% RES penetration scenario. Under those conditions, the BESS is considered as the only unit providing synthetic inertia. Based on 73 BESS controller's inertia gain should be sufficient large to meet the following requirements:

$$H_{syn} \geq \frac{f_{nom} \cdot max(WT_{nom}, PV_{nom})}{2 \cdot ROCOF_{lim} \cdot P^{B}_{max}} \tag{74}$$

As described in the previous section, the BESS should have sufficient headroom in its reserves to modify quickly its power and provide the necessary synthetic inertia. Thus, based on equations () and () the following must hold true in order to provided synthetic inertia of magnitude H_{syn} with the BESS unit:

$$P^{B}_{max} + P^{c,B} - P^{d,B} \geq P^{Dis} = max(P^{WT}, P^{PV}) \tag{75}$$

In different operating states physical inertia are provided by thermal generators too. Under those conditions the necessary headroom for active power in the BESS unit is calculated according to to consider also the impact of the physical inertia. This constraint is introduced to the economic dispatch model of the next section to ensure that the ROCOF is maintained within the desired limits. Obviously, when considering this constraint for the disconnection of a thermal unit P^{Dis} is equal to its production and that units inertia are not considered. For the disconnection of a RES plant additional constraints are introduced as presented in the next section, to ensure that the considered magnitude of disturbance is greater than the production of the RES units.

$$P^{B}_{max} + P^{c,B} - P^{d,B} \geq P^{Dis} = max(P^{WT}, P^{PV}) - 2 \cdot \frac{\sum_{g \in G} op_g \cdot H_g \cdot S^{nom}_g}{f_{nom}} \tag{76}$$

The frequency nadir occurs when the reserves deployed match the disturbance levels stopping the frequency decay. Considering that the time of the frequency nadir occurs after the deployment of the fast FCR provided by the BESS unit and that the ROCOF is zero during the nadir, expression (77) is computed through (70)- (72).

$$t_{nad} = \frac{P^{DIS} - R^{B,FCR}_{max}}{T_g \cdot R^{BG,FCR}_{max}} \tag{77}$$

Solving the differential equation (70) and applying (77) the value of the frequency nadir can be computed, as presented in (78). Thus, the frequency nadir can be constrained through (79).

$$\Delta F_{nad} = -\frac{f_{nom} \cdot (P^{DIS} - R^{B,FCR}_{max})^2 \cdot T_g}{4 \cdot R^{G,FCR}_{max} \cdot (H_{phys} + H_{syn})} - \frac{R^{B,FCR}_{max}}{4 \cdot (H_{phys} + H_{syn})} \tag{78}$$

$$|\Delta F_{nad,limit}| \cdot (H_{phys} + H_{syn}) \cdot R^{G,FCR}_{max} \geq f_{nom} \cdot (P^{DIS} - R^{B,FCR}_{max})^2 \cdot T_g + R^{B,FCR}_{max} \cdot R^{G,FCR}_{max} \tag{79}$$

This project has received funding from the European Union's Horizon 2020 research and innovation programme under grant agreement No 864337

Constraint (79) has certain terms that are quadratic ($(P^{DIS} - R^{B,FCR}_{max})^2$) and bi-linear ($R^{B,FCR}_{max} \cdot R^{G,FCR}_{max}$, $(H_{phys} + H_{syn}) \cdot R^{G,FCR}_{max}$). The quadratic term is linearized through piecewise linear approximations of Special Order Sets (SOS) of type 2. The bilinear term $(H_{phys} + H_{syn}) \cdot R^{G,FCR}_{max}$) comprises the product of binary and continuous variables. They are approximated using auxiliary variable (z) according to (80) where (b) is binary and (c) a continuous variable respectively. M is a sufficient big number. Finally, the bilinear term ($R^{B,FCR}_{max} \cdot R^{G,FCR}_{max}$ is a product of continuous variables that is analyzed to quadratic terms as presented in (81) were c_1 and c_2 are continous variable. THose quadratci terms are again approximated with piesewise linear segments using SOS of type 2.

To sum up, the equation (79) is reformulated to a set of linear constraints through (80), (81) and SOS of type 2. Thus they are included in the economic dispatch formulation that is described in the next section.

$$z \leq c + (1 - b) \cdot M \tag{80a}$$

$$z \geq c - (1 - b) \cdot M \tag{80b}$$

$$- M \cdot b \leq z \leq M \cdot b \tag{80c}$$

$$c_1 c_2 = \frac{(c_1 + c_2)^2 - (c_1 - c_2)^2}{4} \tag{81}$$

Finally, in order to guarantee that the frequency can be restored to its nominal value the sufficient aFRR of the BESS unit and the operating diesel generators should exceed the maximum disturbance that can occur due to an outage of a RES or a thermal unit.

8.3.2 Formulation of stochastic economic dispatch

The stochastic economic dispatch of the small NII have to decide the start up ($su_{g,t}$) and the shut down of the diesel generators ($sd_{g,t}$) for each generator (g) in every time interval (t) in the considered horizon. At the same time it uses probabilistic forecast for the production of RES (PV and WT) as well as the load. Through those forecasts it computes a scenario tree with specific probabilities for each scenario.

According to the scenarios probabilities it computes for every scenario ω the power production of diesel generators ($P^{G}_{g,\omega,t}$) and their respective FCR and FRR upward and downward reserves ($R^{G,[FCR_{u,d},aFRR_{u,d}]}_{g,\omega,t}$). In addition it computes the operating setpoints of the RES generators $P^{[WT,PV]}_{w,t}$ based on the forecasted production and the security constraints. The most critical part is the evaluation of the BESS system charge or discharge power ($P^{[c,d],B}_{\omega,t}$), its reserves ($R^{B,[FCR_{u,d},aFRR_{u,d}]}_{\omega,t}$) and the expected stored energy levels for every scenario in normal operating conditions and after the aFRR deployment $x^{OP,aFRR_{u,d}}_{\omega,t}$. The goal of the formulation is to reduce generation costs (start up and production), while reducing RES curtailment ($Cur^{[WT,PV]}_{w,t}$, P^{Dis}) and load shedding ($L^{Shed}_{\omega,t}$).

The optimization variables are included in the following equation.

Decision variables:

This project has received funding from the European Union's Horizon 2020 research and innovation programme under grant agreement No 864337

$$D = (su_{g,t}, sd_{g,t}, op_{g,t}, P^{G}_{g,\omega,t}, R^{G,[FCR_{u,d},aFRR_{u,d}]}_{g,\omega,t},$$
$$P^{[c,d],B}_{\omega,t}, R^{B,[FCR_{u,d},aFRR_{u,d}]}_{\omega,t},$$
$$B_{\omega,t}, P^{[WT,PV]}_{\omega,t}, x^{OP,aFRR_{u,d}}_{\omega,t}, Cur^{[WT,PV]}_{\omega,t}, P^{Dis}_{\omega,t}, L^{Shed}_{\omega,t})$$

$$\underset{D}{\text{argmin}} \quad \sum_{t\in T}\sum_{g\in G} c^{up}\cdot su_{g,t} + \sum_{\omega\in\Omega} z(\omega) \sum_{t\in} (\sum_{g\in G} c^{prod}(P^{G}_{g,\omega,t}) + w_{cur}\cdot(Cur^{WT}_{w,t} + Cur^{PV}_{w,t}) + w_{LS}\cdot L^{Shed}_{\omega,t} \tag{82a}$$

subject to

$$op_{g,tt} = op_{g,1}, \; g \in G \tag{82b}$$
$$op_{g,tt} = 1 \; g \in G, \; tt \in [1, Ton^{count}] \tag{82c}$$
$$op_{g,tt} = 0 \; g \in G, \; tt \in [1, Toff^{count}] \tag{82d}$$
$$su_{g,t} \geq op_{g,t} - op_{g,t-1}, \; g \in G, t \in [2, T] \tag{82e}$$
$$sd_{g,t} \geq op_{g,t-1} - op_{g,t}, \; g \in G, t \in [2, T] \tag{82f}$$
$$su_{g,t} \leq op_{g,tt}, \; g \in G, tt \in [t, min(t + Ton - 1, T)] \tag{82g}$$
$$sd_{g,t} \geq (1 - op_{g,tt}), \; g \in G, tt \in [t, min(t + Toff - 1, T)] \tag{82h}$$
$$P^{G,ST}_{g,\omega,t} + R^{G,ST,[FCR_u,aFRR_u]}_{g,\omega,t} \leq op^{ST}_{g,t}\cdot P^{max}_{g}, \; g \in G, t \in T, \omega \in W \tag{82i}$$
$$P^{G,ST}_{g,\omega,t} - R^{G,ST,[FCR_d,FRR_d]}_{g,\omega,t} \geq op^{ST}_{g,t}\cdot P^{min}_{g}, \; g \in G, t \in T, \omega \in W \tag{82j}$$
$$0 \leq R^{G,ST,[FCR_{u,d},FRR_{u,d}]}_{g,\omega,t} \leq op^{ST}_{g,t}\cdot R^{max,[FCR_{u,d},FRR_{u,d}]}_{g}, \; g \in G, t \in T, \omega \in W \tag{82k}$$
$$\tag{82l}$$
$$P^{[WT,PV],ST}_{w,t} + Cur^{[WT,PV],ST}_{w,t} = y^{[WT,PV]}_{\omega,t}, \; t \in T, \omega \in W \tag{82m}$$
$$P^{[WT,PV],ST}_{w,t} \leq P^{Dis}_{\omega,t} \tag{82n}$$
$$x^{OP}_{\omega,t+1} = x^{OP}_{\omega,t} + \begin{pmatrix} +\Delta_k\cdot\eta_c \\ -\Delta_k\cdot\frac{1}{\eta_d} \end{pmatrix}^T \begin{pmatrix} P^{c}_{\omega,t}+ \\ P^{d}_{\omega,t} \end{pmatrix} /x_{nom}, \; t \in [2, T], \omega \in W \tag{82o}$$
$$x^{aFRRu}_{\omega,t+1} = x^{aFRRu}_{\omega,t} + \begin{pmatrix} +\Delta_k\cdot\eta_c \\ -\Delta_k\cdot\frac{1}{\eta_d} \end{pmatrix}^T \begin{pmatrix} P^{c}_{\omega,t} + R^{[aFRRu],B}_{\omega,t} \\ P^{d}_{\omega,t} + R^{[aFRRu],B}_{\omega,t} \end{pmatrix} /x_{nom}, \; t \in [2, T], \omega \in W \tag{82p}$$
$$x^{aFRRd}_{\omega,t+1} = x^{aFRRd}_{\omega,t} + \begin{pmatrix} +\Delta_k\cdot\eta_c \\ -\Delta_k\cdot\frac{1}{\eta_d} \end{pmatrix}^T \begin{pmatrix} P^{c}_{\omega,t} - R^{[aFRRd],B}_{\omega,t} \\ P^{d}_{\omega,t} - R^{[aFRRd],B}_{\omega,t} \end{pmatrix} /x_{nom}, \; t \in [2, T], \omega \in W \tag{82q}$$
$$x^{OP}_{\omega,t} = x_{t_0} + \begin{pmatrix} +\Delta_k\cdot\eta_c \\ -\Delta_k\cdot\frac{1}{\eta_d} \end{pmatrix}^T \begin{pmatrix} P^{c}_{\omega,t} \\ P^{d}_{\omega,t} \end{pmatrix} /x_{nom}, \; t = 1, \omega \in W \tag{82r}$$
$$x^{aFFRu}_{\omega,t} = x^{aFFRu}_{t_0} + \begin{pmatrix} +\Delta_k\cdot\eta_c \\ -\Delta_k\cdot\frac{1}{\eta_d} \end{pmatrix}^T \begin{pmatrix} P^{c}_{\omega,t} + R^{[aFRRu],B} \\ P^{d}_{\omega,t} + R^{[aFRRu],B} \end{pmatrix} /x_{nom}, \; t = 1, \omega \in W \tag{82s}$$
$$x^{aFFRd}_{\omega,t} = x^{aFFRd}_{t_0} + \begin{pmatrix} +\Delta_k\cdot\eta_c \\ -\Delta_k\cdot\frac{1}{\eta_d} \end{pmatrix}^T \begin{pmatrix} P^{c}_{\omega,t} - R^{[aFRRd],B} \\ P^{d}_{\omega,t} - R^{[aFRRd],B} \end{pmatrix} /x_{nom}, \; t = 1, \omega \in W \tag{82t}$$
$$x_{min} \leq x^{OP,aFFRu,aFFRd}_{\omega,t} \leq x_{max}, \; t \in T, \omega \in W \tag{82u}$$
$$0 \leq P^{c,ST}_{\omega,t} \leq P^{BESS}_{max}\cdot B^{ST}_{\omega,t}, \; t \in T, \omega \in W \tag{82v}$$

This project has received funding from the European Union's Horizon 2020 research and innovation programme under grant agreement No 864337

$$0 \leq P^{d,ST}_{\omega,t} \leq P^{BESS}_{max} \cdot (1 - B^{ST}_{\omega,t}), \; t \in T, \omega \in W \tag{82w}$$

$$0 \leq R^{[FCR_u,FRR_u],ST}_{\omega,t} \leq P^{BESS}_{max} + P^{c,ST}_{\omega,t} - P^{d,ST}_{\omega,t}, \; t \in T, \omega \in W \tag{82x}$$

$$0 \leq R^{[FCR_d,FRR_d],ST}_{\omega,t} \leq P^{BESS}_{max} + P^{d,ST}_{\omega,t} - P^{c,ST}_{\omega,t}, \; t \in T, \omega \in W \tag{82y}$$

$$\sum_{gg \in G-[g]} R^{G,ST,[FCR_u,aFRR_u]}_{gg,\omega,t} + R^{[FCR_u,FRR_u],ST}_{\omega,t} \geq P^{G,ST}_{g,\omega,t} \; g \in G, t \in T, \omega \in W \tag{82z}$$

$$\sum_{g \in G} R^{G,ST,[FCR_u,aFRR_u]}_{g,\omega,t} + R^{[FCR_u,FRR_u],ST}_{\omega,t} \geq P^{Dis}_{\omega,t}, \; t \in T, \omega \in W \tag{82}$$

$$\sum_{g \in G} R^{G,ST,[FCR_d,aFRR_d]}_{g,\omega,t} + R^{[FCR_d,FRR_d],ST}_{\omega,t} + P^{WT,ST}_{\omega,t} + P^{PV,ST}_{\omega,t} \geq cd \cdot (y^{Load}_{\omega,t} - L^{Shed}_{\omega,t}) \; t \in T, \omega \in W \tag{82}$$

$$ROCOF(op^{ST}_{g,t}, R^{[FCR_u],ST}_{\omega,t}, P^{Dis}_{\omega,t}) \leq ROCOF^{lim} \; t \in T, \omega \in W \tag{82}$$

$$F_{nad}(op^{ST}_{g,t}, R^{[FCR_u],ST}_{\omega,t}, P^{Dis}_{\omega,t}) \leq F^{lim}_{nad} \; t \in T, \omega \in W \tag{82}$$

$$\sum_{g \in G} (P^{G}_{g,\omega,t}) + P^{d}_{\omega,t} - P^{c}_{\omega,t} + P^{WT}_{w,t} + P^{PV}_{w,t} = y^{Load}_{\omega,t} - L^{Shed}_{\omega,t} \; t \in T, \omega \in \Omega \tag{82}$$

In the above formulation the:

- objective function 82a that comprises in its first term the start up cost (c^{up}) of the diesel generators and the dispatch costs weighted with their respective probabilities ($z(\omega)$). The dispatch costs include a quadratic term for the generator's operating costs that is linearized using SOS of type 2, a term that aims to reduce RES curtailment and a term that penalizes the load shedding that could occur if any of the constraints is violated. Both RES curtailment and load shedding are weighted according to the terms w_{cur} and w_{LS} respectively.

- 82c-82k represent the constraints for the diesel generators. The first three ensure that the commitment decision of the previous economic dispatch solution is forced and that the remaining time that those units must remain on (or off($T^{count)_{off}}$)) operation is satisfied. 82e-82f correlate the binary variables indicating the operating status of the generator, the start up and the shut down of the generator.82g-82h take into account the minimum time that a diesel generator must remain connected T^{on} or disconnected T^{off}. Finally, 82i-82k correlate the reserves provided by the generators with their production levels and their technical maximum (P^{max}_g) and minimum (P^{min}_g) limits in every time interval and scenario as well as the maximum reserve levels that a generator can provide ($R^{max,[FCR_{u,d},FRR_{u,d}]}_g$).

- 82m calculates the curtailed RES power in each time interval and scenario according to the production setpoint and the forecast of the available RES power ($y^{[}WT, PV]_{\omega,t}$). Constraint 82n ensures that the production of RES is less than the magnitude of the disturbance that is considered in the ROCOF and frequency nadir constraints.

- 82o-82y are the constraints regarding the operation of the storage system. 82o-82u ensure that the stored energy in the BESS unit remain within the desired threshold for all the operating scenarios and time intervals both for normal operation as well as if the deployment of aFRR (upwards and downward) occurs during a contingency. Constraints 82v-82y correlate the FCR,aFRR levels that can be provided by the BESS unit upward and downward to the discharged/charge levels and the nominal power of the BESS unit.

- Finally, 82z-82 are the constraints that ensure proper frequency control in the island for every time interval and scenario. Constraint 82z ensures that the necessary FCR and aFRR

This project has received funding from the European Union's Horizon 2020 research and innovation programme under grant agreement No 864337

upward levels exists to compensate the disconnection of a diesel generator.Constraint 82 ensures that adequate FCR and aFRR upward levels exist for the disconnection of the largest producing RES plant. Constraint 82 ensure that the downward FCR and aFRR levels can compensate a disconnection of a portion of the predicted load dictated by the factor cd. The RES generators are participating in this service since they can dynamically curtail their production to address overfrequency events. Finally, the last thee constraints represent the frequency nadir and ROCOF constraints derived by the methodology of the previous section and the power balance constraint.

This project has received funding from the European Union's Horizon 2020 research and innovation programme under grant agreement No 864337

9 Case Study of Non Interconnected Island system

The methodology developed for the stochastic frequency dynamic economic dispatch was evaluated through the case study of Astypalea island by using actual data from another greek island that are part of Dataset n°6 in the Smart4RES Data Management Plan. The are no available data for RES or BESS units in Astypalea since the hybrid plant project is in development phase. The overview of the island is presented in Fig.63. This island is considered to host hybrid station due to of its size and the lack of large RES installations, existing or planned. Astypalea is located in the southeastern Aegean Sea and has a population of 1,334, with a peak annual load of 2.73 MW and annual energy demand of 6,600 MWh (year 2015), with the typical summer peaking demand pattern. In this case study the tree main units in the local power station were considered. Their technical characteristics are presented in Table 9 and their economical data in Table 10.

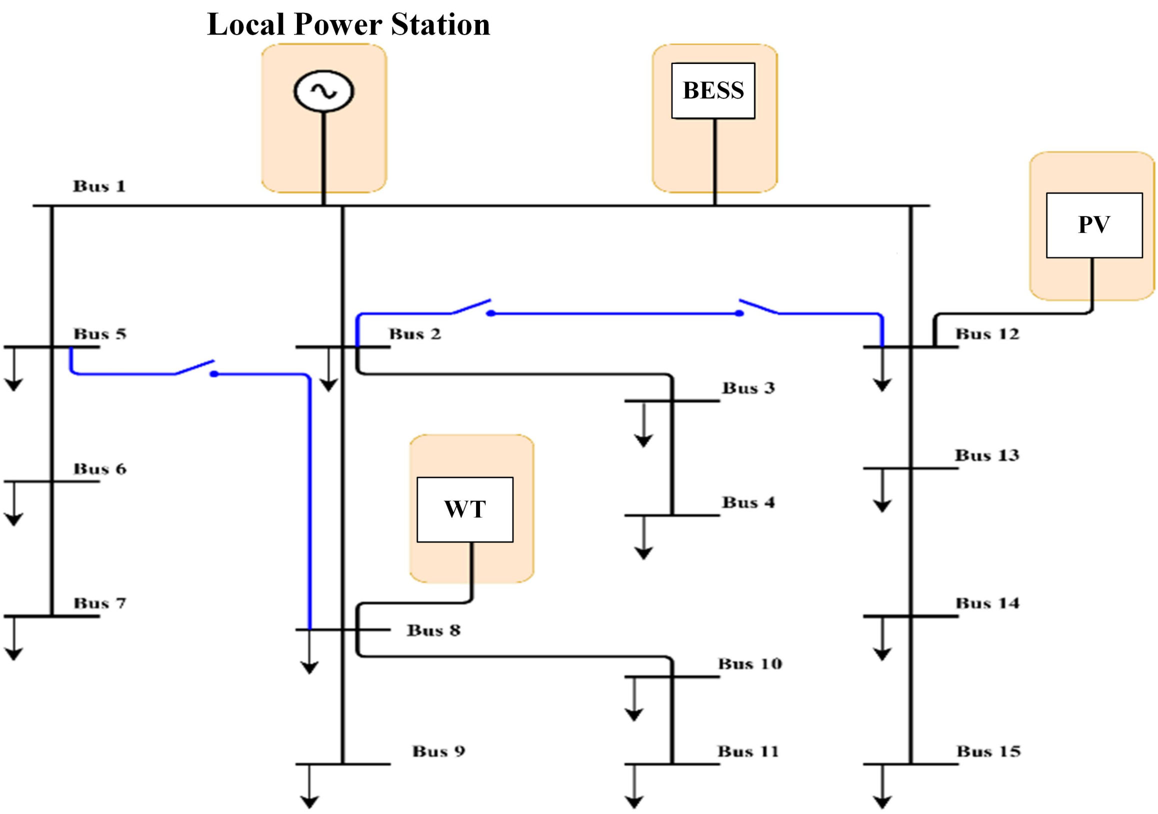

Figure 63: Overview of Astypalea island.

S(MVA)	$P^{max}/P^{nom}(MW)$	$P^{min}(MW)$	$R^{max}_{FCR}(MW)$	$R^{max}_{aFRR}(MW)$	$T_{on}(h)$	$T_{off}(h)$	$H(MWs/MVA)$
1.6	1.1/1.25	0.4	0.3	0.6	1	1	2

Table 9: Astypalea's diesel generator technical data

The hybrid station that is going to be installed is considered to have a WT of nominal production of 2MW, a PV plant of 1MW and a BESS with maximum power of 1.8MW and nominal capacity of 8MWh. Regarding the battery a SOC limits of 95% and 30% was selected both for normal operation and after the deployment of the reserves. The charge/discharge efficiency

This project has received funding from the European Union's Horizon 2020 research and innovation programme under grant agreement No 864337

P^1 (MW)	c^1 (€/MWh)	P^2 (MW)	c^2 (€/MWh)	P^3 (MW)	c^3 (€/MWh)	c^{su} €
0.4	412.40	0.937	388.74	1.25	386.43	60

Table 10: Astypalea's diesel generator economic data

parameters was selected at 0.9.

This project is in development phase, thus there are no actual data regarding the RES units that mentioned previously. This case study data are based on historical time-series of wind and solar power production and load measurements (1 year at 15-min resolution). This time series come from Dataset 6 of the Smart4RES Data Management Plan (cf. Table 1) for Rhodes island. A WT of 3MW was used for the WT forecast scaled its forecast and actual production values at 2MW, while the Rhodes PV production was scaled to 1MW and its load to Astypalea using the peak demand values experienced in the island (Rhodes:223 MW and Astypalea: 2.73MW).

Dataset Index	Dataset Name	Data types used	Use in Deliverable
Dataset 6	Wind + Load + pv in Rhodes (HEDNO$_{Rhodes}$)	Wind and solar power and load time series	RES and load probabilistic forecasting Model validation

Table 11: Use of Smart4RES datasets

The configuration of the training, validation and testing sets for the wind and solar power forecasting model and load forecasting is given in Table 12. The testing set is chosen as the evaluation period for the optimization framework.

Set type	Start	End	Duration	Comments
Training set	2018-01-01	2018-10-31	10 Months	
Validation set	2018-11-01	2018-11-30	1 Month	
Testing set	2018-12-01	2018-12-31	1 Months	

Table 12: Definition of training, validation, testing set

The rest of the configuration is listed below:

- Intraday probabilistic prediction horizons: 1hour to 5 hours
- Number of predicted quantiles : 9
- Number of wind power trajectories : 45
- Number of solar power trajectories : 45
- Number of load trajectories : 45

The stochastic optimization problem had a horizon of 4 hours and time intervals of 20 minutes, in accordance to the greek NII code. For the whole month, every 20 minutes the new forecasts were used together with the existing measurements of RES and load in order to calculated the power dispatch of the next 4 hours.

Astypalea's power system consist of three different MV feeders as presented in Fig.63. The downward FCR and aFRR levels are selected to match the disconnection of the most loaded feeder. Thus, based on the nominal ratings of MV/LV substations installed in each feeder 40%

of the load was considered as the requirement of FCR and aFRR levels. Thus, the term *cd* of the optimization problem was selected 0.4.

The ROCOF threshold according to the greek NII code is 1Hz/s, thus this value is used in the constraints of FDED. For the frequency nadir a total deviation of 0.4Hz was considered as limit. The existing UFLS relays in Astypalea has settings at 48.5Hz. However, islanding detection protection equipment could calculate ROCOF at measurement windows *e.g.* of 20 cycles (*i.e.* 0.4s) to compute the ROCOF value (ref eq). Thus a deviation of frequency of 0.4Hz was selected to avoid tripping of islanding detection equipment of such settings.

The BESS control used in the dynamic model to evaluate the economic dispatch controls is presented in Fig.64. The emulated inertia and the FCR are selected from the power filter measurement ($H_{syn} = \frac{1}{2 \cdot drp \cdot wc}$) and the droop control gain (drp). The drp was selected at 0.5% and wc=3.57 to ensure that the synthetic inertia gain maintain the ROCOF at 1Hz/s if the WT is disconnected at its nominal rating at 100% RES penetration.

An external isochronous central controller deploys the aFRR and updates P_{AGC}. The black start module could update the voltage reference during black start, otherwise the voltage amplitude is modified according to a Q(V) characteristic through the droop gain in voltage (drv). The drv was selected 5%. The angle and voltage amplitude setpoints are fed to a model that contains an inner voltage control and a current control as well as a current limitation. The FRT requirement can be included also in the controller to control the circuit breaker of the BESS unit according to the voltage measurements at the point of common coupling. The maximum power of 1.8 MW of the BESS unit was considered as the maximum power used in the computation of ROCOF constraints and in the computation of the available FCR and aFRR.

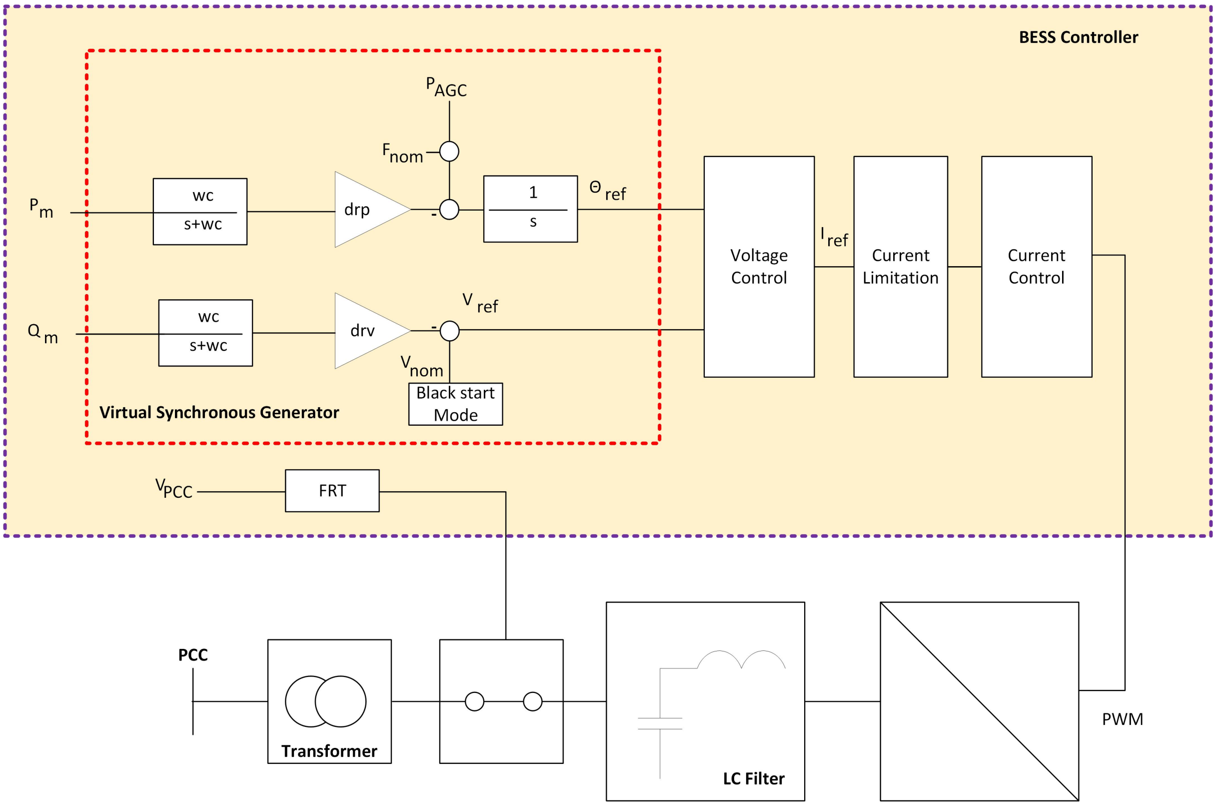

Figure 64: Overview BESS controller.

This project has received funding from the European Union's Horizon 2020 research and innovation programme under grant agreement No 864337

10 Evaluation of advanced ancillary services in small NII

The algorithm for the economic dispatch for small NII operating in high RES penetration was evaluated basically for its ability:

- a) to ensure frequency security. A set of 2000 operating conditions was considered in this scenario. It included the operating points in the data of table 11 as well as additional operating points sampled randomly to include a more broad spectrum of operating points.For every operating point the stochastic economic dispatch was solved using a conventional method and the proposed. In the conventional method the aFRR and FCR of BESS and the diesel generators have to compensate the loss of the largest producing RES unit, similar to what is proposed in [20]. The control actions computed with every method (generator's production, BESS charge/discharge, aFRR and FCR levels, etc.) was collected for every operating point considered and uploaded in the dynamic model of Astypalea island in Powerfactory. The largest RES outage was considered as contingency and the frequency and ROCOF transients were collected in order to compare them with the desired thresholds (49.6Hz and 1Hz/s). Surpassing those thresholds is considered to result in additional outage of generating units in order to protect them from high ROCOF transients or due to tripping of islanding protection. Since a cascaded outage of generation would result in load shedding or even total system outage, we considered every threshold in frequency or in ROCOF as a case that results in load shedding.
- b) to address uncertainty. The probabilistic forecast services and the stochastic formulation of the FDED formulation proposed was compared with a deterministic forecast and FDED formulation in order to assess the impact of advanced forecast services and the stochastic optimization. For both formulations the FDED was solved considering 4 horizon with 20 minute steps. The diesel generators in Astypalea island can not immediately start and require a warm up procedure of around several minutes. Thus, the commitment solution (generator start or shut down) obtain with any of the optimization approaches in t time interval for t+1 interval is maintained fixed for the first interval of the optimizations solved in t+1 interval. The forecasts are updated every hour but the economic dispatch problems are solved every 20 minutes using existing measurements and forecasts. If the economic dispatch formulations can not fullfill the problem constraints the load shedding will be forced to be greater than 0 to make the problem feasible. The cost W_{LS} correlated with load shedding in the optimization describe the costs for deploying costly emergency units to meet the desired FCR and aFRR levels or disconnecting customers to ensure frequency security. Thus, the two approaches are mainly compared in terms of the total load shedding that they computed for the period under stude. Other metrics are provided as well regarding the operating costs, RES penetration and RES curtailment. FInally, in the same context, PV forecasts using satellite images are compared with conventional PV forecast.

For the stochastic approach the Q_{10}, Q_{50} and Q_{90} quantiles were used. The probabilities in every scenario are computed according to [ref strbac 2012]. In the scenario tree branching occurs only at the root node and at t=1 the existing measurement is used instead of forecast. The scenario tree is presented in Fig.65. Three scenarios are considered in every time interval which are:

- the mean scenario. This scenario includes the Q_{50} quantile of RES and Load forecast.

- high demand low RES scenario. This scenario includes the Q_{10} quantile in RES power forecast and the Q_{90} in load.
- low demand high RES scenario. This scenario includes the Q_{90} quantile in RES power forecast and the Q_{10} in load.

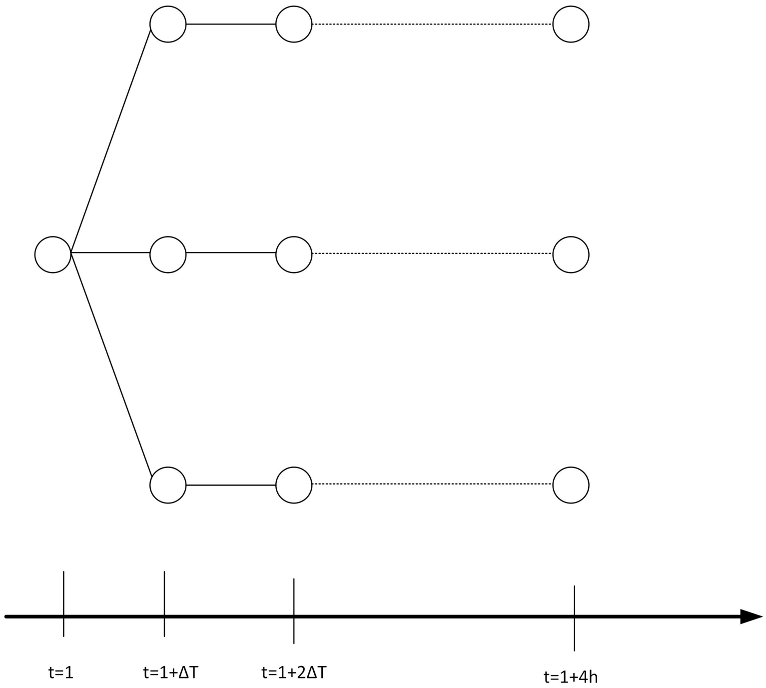

Figure 65: Scenario tree considered in Astypalea case.

The weights of the load shedding cost w_{LS} and the RES curtailment W_{cur} was selected to vary and the formulation performance for those values will be presented in the following section.

The main aim the aforementioned formulation is to ensure security at small NII at high RES penetration levels. Thus, the more relevant KPI defined in Smart4RES Project is $KPI_{1.3.a}$ that describes the % decrease of load shedding events in isolated power systems. The project target is to reach $KPI_{1.3.a} \geq 80\%$.

This project has received funding from the European Union's Horizon 2020 research and innovation programme under grant agreement No 864337

11 Results on small NII

In this section the results for the Astypalea case study are presented using the evaluation approach presented in the previous chapter. The results are divided in two sections:

- **Evaluation of frequency dynamics constraints**. In this an evaluation of the methodology of the BESS services introduction in frequency correlated constraints takes place. It is compared against a conventional approach for the calculation of the economic dispatch control actions. Both approaches aim to have adequate reserves to meet the disconnection of the largest producing unit in order to have a fair comparison between the methodology presented to compute the necessary reserves and a conventional methodology. The conventional approach uses the method presented in [20].
- **Comparison of deterministic and stochastic approach**. In this subsection the impact of the probabilistic forecast and the stochastic optimization approach is compared to existing methodologies that use deterministic forecast and optimization.

11.1 Evaluation of frequency dynamics constraints

In this section a set of 2000 operating points was used. It consists of several scenarios from the test set presented in section 9 as well as additional operating conditions to have a more vast spectrum of operating points.

Only the existing point was considered with no horizon and it was solved with two optimization approaches, the proposed and an conventional one. The conventional approach considered that the FCR and aFRR of BESS and diesel units should surpass the production of the largest producing RES plant. Creating the controls for each operating point the contingency of largest RES outage was considered at the dynamic model of the NII in Powerfactory for both methodologies capturing the resulting frequency transients. The frequency transients for the conventional approach and the proposed approach are presented in Fig.66 and in Fig.67 respectively. The ROCOF transients are presented in Fig.68 and Fig.69

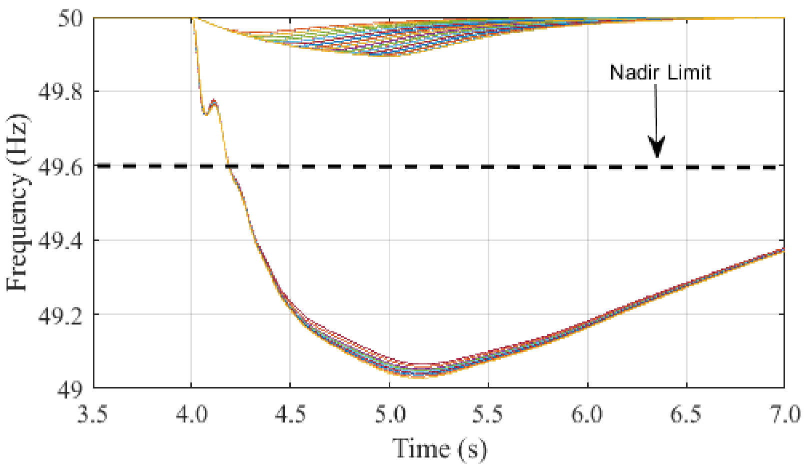

Figure 66: Frequency Transient in contingencies performed in operating points extracted with conventional Economic Dispatch.

As presented in these figures there are certain scenarios that the conventional approach fails to ensure that the frequency and ROCOF remain above the desired thresholds for all scenarios,

This project has received funding from the European Union's Horizon 2020 research and innovation programme under grant agreement No 864337

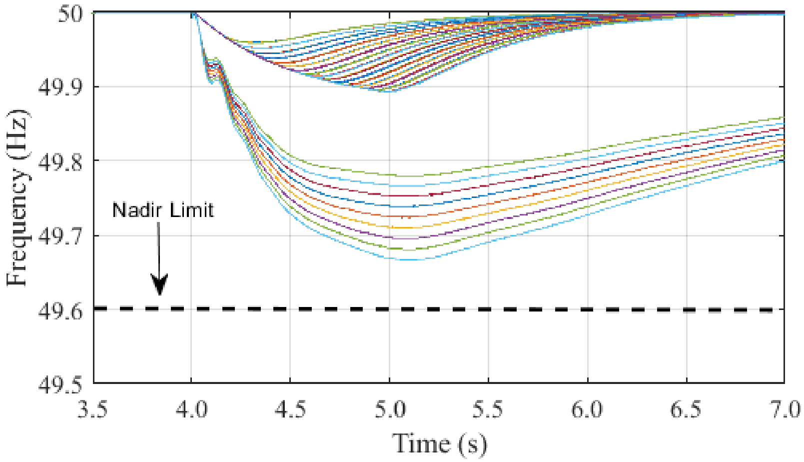

Figure 67: Frequency Transient in contingencies performed in operating points extracted with Frequency Dynamic Economic Dispatch.

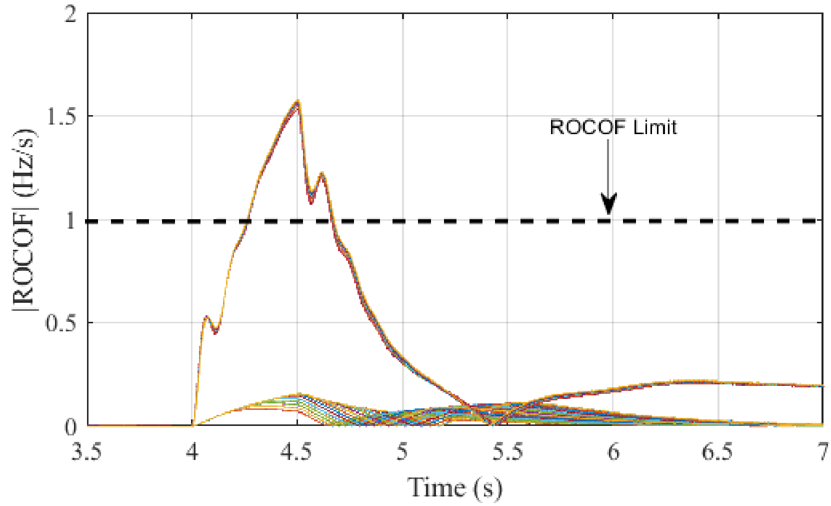

Figure 68: ROCOF Transient in contingencies performed in operating points extracted with conventional Economic Dispatch.

while the proposed methodology ensure frequency and ROCOF security for every scenario. Those mainly occur in high RES penetration scenarios at medium to high demand levels that result in the largest frequency deviation in these figures. For example, among the cases there a scenario of 2.5 MW load, 2MW WT production, 0.4MW of diesel generation and 0.1MW of BESS discharge. According to this operating condition the FCR levels of the BESS are 1.7MW and the diesel generators are 0.3MW covering the WT outage. Thus, the conventional approach considers this scenario secure. However, at the disconnection of the WT the BESS reaches its power limitation thus it can not provide adequate synthetic inertia case, as dictated by (76). In contrast to the conventional approach the proposed methodology identifies this issue and requests higher generation production levels from the diesel generator (0.472MW) to ensure that enough power levels are available in the BESS unit for the provision of the synthetic inertia services.

There is a total of 9 scenarios that the conventional approach fails to evaluate frequency security properly. The high ROCOF values could result in tripping of islanding protection or other

This project has received funding from the European Union's Horizon 2020 research and innovation programme under grant agreement No 864337

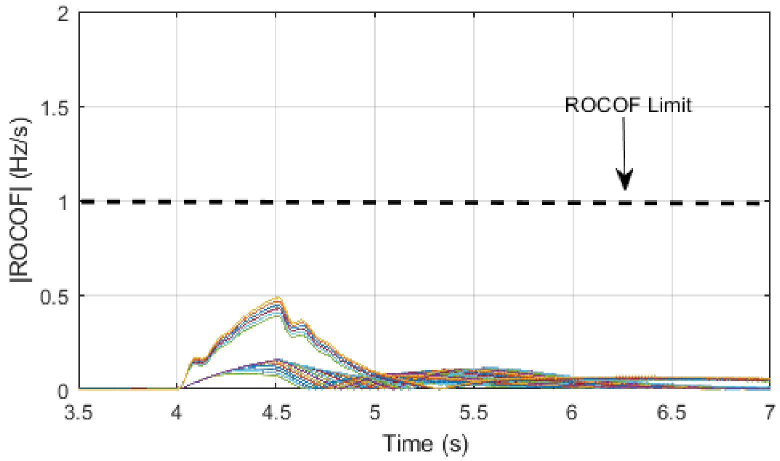

Figure 69: ROCOF Transient in contingencies performed in operating points extracted with Frequency Dynamic Economic Dispatch.

generators protection since it surpasses the threshold dictated by the greek NII code. As a result, further generators could be disconnected resulting in system outage or load shedding. Compared to the conventional approach, the proposed method achieves to maintain the desired security metrics within thresholds thus it can be assumed that it decreases the load shedding occurrence totally compared to the conventional approach.

11.2 Comparison of stochastic and deterministic economic dispatch

The actual 1 month of data presented in Section 9 was used to evaluate the economic performance and security of the proposed formulation of ED versus a deterministic ED that uses deterministic forecasts.

The forecasts were updated every hour provided the trajectories of 9 quantiles, *i.e.* Q10 to Q90, for the next five hours. The actual measured values were used for t=1 in both stochastic and deterministic ED. The load, PV production and WT measured power are presented in Fig.70. It is clear that there are days with high RES production as well as days where the demand surpasses existing RES production. The trajectories of the forecasts that the FDED receives as input are presented in 70 for the timestamp 09/12/2018 03:00 PM.

Using this trajectories the scenarios for the stochastic FDED are created the way it is described in the previous section. by solving the optimization problem the optimal trajectories for BESS and diesel generators power output are calculated (Fig. 72) ensuring that the state of charge of the BESS remains within the desired thresholds both during normal operation or if deployment of aFRR is needed (Fig. 73)

The SOC values for the whole month in normal operation and after the deployment of aFRR are presented in Fig.74. The proposed formulation is able to maintain the SOC within the desired levels. The aFRR provided by the BESS unit are presented in . The upward aFRR are reduced only when the SOC of the BESS is not close to its lower limit (30%) and the diesel generator provides the remaining aFRR. The downward aFRR are reduced at high SOC where mainly the RES can provide the required levels of downward aFRR.

The load shedding action introduced in the FDED proposed for the islands will force disconnection of load if any of the SOC or security constraints are violated. In actual operation, the

This project has received funding from the European Union's Horizon 2020 research and innovation programme under grant agreement No 864337

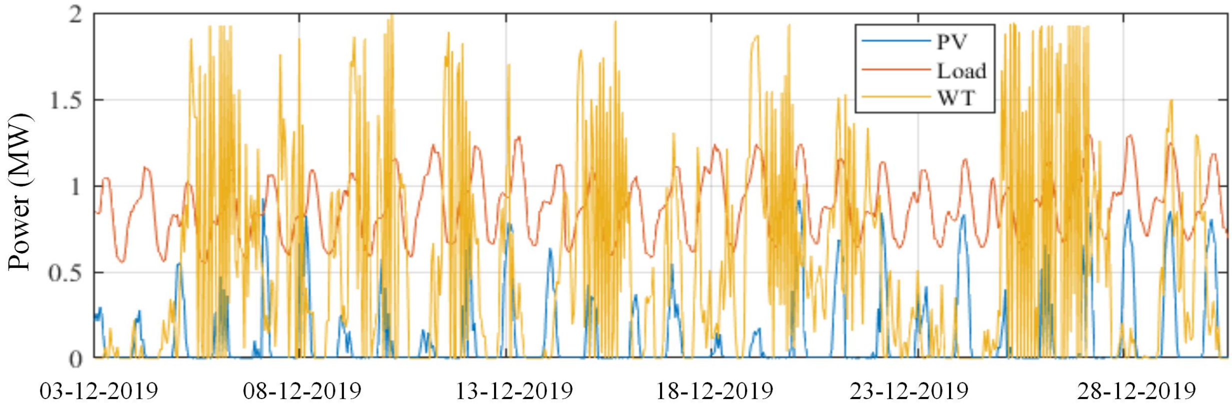

Figure 70: Load and available RES power for the testing period considered.

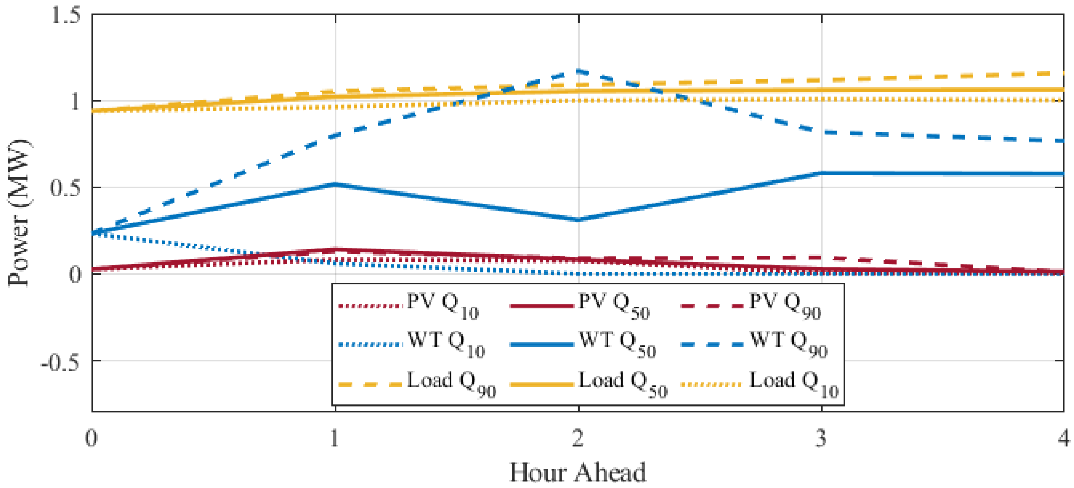

Figure 71: Trajectories received as input by the FDED at 15/12/2018 03:00 PM.

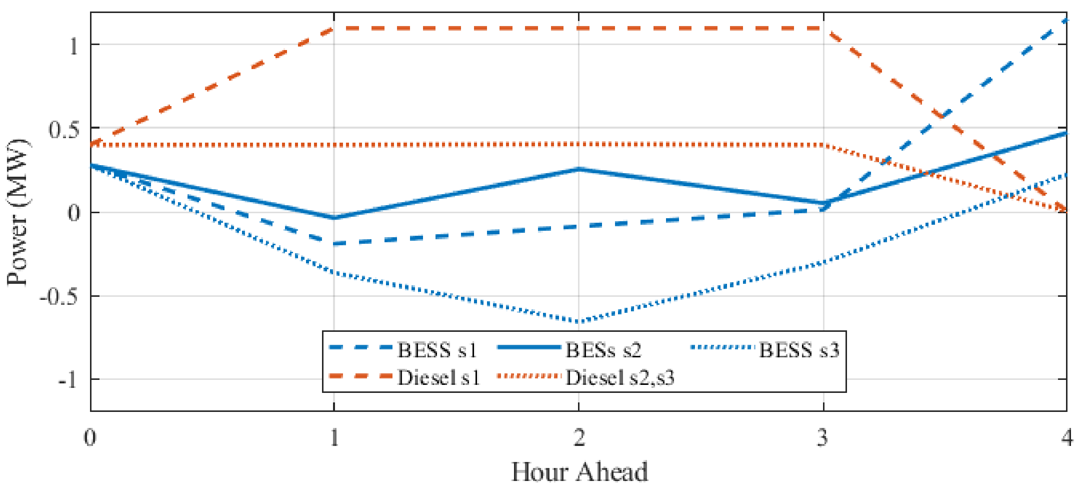

Figure 72: Trajectories of BESS and diesel generator power output at 15/12/2018 03:00 PM

This project has received funding from the European Union's Horizon 2020 research and innovation programme under grant agreement No 864337

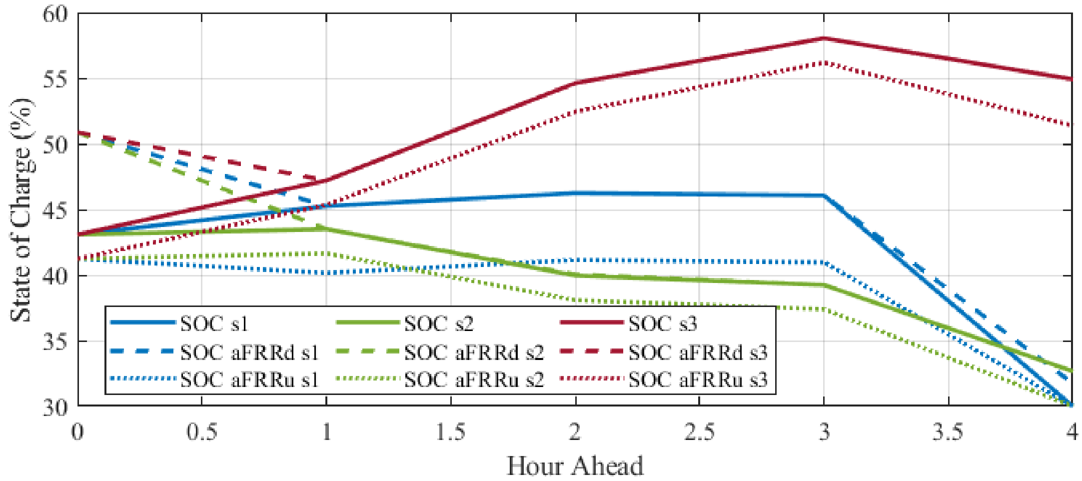

Figure 73: Trajectories of SOC in normal operation or if aFRR computed at 15/12/2018 03:00 PM.

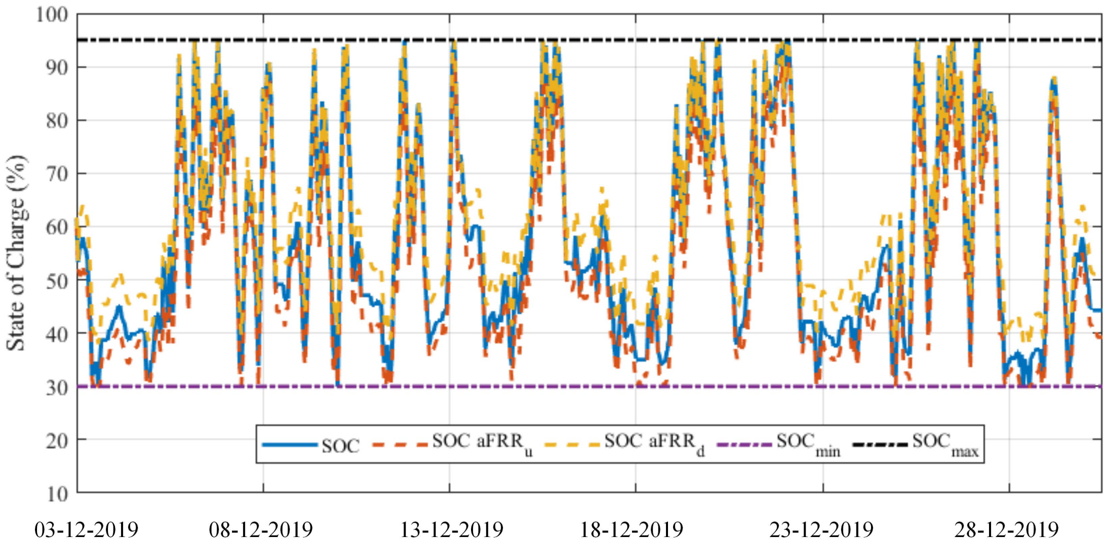

Figure 74: State of charge in normal operation and after the deployment of aFRR.

system operator could suffer lower SOC or less amount of reserves until it dispatches additional thermal units. Therefore, it is an indicator of the security of the control actions computed by the deterministic or the stochastic approach.

The objective function of the FDED presented for NII includes the power generation costs (start up and production costs of the diesel generators) and the load shedding and RES curtailment weighted with their repsective factors. In Fig.76 the production costs and the resulting load shedding for different values of W_{LS} are presented. As the weight W_{LS} increases the security of the FDED increases resulting at lower total load shedding levels. However, it has an impact on the overall generation costs which increase as the overall to address the security in the system. In Fig.77 the production costs and the resulting load shedding for different values of W_{cur}. Higher values of W_{cur} penalize more the RES curtailment in the objective function thus they result in higher RES acceptance and lower production costs. However, this affects the trade-off with the security therefore for high W_{cur} values result in worse performance in the total

This project has received funding from the European Union's Horizon 2020 research and innovation programme under grant agreement No 864337

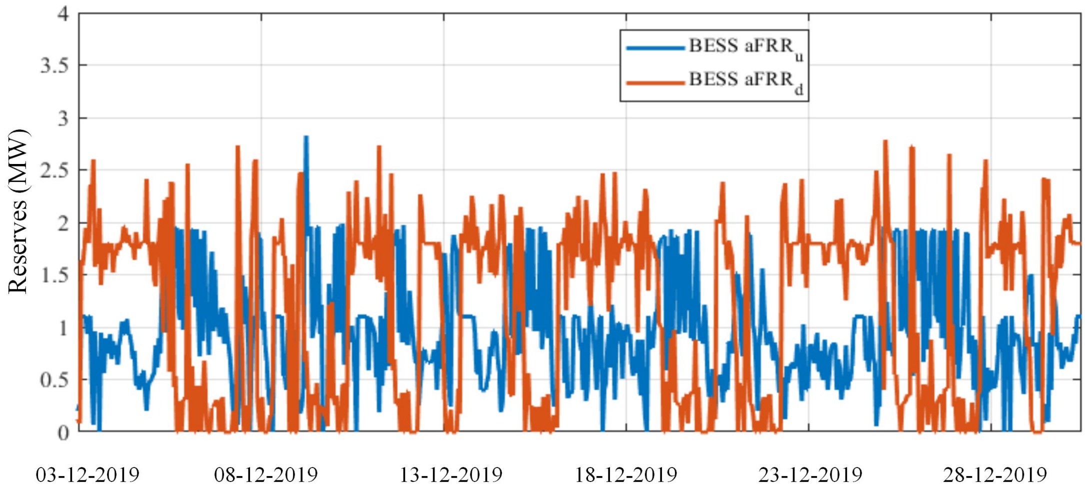

Figure 75: Automatic FRR provided by the BESS.

load shedding throughout the test period considered.

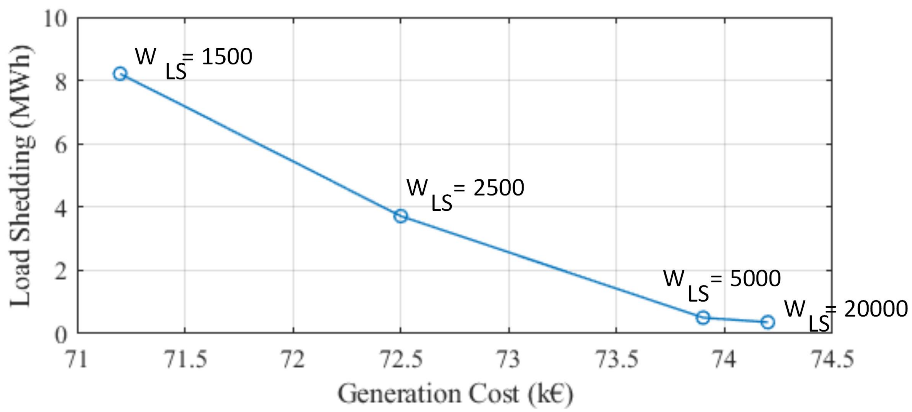

Figure 76: Cost and Load shedding for different values of the load shedding weight W_{LS}.

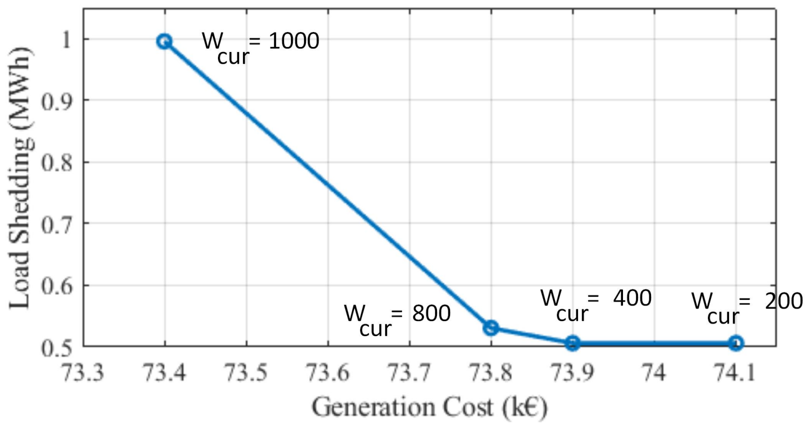

Figure 77: Cost and Load shedding for different values of the RES curtailment weight W_{cur}.

Using $W_{cur} = 400$ and $W_{LS} = 5000$ the deterministic forecast and FDED are compared with the

This project has received funding from the European Union's Horizon 2020 research and innovation programme under grant agreement No 864337

stochastic FDED that uses probabilistic forecast. The load shedding values of the two methods are presented in Fig.78. In the stochastic approach there is a total number of 9 occurrences that the ED was not secure. On the contrary, the deterministic approach was less secure resulting in 42 cases of insecure dispatch. Furthermore, the stochastic approach resulted in mainly in small values of load shedding (<0.1 MW), while the deterministic approach has an overall number of 18 cases of Load shedding surpassing 0.25 MW. At those cases, the absence of adequate levels of reserves or the low SOC levels could result in dispatching additional emergency generators to avoid improper frequency control if a contingency occurs.

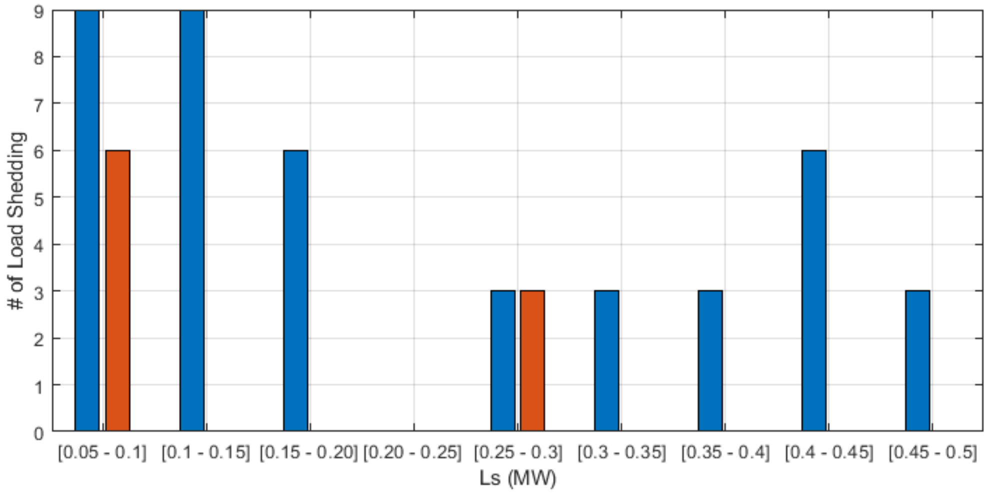

Figure 78: Load shedding levels and their number of occurrence for deterministic (blue) and stochastic (orange) approach.

The insecure cases mainly resulted in low SOC levels where possible deployment of upward aFRR can result in surpassing the desired thresholds of SOC and inability from the BESS system to maintain this service for 20 minutes as requested by the greek NII code. The incidence rate of the different SOC levels throughout the month for the deterministic and the stochastic approach are presented in Fig.79. It is clear that the stochastic approach is more conservative reaching fewer times low SOC levels compared to the deterministic resulting in adequate room for the upward aFRR deployment.

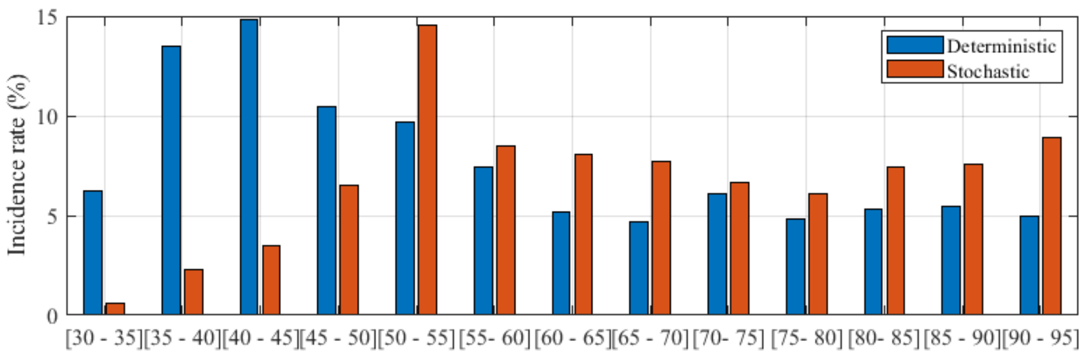

Figure 79: Incidence rate of SOC levels and their number of occurrence for deterministic (blue) and stochastic (orange) approach.

The two approaches are compared also in terms of economic performance, RES penetration, RES curtailment and total demand shed. The results are presented in Table 13. The

This project has received funding from the European Union's Horizon 2020 research and innovation programme under grant agreement No 864337

stochastic approach results in a reduction of load shedding compared to the deterministic. The $KPI_{1.3.a}$, that indicates the decrease of load shedding events in isolated power systems, of the project was used to compare the two approaches. Through the stochastic approach we have a decrease of 84.5% which is greater than the project's target of 80%. The KPI is computed according to the formula in (83).

To achieve this decrease in load shedding the stochastic approach dispatches the BESS and thermal units more conservatively compared to the deterministic approach resulting in 2% decrease in RES penetration, 5.2% more RES power curtailment and an increase of 5.8% in costs (thermal generator production and start up costs). However, in the cost calculation the emergency start up of back up generators or the load shedding costs if a contingency occur are not calculated. In a similar fashion to (ref), this costs can be computed by the load shedding occurring in the optimization, where a value of 5000$/MWh is considered for the load shedding cost. Considering a cost of 2000€/MWh for the load shedding in this case, the total costs of the stochastic approach reach 74.8k€ while the deterministic approach reach 75.98k€.

$$KPI_{1.3.a} = 100\frac{L_{sd}^{Det} - L_{sd}^{sto}}{L_{sd}^{Det}} = -84.5\% \tag{83}$$

Method	RES Penetration (%)	Production cost (k€)	Load Shedding (MWh)	RES Curtailment (MWh)
Deterministic	70.04	69.5	3.24	187.81
Stochastic	67.93	73.8	0.5	198.32

Table 13: Comparison of stochastic and deterministic approach

Furthermore, a comparison is made between two stochastic approaches to evaluate the impact of the satellite PV forecasts developed in WP3. In the first case a conventional probabilistic forecast is used. On the second, a probabilistic PV forecast that uses satellite images. The results are presented in Table 14. In all the metrics the WP3 forecast modules result in better results making the system more secure (less load shedding) but also more economic profitable.

Method	RES Penetration (%)	Production cost (k€)	Load Shedding (MWh)	RES Curtailment (MWh)
Conventional	67.57	7.46	0.75	199.4
Satellite	67.93	7.38	0.5	198.32

Table 14: Comparison of stochastic solutions with conventional PV forecast and WP3 satellite PV forecast

This project has received funding from the European Union's Horizon 2020 research and innovation programme under grant agreement No 864337

12 Conclusion

The first approach proposed in this Deliverable is a complete framework to solve the problem of provisioning energy and AS, by means of an hybrid system (RES power plant + BESS). This problem is structured in three different steps (forecasting, day-ahead trading and short-term control). The former one is not directly part of this work, but it represents a necessary input for the framework. The second one consists in the stochastic optimization of the DA Trading problem, considering in the first place the unique problem of bidding on the electricity market, added after the provision of AS. The latter phase is where the main original contribution of this work has been given. Here different MPC strategies are proposed, starting from the standard canonical formulation of a reference tracking controller (DRT-MPC), moving to an economic MPC which is proposed in a stochastic formulation (SEMPC) and is compared to a deterministic alternative (DEMPC). These control strategies are then extended to also take into account the problem of energy + AS provision. Both trading and control allow for a multi-objective formulation which applies distinct weights to market costs and BESS degradation cost, evaluated thanks to a linear approximation for cycling and calendar ageing.
Finally, some evaluation scores are formulated to assess in a quantitative way the performance of this framework and some plots and distributions are shown to analyze qualitatively its behaviour. Using data from a real hybrid system Wind Power Plant (WPP) + BESS, some simulations are performed to observe the behavior of the different combinations of modules, for trading and control, in which the framework is articulated. The obtained results show the performance of the different modules and, *ex-post*, of the different chains in the framework. In particular the economic MPC is proven to overcome, both on the revenue and on the BESS degradation sides, the performance of the reference tracking controller. The stochastic formulation of the economic MPC is also less sensitive to large RES forecasting errors than its deterministic counterpart.

Non-interconnected island power systems operate in geographical islands without interconnections to the mainland grid. Typically, the energy production of these systems relies on diesel generators, which are both costly and environmentally polluting. Hybrid solutions that include renewable energy generators, energy storage units and advanced control methods are able to achieve very high penetration of renewables in such systems.

The provision of AS by the BESS is crucial to maintain security in the islands power supply. The most crucial threat is the overall reduction in the system's inertia due to the replacement of conventional plants with power electronic based resources. The reduced amount of inertia leads to more severe transients when power imbalances in the system occur both in terms of frequency and ROCOF. Such events can lead to disconnection of consumers, through an activation of under frequency load shedding relays, as well as generating units. The provision of fast FCR by the BESS unit has been introduced in larger systems to address the decreased inertia concern. However, simulations on a dynamic model of the island of Astypalea have shown that this service alone might not be able to ensure proper frequency control. The synthetic inertia service by the BESS unit is critical to mitigate further the frequency transient to acceptable levels. Automatic FRR are also important since the remaining diesel generators operating at high RES penetration might have inadequate aFRR levels to restore the frequency.

There are also other crucial services that should be provided by the BESS unit. Since the presence of the BESS unit is necessary to the proper operation of the system, its ability to remain connected during faults is of paramount importance. More strict requirements, compared to the FRT requirements described in the greek NII code, can be adopted to increase the time that the BESS unit remains during fault. Its dynamic voltage support during the faults can increase the

This project has received funding from the European Union's Horizon 2020 research and innovation programme under grant agreement No 864337

voltage at the terminal of the unit allowing to remain connected for larger time intervals but also to increase fault current levels, leading to faster fault detection and clearance. Furthermore, the voltage can be supported in normal operation through a Q(V) control or through a reactive power setpoint provided by the system operator.

The aforementioned services can be also provided in grid forming control. Nevertheless, the grid forming ability is a prerequisite for the BESS in order to act as a black start unit or to operate the island in 100% RES penetration levels. The aforementioned services can be also provided in grid forming control. It's main advantage compared to a grid following control is its ability to seamlessly transit between states (from and to 100% when a diesel generator connects/disconnects). This is highlighted through a in the dynamic model of Astypalea island.

The fast FCR, the synthetic inertia and the aFRR provision of the BESS are affected by the dispatch of the different units in the island. In addition, considering the FCR provided by the BESS and the diesel units as similar can lead to insecure dispatches as indicated in the results presented. To this end, a methodology to correlate the impact of the fast FCR and synthetic inertia in linear rules for the economic dispath of the system is presented. At the same time adequate energy levels must be available in the BESS unit in order to provide the aFRR. However, the stored enegy could vary in the horizon considered in the economic dispatch due to the uncertainty introduced by RES and load. The proposed stochastic frequency dynamic economic dispatch (FDED) can ensure the frequency security in the system taking into account the uncertainty in RES production and load. Advanced forecast techniques developed in the SMART4RES project are required for the implementation of the stochastic FDED. Based on actual forecasts this stochastic FDED is compared to a conventional deterministic economic dispatch. Based on the results the stochastic approach achieves more secure operation resulting in a reduction of load shedding, greater than 80%, which was the among the KPIs of the project.

12.1 KPIs and Milestones

The following KPIs have been fulfilled, under the assumptions detailed in the sections relative to each approach:

- The proposed trading and control approach enables to increase potential revenue when offering energy and AS compared to energy only. The value of the corresponding $KPI_{1.3.d}$ is $\approx 20\%$. Additionally, the proposed economic control enables a $12-13\%$ increase in the revenue compared to a standard control which tracks reference signals for energy and AS market offers.
- A Specific KPI has been proposed to quantify the gain in BESS degradation cost with the proposed framework. The proposed economic control achieves a $KPI_{degradation} \geq 23\%$, *i.e.* 23 % reduction in degradation cost compared to a state-of-the-art model with reference-tracking control.
- Smart4RES Project KPI on decrease of load shedding events in isolated power systems, $KPI_{1.3.a}$ $84.5\% \geq 80\%$

12.2 Achieved TRL levels

The proposed approaches / methods in this work have reached the following TRLs:

This project has received funding from the European Union's Horizon 2020 research and innovation programme under grant agreement No 864337

- Multi-objective optimization framework for hybrid RES system providing multiple services: TRL 4
- Battery design for advanced ancillary service provision in isolated power systems: TRL 3
- Stochastic frequncy dynamic economic dispatch : TRL 3

12.3 Key messages

The following key messages can be drawn from this study:

- Degradation-aware predictive control approaches ensure the feasibility and profitability of hybrid RES systems providing multiple services.
- Economic predictive control outperforms traditional reference tracking predictive control in the context of multiple services by a hybrid RES system.
- The synthetic inertia service provision by a centralized BESS is crucial to maintain frequency security in non interconnected island operating in high RES penetration levels. PV and WT can provide synthetic inertia to assist in the island security too. However, it could be at the cost of power curtailment.
- Grid forming control and more strict fault ride through requirements can increase the overall security of the system during faults and transitions between island states.
- The introduction of the different characteristics of BESS FCR and synthetic inertia compared to the diesel generators in the economic dispatch formulation can avoid the computation of frequency insecure control actions.
- Advanced forecasts modules (probabilistic) and optimization techniques that consider uncertainty (stochastic) can increase the overall security in an isolated power system.

This project has received funding from the European Union’s Horizon 2020 research and innovation programme under grant agreement No 864337

1 Appendix - Forecasting

The optimization framework proposed in Section 4 relies on the forecasting of uncertain variables. As the Deliverable focuses primarily on the impact of RES uncertainty on decisions, only forecasting of RES production is considered. The sections below present the state-of-the-art forecasting methods employed for day-ahead and short-term RES forecasting.

The day-ahead forecasting model of RES production is a Gradient Boosting Regression Tree (GBRT), which is a state-of-the-art regression model employed in RES forecasting [35]. This model fits shallow decision trees per quantile τ of the expected distribution, so that the pinball loss function L defined in (84) between predicted RES production $\hat{y}_t$ and observed production y_t is minimized:

$$L_\tau(\hat{y}_t, y_t) = (\mathbf{1}_{y_t \leq \hat{y}_t} - \tau)(\hat{y}_t - y_t) \quad \forall t \tag{84}$$

Based on a set s_t of explanatory variables, the forecasts at the $\mathcal{N}$ terminal nodes ρ_n, $n \in \mathcal{N}$ of decision trees are iteratively optimized to minimize the loss function:

$$\rho_n = \text{argmin}_\rho \sum_{s_t inS_n} L_\tau(g_\tau(s_t) + \rho, y_t) \tag{85}$$

Where $g_\tau(.)$ is the function corresponding to the prediction of a given tree.

The quantiles obtained from the probabilistic forecasts are subsequently converted into trajectories that model the temporal correlation of the production signal. The method followed is composed of four steps [36]:

1. In a validation set, locate the position u_{t+K} of observed production within the predicted distribution:

$$u_{t+K} = \hat{F}_{t+k}(y_{t+k}), \quad \forall t \in T, k \in K \tag{86}$$

2. If the forecast is reliable, then these positions are uniformly distributed in $[0, 1]$. The distribution is converted into a real-valued random variable $\xi \in \mathbb{R}$ using the logit function Φ in order to evaluate the covariance matrix between different prediction horizons:

$$\xi_{t+k} = \Phi(u_{t+k}) \quad \forall t, k \tag{87}$$

3. Fit the multivariate Normal distribution X of the obtained positions ξ. This distribution is defined by a covariance matrix $\Sigma_{k,k'}$ for each pair of horizons (k, k') in the horizon range. It is then converted back to a Uniform distribution

$$X_{k,k'} \sim \mathcal{N}(0, \Sigma_{k,k'}), \quad \forall k, k' \tag{88}$$

$$U_{k,k'} \sim U(X_{k,k'}), \quad \forall k, k' \tag{89}$$

4. Derive trajectories by sampling the distribution Ω times for each t in the testing set and inverting the Cumulative Distribution Function

$$\hat{y}^\omega_{t+K} = \hat{F}_{t+k}(U^{(\omega)}_{k,k'}) \quad \forall t, k, \omega \in \Omega \tag{90}$$

This project has received funding from the European Union's Horizon 2020 research and innovation programme under grant agreement No 864337

A large number of scenarios needs to be generated in order to obtain a good representation of the temporal correlation. However, the complexity of the stochastic optimization using these scenarios scales linearly with the number of scenarios Ω. This is why in this work a set of $\Omega = 100$ scenarios is generated and subsequently reduced to a set $\Omega^{'}$ that maximizes the preservation of the temporal correlation. The scenario reduction can be approached by clustering methods, importance sampling or probability metrics. For the sake of simplicity, a probability metric method will be employed following [33]. The principle consists in selecting the most equidistant trajectories in the full set according to a distance $d(\omega, \omega') = \sqrt{\sum_t (\hat{y}^{\omega}_{t+k} - y_{t+k})^2}, \forall \omega, \omega'$, and repeat this selection on the remaining trajectories until the desired cardinality is reached.

Table 15 below summarises the forecasting scores of the GBRT day-ahead forecasts, averaged over the horizon range. Values are acceptable considering the state of the art and the size of training and testing set (51552 and 33408 points respectively). An example of day-ahead forecast is shown in Fig. 80. We can see that the median predicted quantile (orange series) reproduces the general production pattern at low and wind speed regimes, albeit missing some fast ramps (*e.g.*, September 5) that have not been anticipated by the weather predictions used as inputs. It also avoids the positive biases exhibited by a physical model (green series) which converts weather predictions into power without statistical learning capacities. The RMSE of the GBRT has a 6% relative improvement with respect to the physical model.

RMSE	MAE	CRPS
15.9	10.9	6.06

Table 15: Deterministic and Probabilistic Scores of day-ahead forecasts, scaled by $\% P_{max}$

The reduced set of trajectories in Fig. 81, although visibly originating from sampling, offer a sufficient model of the temporal variability in the RES production. The selected trajectories, represented in different grey levels, cover the uncertainty range quantified by the probabilistic forecast.

For intraday forecasting, the GBRT considers as input recent lags of production measurement up to the past 6 hours, as well as the freshest NWP available, generally produced at least 6 hours before the runtime of the intraday RES forecasting. The RMSE ranges from 5% at 5 min to 10 % at 15 min, against 12% at 15 min for persistence benchmark, which translates into a relative improvement of 20%.

This project has received funding from the European Union's Horizon 2020 research and innovation programme under grant agreement No 864337

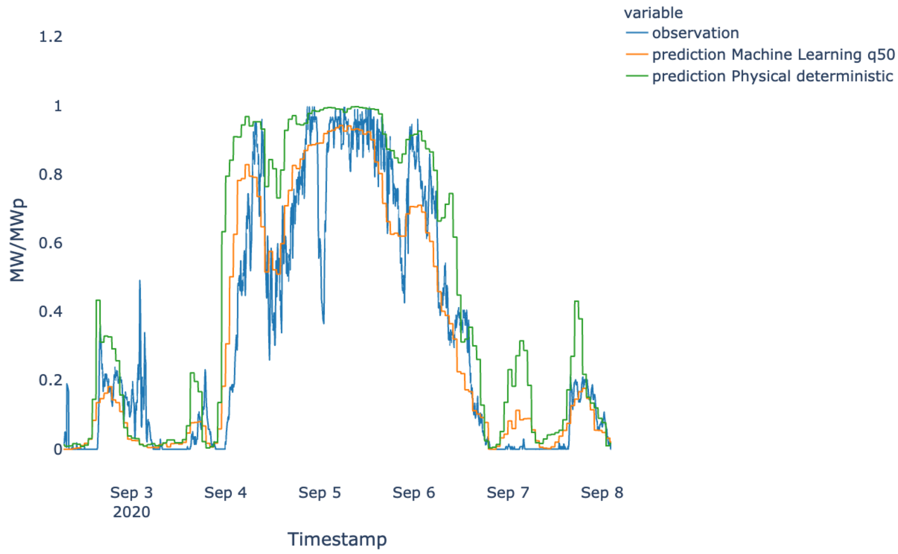

Figure 80: Example of RES forecasting at day-ahead horizon. The orange curve is the 50% quantile of the predicted distribution, compared against a physical deterministic model (calibrated wind speed / wind power curve) as benchmark.

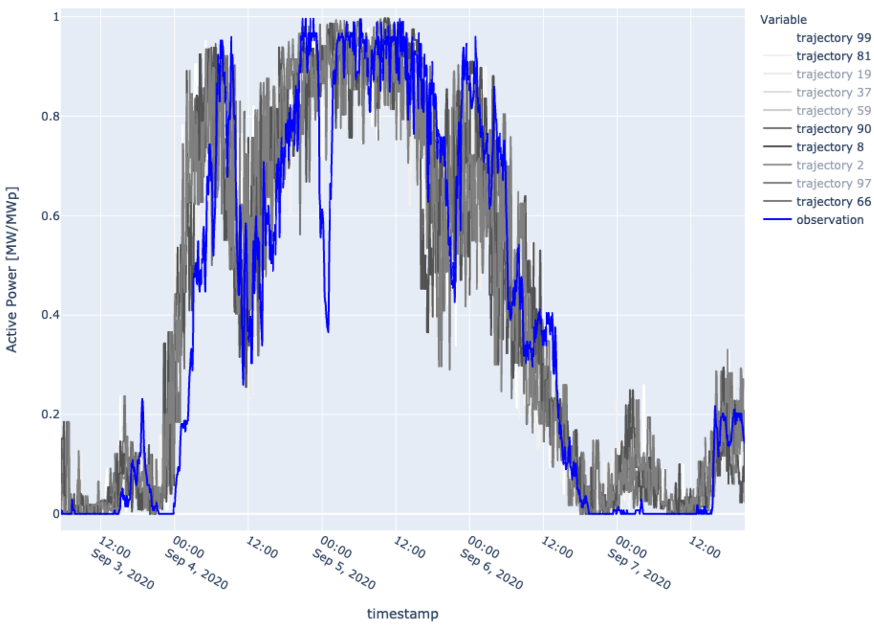

Figure 81: Reduced trajectories of RES production obtained from day-ahead forecasts

This project has received funding from the European Union's Horizon 2020 research and innovation programme under grant agreement No 864337

Bibliography

[1] Seth Mullendore. Energy storage and electricity markets. the value of storage to the power system and the importance of electricity markets in energy storage economics. https://www.cleanegroup.org/wp-content/uploads/Energy-Storage-And-Electricity-Markets-August-2015.pdf, 2015.

[2] Entsoe. Overview of the european balancing market and electricity balancing guideline, 2018.

[3] Lexuan Meng, Jawwad Zafar, Shafiuzzaman K. Khadem, Alan Collinson, Kyle C. Murchie, Federico Coffele, and Graeme M. Burt. Fast frequency response from energy storage systems—a review of grid standards, projects and technical issues. *IEEE Transactions on Smart Grid*, 11(2):1566–1581, 2020. doi: 10.1109/TSG.2019.2940173.

[4] Karin Kreuzer. Participation des éoliennes aux services système en allemagne et en france rôle , cadres réglementaires et défis futurs novembre 2016, 2016.

[5] Nikos Hatziargyriou, Ioannis Margaris, Irene Stavropoulou, Stavros Papathanassiou, and Aris Dimeas. Noninterconnected island systems: The greek case. *IEEE Electrification Magazine*, 5(2):17–27, 2017. doi: 10.1109/MELE.2017.2685739.

[6] Stavros A. Papathanassiou and Nikos G. Boulaxis. Power limitations and energy yield evaluation for wind farms operating in island systems. *Renewable Energy*, 31(4):457–479, 2006. ISSN 0960-1481. doi: https://doi.org/10.1016/j.renene.2005.04.002. URL https://www.sciencedirect.com/science/article/pii/S0960148105000923.

[7] Carlos Adrian Correa-Florez, Andrea Michiorri, and Georges Kariniotakis. Robust optimization for day-ahead market participation of smart-home aggregators. *Applied Energy*, 229:433–445, 2018. ISSN 0306-2619. doi: https://doi.org/10.1016/j.apenergy.2018.07.120. URL https://www.sciencedirect.com/science/article/pii/S0306261918311553.

[8] Unnikrishnan Raveendran Nair, Monika Sandelic, Ariya Sangwongwanich, Tomislav Dragičević, Ramon Costa-Castelló, and Frede Blaabjerg. Grid congestion mitigation and battery degradation minimisation using model predictive control in pv-based microgrid. *IEEE Transactions on Energy Conversion*, 36(2):1500–1509, 2021. doi: 10.1109/TEC.2020.3032534.

[9] Dennis Van der Meer, Guang Chao Wang, and Joakim Munkhammar. An alternative optimal strategy for stochastic model predictive control of a residential battery energy management system with solar photovoltaic. *Applied Energy*, 283:116289, 2021.

[10] Tobias Gybel Hovgaard, Kristian Edlund, and John Bagterp Jørgensen. The potential of economic mpc for power management. In *49th IEEE Conference on Decision and Control (CDC)*, pages 7533–7538, 2010. doi: 10.1109/CDC.2010.5718175.

[11] Huajie Ding, Pierre Pinson, Zechun Hu, and Yonghua Song. Optimal offering and operating strategies for wind-storage systems with linear decision rules. *IEEE Transactions on Power Systems*, 31(6):4755–4764, 2016.

[12] Rishi Amrit, James B. Rawlings, and David Angeli. Economic optimization using model predictive control with a terminal cost. *Annual Reviews in Control*, 35(2):178–186, 2011. ISSN 1367-5788. doi: https://doi.org/10.1016/j.arcontrol.2011.10.011. URL https://www.sciencedirect.com/science/article/pii/S136757881100040X.

[13] Matthias A. Müller and Lars Grüne. Economic model predictive control without terminal constraints for optimal periodic behavior. *Automatica*, 70:128–139, 2016. ISSN 0005-1098. doi: https://doi.org/10.1016/j.automatica.2016.03.024. URL https://www.sciencedirect.com/science/article/pii/S0005109816301042.

[14] Matthias A. Müller, David Angeli, and Frank Allgöwer. Economic model predictive control with self-tuning terminal cost. *European Journal of Control*, 19(5):408–416, 2013. ISSN 0947-3580. doi: https://doi.org/10.1016/j.ejcon.2013.05.019. URL https://www.sciencedirect.com/science/article/pii/S0947358013000885. The Path of Control.

[15] Emil Namor, Dimitri Torregrossa, Fabrizio Sossan, Rachid Cherkaoui, and Mario Paolone. Assessment of battery ageing and implementation of an ageing aware control strategy for a load leveling application of a lithium titanate battery energy storage system. In *2016 IEEE 17th Workshop on Control and Modeling for Power Electronics (COMPEL)*, pages 1–6, 2016. doi: 10.1109/COMPEL.2016.7556779.

[16] Andrea Michiorri, Giovanni Lupaldi, and Davide Bertelli. Optimal hybrid pv-battery residential system management and sizing taking into account battery thermal behavior and ageing. In *CIRED 2020 Workshop*, pages 4–5, 2020.

[17] E.M.G. Rodrigues, G.J. Osório, R. Godina, A.W. Bizuayehu, J.M. Lujano-Rojas, and J.P.S. Catalão. Grid code reinforcements for deeper renewable generation in insular energy systems. *Renewable and Sustainable Energy Reviews*, 53:163–177, 2016. ISSN 1364-0321. doi: https://doi.org/10.1016/j.rser.2015.08.047. URL https://www.sciencedirect.com/science/article/pii/S1364032115009107.

[18] Greek non-interconnected island code. https://deddie.gr/en/themata-tou-diaxeiristi-mi-diasundedemenwn-nisiwn/ruthmistiko-plaisio-mdn/kwdikas-diaxeirisis-ilektrikwn-sustimatwn-mdn/kwdikas-diaxeirisis-mdn/. Accessed: 2010-09-30.

[19] Ioannis D. Margaris, Stavros A. Papathanassiou, Nikos D. Hatziargyriou, Anca D. Hansen, and Poul Sorensen. Frequency control in autonomous power systems with high wind power penetration. *IEEE Transactions on Sustainable Energy*, 3(2):189–199, 2012. doi: 10.1109/TSTE.2011.2174660.

[20] Georgios N. Psarros, Eleni G. Karamanou, and Stavros A. Papathanassiou. Feasibility analysis of centralized storage facilities in isolated grids. *IEEE Transactions on Sustainable Energy*, 9(4):1822–1832, 2018. doi: 10.1109/TSTE.2018.2816588.

[21] Luis Badesa, Fei Teng, and Goran Strbac. Simultaneous scheduling of multiple frequency services in stochastic unit commitment. *IEEE Transactions on Power Systems*, 34(5):3858–3868, 2019. doi: 10.1109/TPWRS.2019.2905037.

This project has received funding from the European Union's Horizon 2020 research and innovation programme under grant agreement No 864337

[22] Vaclav Knap, Sanjay K. Chaudhary, Daniel-Ioan Stroe, Maciej Swierczynski, Bogdan-Ionut Craciun, and Remus Teodorescu. Sizing of an energy storage system for grid inertial response and primary frequency reserve. *IEEE Transactions on Power Systems*, 31(5): 3447–3456, 2016. doi: 10.1109/TPWRS.2015.2503565.

[23] Hrvoje Pandžić, Yury Dvorkin, Ting Qiu, Yishen Wang, and Daniel S. Kirschen. Toward cost-efficient and reliable unit commitment under uncertainty. *IEEE Transactions on Power Systems*, 31(2):970–982, 2016. doi: 10.1109/TPWRS.2015.2434848.

[24] Dimitris T. Lagos and Nikos D. Hatziargyriou. Data-driven frequency dynamic unit commitment for island systems with high res penetration. *IEEE Transactions on Power Systems*, 36(5):4699–4711, 2021. doi: 10.1109/TPWRS.2021.3060891.

[25] Jorn Reniers, Grietus Mulder, and David Howey. Review and performance comparison of mechanical-chemical degradation models for lithium-ion batteries. *Journal of The Electrochemical Society*, 166:A3189–A3200, 01 2019. doi: 10.1149/2.0281914jes.

[26] Emil Namor, Dimitri Torregrossa, Fabrizio Sossan, Rachid Cherkaoui, and Mario Paolone. Assessment of battery ageing and implementation of an ageing aware control strategy for a load leveling application of a lithium titanate battery energy storage system. pages 1–6, 06 2016. doi: 10.1109/COMPEL.2016.7556779.

[27] Madeleine Ecker, Nerea Nieto, Stefan Käbitz, Johannes Schmalstieg, Holger Blanke, Alexander Warnecke, and Dirk Uwe Sauer. Calendar and cycle life study of li(nimnco)o2-based 18650 lithium-ion batteries. *Journal of Power Sources*, 248:839–851, 2014. ISSN 0378-7753. doi: https://doi.org/10.1016/j.jpowsour.2013.09.143. URL https://www.sciencedirect.com/science/article/pii/S0378775313016510.

[28] Michael Merten, Fabian Rücker, Ilka Schoeneberger, and Dirk Uwe Sauer. Automatic frequency restoration reserve market prediction: Methodology and comparison of various approaches. *Applied Energy*, 268(April):114978, 2020. ISSN 03062619. doi: 10.1016/j.apenergy.2020.114978. URL https://doi.org/10.1016/j.apenergy.2020.114978.

[29] Jeremie Bottieau, Louis Hubert, Zacharie De Greve, Francois Vallee, and Jean-Francois Toubeau. Very-Short-Term Probabilistic Forecasting for a Risk-Aware Participation in the Single Price Imbalance Settlement. *IEEE Transactions on Power Systems*, 8950(c):1–1, 2019. ISSN 0885-8950. doi: 10.1109/tpwrs.2019.2940756.

[30] Akylas Stratigakos, Simon Camal, Andrea Michiorri, and Georges Kariniotakis. Prescriptive trees for integrated forecasting and optimization applied in trading of renewable energy. *IEEE Transactions on Power Systems*, pages 1–1, 2022. doi: 10.1109/TPWRS.2022.3152667.

[31] Dimitris Bertsimas and Nathan Kallus. From predictive to prescriptive analytics. *Management Science*, 66(3):1025–1044, 2020.

[32] Angelos Georghiou, Daniel Kuhn, and Wolfram Wiesemann. The decision rule approach to optimization under uncertainty: methodology and applications. *Computational Management Science*, 16(4):545–576, 2019.

[33] J Dupačová, · N Gröwe-Kuska, and · W Römisch. Scenario reduction in stochastic programming An approach using probability metrics. *Math. Program., Ser. A*, 95:493–511, 2003. doi: 10.1007/s10107-002-0331-0.

This project has received funding from the European Union's Horizon 2020 research and innovation programme under grant agreement No 864337

[34] AEMO. Fast frequency response in the nem. *VIC, Australia, Working Paper*, 2017.

[35] D. W. van der Meer, J. Munkhammar, and J. Widén. Probabilistic forecasting of solar power, electricity consumption and net load: Investigating the effect of seasons, aggregation and penetration on prediction intervals. *Solar Energy*, 171(July):397–413, 2018. ISSN 0038092X. doi: 10.1016/j.solener.2018.06.103. URL https://doi.org/10.1016/j.solener.2018.06.103.

[36] P. Pinson and R. Girard. Evaluating the quality of scenarios of short-term wind power generation. *Applied Energy*, 96:12–20, 2012. ISSN 03062619. doi: 10.1016/j.apenergy.2011.11.004.

This project has received funding from the European Union's Horizon 2020 research and innovation programme under grant agreement No 864337